0-315-91854-3

COMPRESSION CREEP MEASUREMENTS IN PULTRUDED ANGLE SECTIONS MADE OF FIBRE GLASS REINFORCED PLASTIC

BY

YAGHOUB MOHAMMADI

A Thesis submitted to the Faculty of Graduate Studies and Research in partial fulfilment of the requirements for the degree of Master of Engineering

Department of Civil Engineering and Applied Mechanics

McGill University

Montreal, Quebec, Canada, H3A 2K6

June, 1993

SHORT TITLE:

CREEP IN ANGLE SECTIONS MADE OF FIBRE GLASS REINFORCED PLASTIC

In the Name of Allah

The Beneficent, The Merciful

To:

My Parents

For their encouragement

and

My Family

For their patience and understanding

ABSTRACT

A study aimed at investigating the performance of pultruded fibre glass reinforced plastic (FGRP) materials subjected to both the time-independent and the time-dependent response of angle stubs and coupons was conducted. Angle stubs and coupons were made of isophtalic polyester resin reinforced with an E-glass fibre glass mat of 35%-45% of the weight. The stub dimensions were of 50.8 mm x 50.8 mm x 6.35 mm (2 in. x 2 in. x 1/4 in.) and their length was 305 mm (6 in.). The compression coupons were cut in a prismatic shape according to ASTM Standard D695-89 with 12.70 mm x 6.35 mm (1/2 in. x 1/4 in.) cross-section and a length of 31.75 mm (1 15 in.).

In the time-independent short-term study, the FGRP angle stubs and coupons were subjected to axial compression loading with two different testing configurations in order to find the best loading arrangement to be used in the long-term study.

In the time-dependent long-term study, three angle stubs were first subjected to a 350 hour preliminary creep test, followed by 150 hours of creep recovery, with three lengths and configurations of strain gauges. These preliminary tests were necessary to validate and finalize the design of the experimental set-ups and testing variables. Finally, a last series of tests was carried out on three angle stubs instrumented with 12 5-mm long gauges. Coupon creep tests were carried out in parallel with the stub tests, and results of the two series of tests were compared in

view of validating the use of coupon test results for predicting creep deformations of full-sized members. The total duration of the tests was 2500 hours in creep and 250 hours in creep recovery Results indicate a scatter in the order of 15% in creep strain measurements after 2500 hours, for both stub and coupon tests. Predictions using Findley's power law with creep parameters determined from the stub tests and coupon tests are in excellent agreement, both with one another and with actual creep strain measurements on the stubs. The Boltzman superposition principle was used to compare the experimental creep recovery results with predictions from Findley's model, and excellent agreement was also observed.

SOMMAIRE

L'auteur présente les résultats d'une étude expérimentale sur le comportement mécanique à long terme de cornières pultrudées en matériau composite, chargées en compression uniaxiale. Le matériau utilisé est une résine polyester isophtalique renforcée d'une natte de fibres de verre de type E dans une proportion de 35%-45% en poids. Les essais ont été faits sur des courtes sections de cornières à ailes égales ainsi que sur des éprouvettes. Les cornières testées sont de dimensions 50.8 mm x 50 8 mm x 6.35 mm (2 in. x 2 in. x 1/4 in.) et d'une longueur de 305 mm (6 in.). Les éprouvettes de compression ont été prélevées des cornières, et leurs dimensions sont de 12.70 mm x 6.35 mm (1/2 in. x 1/4 in.) et la longueur de 31.75 mm (1.15 in.), conformément aux exigences de la norme ASTM D695-89.

Des essais à court terme ont d'abord été faits sur les cornières et les éprouvettes afin de valider et finaliser la configuration de l'essai de fluage. Ensuite, des essais préliminaires d'une durée de 350 heures en compression suivies de 150 heures en relaxation, ont été réalisés sur trois prototypes de cornières avec différents arrangements de jauges de contraintes, en vue de valider la procédure expérimentale. La série finale d'essais — 2500 heures en compression suivies de 250 heures en relaxation — a été réalisée sur trois sections de cornières, chacune instrumentée avec 12 jauges de 5 mm, et sur trois éprouvettes de compression. Les résultats de ces deux séries d'essais ont été comparés afin de vérifier la fiabilité des essais sur éprouvettes

pour prédire le comportement à long terme des sections de cornières de dimensions réelles.

Les résultats indiquent une variation de $\pm 15\%$ dans les mesures de déformations après 2500 heures, et cette variation est la même pour les éprouvettes et les sections de cornières. Le modèle théorique de Findley a été utilisé pour prédire les déformations, en y substituant les paramètres de fluage obtenus par traitement des résultats expérimentaux. Ces prédictions sont très proches des mesures prises, tant pour les mesures individuelles des éprouvettes et des cornières, que pour les prédictions du fluage réel sur les cornières à partir des paramètres obtenus avec les mesures sur éprouvettes. Il en est de même pour les déformations de relaxation, calculées en appliquant le principe de superposition de Boltzman au modèle de Findley.

ACKNOWLEDGEMENTS

The author wishes to express his sincere appreciation and gratitude to his research supervisor; Professor G. McClure for her guidance, assistance, advice, patience and constructive criticism throughout the preparation of this thesis.

The author is grateful to the Ministry of Culture and Higher Education of the Islamic Republic of IRAN for sponsoring his study at McGill University, Montreal, Canada.

The author would like to thank the following people:

Mr. M. Caron for his assistance in preparing the experimental set-up.

Messrs. M. Przykorski, J. Bartczak, R. Sheppard and D. Kiperchuk for their laboratory technical assistance.

My graduate colleagues who in one way or another offered a helping hand in preparing the manuscript of this thesis.

Finally, the author would like to express his heartfelt thanks to his parents and his family for their unfailing encouragement and support during the entire preparation of the thesis.

TABLE OF CONTENTS

LIST OF TABLES

LIST OF FIGURES

LIST OF SYMBOLS

Symbol	Description	Dimension
E	modulus of elasticity	MPa
E_m	Maxwell proportionality constant	MPa
E_t	time-dependent modulus of elasticity	MPa
E_v	Voigt proportionality constant	MPa
E_v	viscoelastic axial modulus of elasticity	MPa
E_0	time-independent modulus of elasticity	MPa
m	coefficient of time-dependent creep	$\mu\epsilon$
n	stress-independent material creep constant	none
P	concentrated vertical force	kN
t	time after loading	hr
t_0	unit time	hr
t_u	time of unloading	hr
V_c	rate of creep	mm/mm/hr
ϵ	total axial creep strain	$\mu\epsilon$
ϵ_0	instantaneous creep strain	$\mu\epsilon$
σ_i	stress produced by the initial load	MPa
σ_f	stress produced by the final load	MPa
σ_m	stress at time t	MPa

σ_t	stress at time t_0	MPa
ϕ_c	creepocity	%
η_m	Maxwell proportionality constant in Newtonian viscosity	Pa s
η_v	Voigt proportionality constant in Newtonian viscosity	Pa.s

CHAPTER 1

INTRODUCTION

1.1 Introduction

Natural occurring composites, such as feathers and woods, have been known for thousands of years. While their history is several thousands shorter, man-made composites have been available for over 7000 years and some of the arts of making composites are still in use in developing nations. For example, Reeds were used to reinforce pitch for composite boats in the Middle East in 5000 B.C., and wood laminated with shellac was produced in Thebes and India over 3000 years ago (Sheldon, 1982).

In 1931, the Owens Illinois Glass Company and Corning Glass forced molten glass through fine orifices and obtained glass filaments which they called "fibre glass". Since then chopped fibre strand has been used for reinforcing mats and continuous glass filaments have been used in the filament winding and pultrusion processes. This technique was used for winding tubes as early as in 1952, while Al Meyer and A. Howell had patented the pultrusion process in 1951 (Seymour, 1987).

There are currently three main methods of producing composite products: lay

up, filament winding, and pultrusion. In this work, composite shapes manufactured by pultrusion are studied. Pultrusion is the process of continually pulling fibres through a resin bath and then a heated die, producing structural shapes of constant cross section including rods, box and I-beams, and channels. The process of pultrusion, illustrated in Fig. 1.1, allows some latitude for varying the orientation of the fibres.

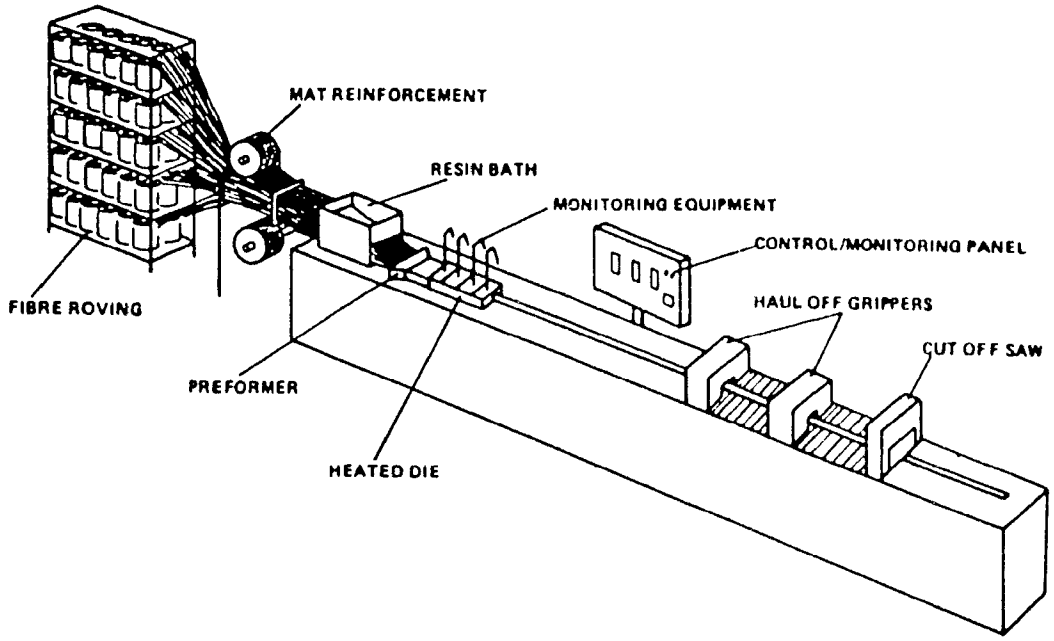

Fig. 1.1. The pultrusion process (From Bishop and Sheard, 1992)

For the last twenty years, fibre-reinforced composite materials have been used successfully in the aerospace industry. The use of this technology began with the development of fibre-reinforced plastic composites in the 1940s, when engineers were looking for alternatives to expensive or scarce steels and alloys. Since then, the

military and aerospace industries have developed a variety of applications for composites: rockets, satellite components, wing skins and small structural beams for aircrafts, main rotor blades on helicopters, booms and bucket trucks.

Today, the term composite refers to fibre-reinforced plastics (FRP) manufactured from fibres and resins. Composites offer many advantages as a construction material. Fibres have a high static and fatigue strength, and composites are up to five times lighter than steel and concrete. Composites are also highly resistant to chemicals and corrosion, and are versatile in the fabrication process. Drawbacks include low modulus of elasticity, susceptibility to deformation under long-term loads, and, at present, high cost (Ballinger, 1990).

More recently, the use of these materials in civil engineering applications has been considered. Electrically non-conductive extension ladders used by utilities are a familiar example. Another one is the Sun Bank high-rise building, in Orlando (Florida, USA), which has four 10.7 m (35 ft) high by 10.7 m (35 ft) square rooftop turrets that house radio antennae. These electro-magnetically transparent enclosures are made with 254 mm (10 in.) by 254 mm (10 in.) by 12.7 mm (1/2 in.) fibre-glass wide flange beams. These turrets were designed to withstand hurricane winds. Glass-reinforced plastics have now been used in the structural engineering field in a variety of applications, in particular in lightly loaded roofs, pipes, chimneys, and in structural strengthening systems for bridges and decking. In Japan, for example, several composites have been used to strengthen tall chimneys by wrapping them with carbon fibre tape materials. Also, in the U.S., the California Highway Department has

recently strengthened several bridge columns in the Los Angeles area by wrapping them with fibre-glass-polyester materials, to provide increased structural strength and safety against earthquake damage. The U.S. Department of Transportation is developing a concept of fully fibre-glass bridge deck.

Antenna-supporting structures are interesting applications for pultruded composite shapes. Electromagnetic transparency is an important advantage in FM and multi-directional antennae, whose radiation pattern is disturbed by the presence of metallic obstacles. Especially in structures operating in cold regions where ice and snow loads amplify wind effects, large loads can prevail for relatively long durations, ranging from a few days to several months, and creep investigations become necessary if pultruded glass fibre-reinforced plastics (FRP) are to be considered as alternatives to traditional structural materials. Furthermore, geometrical integrity of telecommunication structures is crucial for reliable serviceability (McClure and Mohammadi, 1993).

1.2 Research Objectives

Little work has been done in the investigation of the overall behaviour of structures made of commercially produced FRP pultruded sections. The expanding use of composite materials in recent years has resulted in an increase in the number and kinds of characterization tests. Well-defined procedures are used for some of the properties of these materials, such as simple coupon tests in compression and tension or simple beam-type tests in bending. Coupon testing procedures are becoming

available to determine creep characteristics of FRP, but very few investigations have been done on full scale structural elements or complete structures made of commercially produced pultruded shapes. As a result, the question of extrapolation of coupon creep data to large elements remains problematic, especially in view of the variability of the properties measured in low-cost mass-produced pultruded shapes.

Even though creep testing is a primary method of gathering engineering data for any material which demonstrates time-dependent mechanical behaviour, there is no established procedure for compression creep testing of composites. A very limited number of research projects relating to the compression creep behaviour of FRP structural elements have been reported (Irion, 1981).

The two main objectives of this research were to investigate, both experimentally and theoretically, the compression creep behaviour of angle stubs, and to correlate the results with creep measurements on coupons. The time-dependent response characteristics were investigated in order to provide a clear understanding of the behaviour of such structural elements under long-term heavy loads.

1.3 Methodology

In this research, an experimental investigation was conducted to study the creep behaviour of three pultruded angle sections constructed of standard FRP material commercially available. The basic objective of the experimental program was to determine the validity of the existing theoretical creep and creep recovery models for this material, and also to make recommendations for the improvement of the

theoretical model, if needed.

All samples used in the experiment, both stubs and coupons, had the same composition: mat reinforced isophtalic polyester resin, with 35-45% in weight of E-glass fibre. Three identical equal leg angle stubs were tested. The length of each angle stub was of 152.4 mm (6 in.) and their cross-sectional dimensions were of 50.8 mm (2 in.) x 50.8 mm (2 in.) x 6.35 mm (1/2 in.). Three coupons were also tested; a typical flat coupon is of 31.75 mm (1.15 in) x 12.7 mm (1/2 in.) x 6.35 mm (1/4 in.). The loading duration for the long-term creep tests was 2500 hours (103 days), and 250 hours for creep recovery. Before the formal creep and creep recovery tests were carried out, three angle stubs were subjected to a 350-hour preliminary creep test (and 150 hours of creep recovery) in order to validate and finalize the design of the experimental set-ups, the load level to be used, and the optimum strain gauge arrangement on the angle stubs.

The final phase of the research was the analysis of the creep data obtained from both stub and coupon tests. Different creep strain curves were plotted, as well as deflection creep curves. Findley's theory (1960) was employed to model the creep behaviour of both the stubs and coupons, using a linear viscoelasticity assumption with Findley's creep parameters.

1.4 Organization of Thesis

The thesis comprises eight chapters.

Chapter 1 contains a brief history of composite materials and a description of the

pultruded process. The objectives and methodology of the present research are also outlined.

Chapter 2 contains a review of previous work in this area. The basic models of creep and recovery in composites and viscoelastic materials are also reviewed.

Chapter 3 describes the tension and compression tests carried out on stubs and coupons, to characterize the elastic properties of the material.

Chapter 4 contains a description of the experimental set-up of the creep tests for both stub and coupon specimens. Special considerations, such as specimen stability and end effects are also discussed.

Chapter 5 presents the preliminary creep and relaxation investigation (500 hour duration) aimed at validating and refining the methodology and experimental set-up for the long-term creep and creep recovery tests of a total duration of 2750 hours.

Chapter 6 describes the 2500-hour creep test and 250-hour relaxation test for the stub and coupon specimens.

Chapter 7 compares the theoretical response of stubs and coupons with corresponding experimental results. The correlation between the stub and coupon

results is also presented.

Chapter 8, in conclusion, highlights the key results and presents suggestions for future work.

CHAPTER 2

LITERATURE REVIEW

2.1 Introduction

The fundamental theory of mechanics of composite materials and the study of the behaviour of structures composed of composite materials have been the topic of numerous texts and research papers. The mechanical characterization of composite materials has been the subject of much theoretical and experimental work, and is discussed in several texts such as those by Whitney (1982), Tsai and Hahn (1980), and Jones (1975). Johnson and Sims (1983) have presented a simplified procedure for the design and analysis of FRP rectangular plates loaded in flexure, while Vinson and Sierakowski (1987), Vinson and Chou (1975), and Calcote (1969) have discussed the overall behaviour of structures made of composite materials. Most of these communications concentrated on the characterization and the behaviour of laminated plate structures used in aerospace applications. For structural applications, the American Society of Civil Engineers (ASCE) has published its Structural Plastic Design Manual (1984). Books by Holmes and Just (1983), Benjamin (1982), and,

especially, Hollaway (1978), and Skeist (1966), provide useful information.

Holmes and Rahman (1980) have performed an experimental investigation on the time-dependent response of hand-made FRP, rectangular box beams under different loading conditions. Their experimental data has revealed important information concerning the low resistance of the FRP box beams to deflection creep (110% increase of initial elastic deflection after 15000 hours), and even under short term loading (over 80% increase of the initial elastic deflection after only 1000 hours). McCormick (1975, 1990), and Alper et al. (1977), have investigated both the creep and fatigue behaviours of a FRP bridge for highway applications. Optimisation studies were performed on the basis of both theoretical analysis and experimental results. Opliger et al. (1983) have conducted experimental and theoretical studies on the behaviour of tent frameworks constructed with pultruded members. An investigation on both the short and long-term responses of a double layer skeletal structure manufactured from pultruded composites was conducted by Hollaways and Howard (1985). In this work, long-term response of three-dimensional truss systems loaded monotonically to failure were investigated. The long-term results have been related to the short-term loading characteristics of the structure derived from experimental and both linear and nonlinear analytical techniques Johansen and Roll (1990) have conducted experimental and theoretical studies on the strength/stiffness characteristics of a lightweight composite structural system made of FRP tubes and Kevlar 49 cables. Bank and Mosallam (1990) have presented results of a theoretical and experimental study of the long and short-term behaviour of a full-sized portal

frame made of wide flange pultruded glass/vinylester sections. Their work dealt with tensile and shearing creep strain measurements, and they have concluded that creep parameters obtained from coupon tests can be used to describe the creep behaviour of FRP structures. The small number of points of strain measurements considered on the structure (a total of 20 for the entire structure), however, makes it difficult to assess the variability of the results in relation to acceptable levels of variability for design purposes.

2.2 Creep Mechanisms in Composite Materials

The creep behaviour of composite materials has received considerable attention in recent years. Because fibres are not only stronger but also stiffer than resin materials, they carry almost all the load in unidirectional composites which are stressed along the fibre axis. Consequently, if the fibres are elastic, no significant creep of the composite is expected but small amounts may be detected. This occurs in the following way. The fibres and matrix of any composite experience almost identical strains. When the load is applied, the matrix responds by imposing a stress in both fibre and resin. If the fibres do not creep, the matrix is also restrained from creeping but being viscoelastic, it undergoes stress relaxation, transferring part of its loading onto the adjacent fibres, and hence, straining them by a further small increment. This, to all outward appearances, is creep. It is not caused by creep of either component but rather by stress relaxation of one of them and may be called "relaxation creep". The maximum strain which can be developed by this process is

easily estimated.

A typical total creep curve for such composite materials under uniaxial stress, σ, and constant temperature, T, can be described with five components (Fig. 2.1):

-Initial strain, which is the sum of the elastic and plastic components, also referred to as intercept strain.

-Primary creep, which is the strain that occurs rapidly at a decreasing rate.

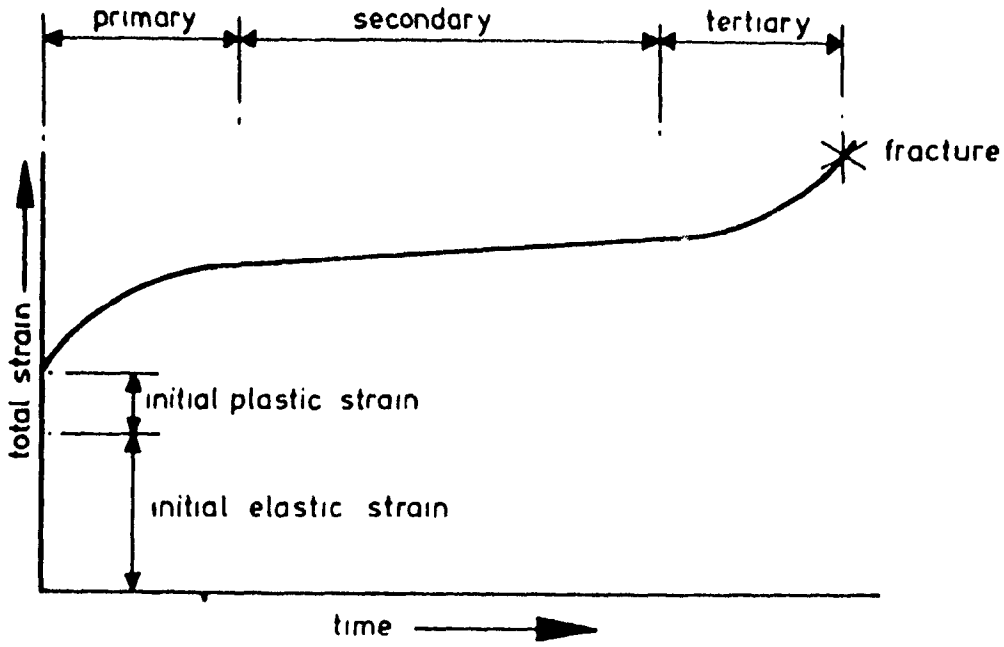

Fig. 2.1. Total creep for a highly idealized viscoelastic material (uniaxial stress and constant temperature)

-Secondary creep, which is the strain that occurs at a steady-state or

minimum rate (i.e. straight portion of the curve). At this stage the material behaves as a linear viscous material.

-Tertiary or terminal creep, which results in fracture.

It will be understood that some materials do not exhibit a secondary type creep while others do not have a tertiary region; also it is common to find that in some materials the tertiary creep is evident only at high stresses. A typical family of creep curves (total strain-vs-time) is given in Fig. 2.2 (Hollaway, 1978).

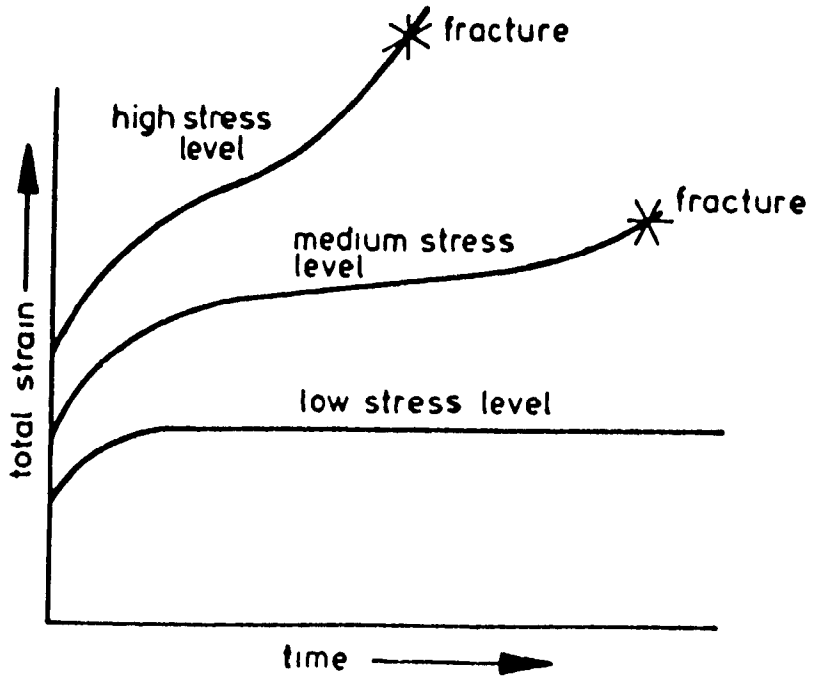

Fig. 2.2. Typical family of creep curves in viscoelastic materials (uniaxial stress and constant temperature)

2.3 Viscoelastic Behaviour of FRP Pultruded Materials

Viscoelasticity is a property that describes the behaviour of materials exhibiting strain rate effects under applied stresses. These effects are demonstrated by creep phenomena under constant stress and by stress relaxation under constant strain. The viscoelastic behaviour of FRP materials is illustrated by the curve in Fig. 2.3. Upon loading, an initial elastic strain is obtained instantaneously (1-2). This initial strain is followed by a slow but sustained increase in strain for which the rate of creep decreases with time (2-3). Immediately after load removal, an instantaneous strain

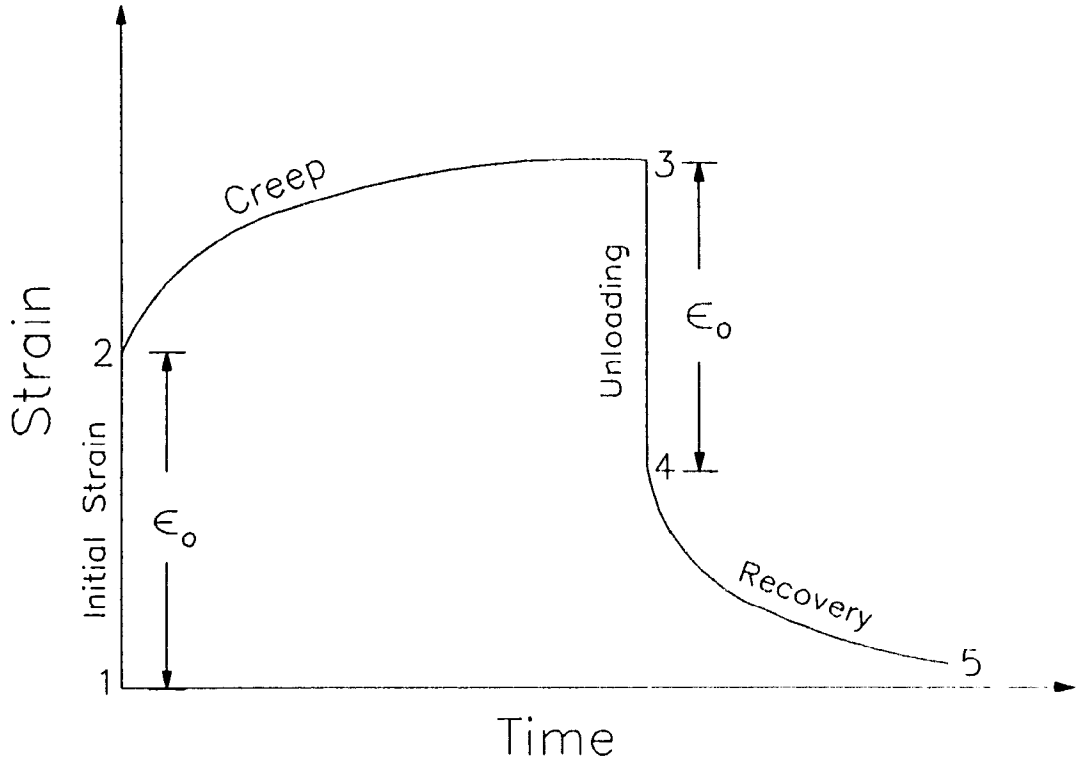

Fig. 2.3. Viscoelastic behaviour of FRP materials under constant load

recovery (3-4) occurs that is theoretically equal to the initial instantaneous strain (1-2) developed. This instantaneous strain recovery is followed by a continuous, slow strain recovery process.

Some materials exhibit linear or nearly linear viscoelastic response while others exhibit non-linear viscoelastic behaviour. For linear viscoelasticity, a viscoelastic modulus expresses the relationship between the stresses and strains. This modulus depends only on the duration of the applied loading for a given temperature. On the other hand, the nonlinear viscoelastic modulus depends on both the magnitude and duration of the applied loading.

The viscoelastic theory usually considers the combination of two basic types of behaviours; these are Hookean elasticity and Newtonian viscosity. The Hookean elasticity can be represented by a linear algebraic equation describing the response of a linear elastic spring, and the Newtonian viscosity can be represented by a linear differential equation describing the response of a linear dashpot.

A combination of the Voigt and Maxwell models in series (Baer, 1968), shown in Fig. 2.4, reproduces the initial elastic strain, creep and instantaneous elastic recovery, but can only represent a linear relationship between stress and strain and between stress and rate of strain. Although these models have been used to describe creep and relaxation in several materials, they are not applicable to a wide variety of either materials or temperatures, and they describe the properties of plastics only very approximately. However, by refining this combined model, a more accurate representation may be obtained for FRP composites. Note that the terms appearing

in the Voigt and Maxwell models of Fig. 2.4 are defined as follows:

E_m and E_v = Maxwell and Voigt proportionality constants in Hookean elasticity behaviour respectively

η_m and η_v = Maxwell and Voigt proportionality constants in Newtonian viscosity behaviour respectively.

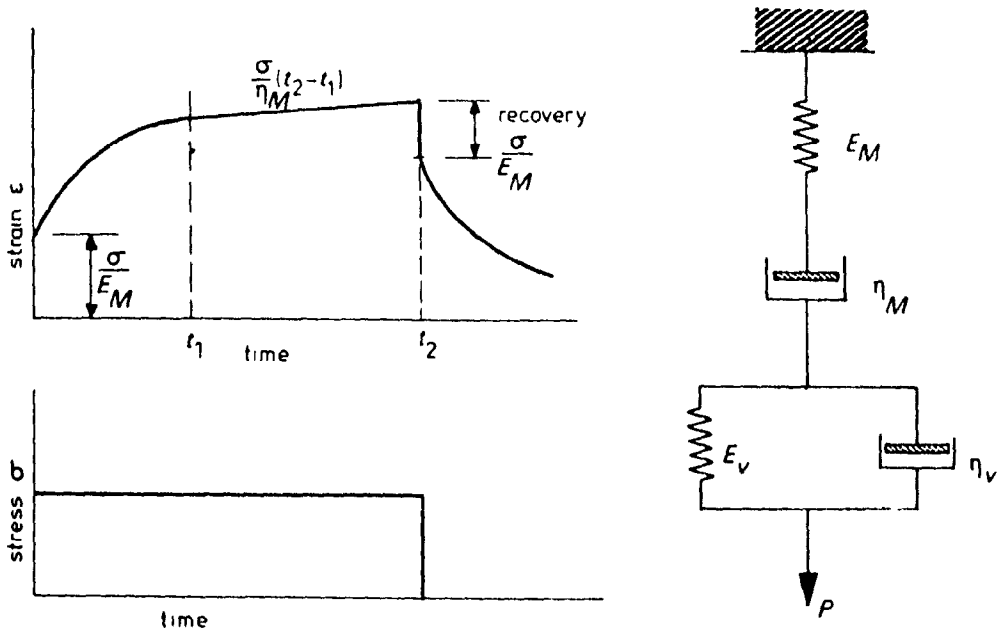

Fig. 2.4. Combination of Voigt and Maxwell models in series

2.4 Findley's Theory

Many mathematical methods have been proposed to describe the creep behaviour of plastics in terms of stress, strain, and time. The creep model used here is the power law due to Findley (1960); it is recommended by the ASCE in its Structural Plastics Design Manual (1984) because of its simplicity and its capability

of successfully describing the creep response of different types of plastics, namely reinforced plastics and laminated plastics. In addition, the validity of this model has been proven from creep tests with a total duration of up to 26 years (Findley, 1987) for tension, compression and combined tension and torsion. In this model, the creep response is described by separable time-independent and time-dependent strains. Under constant stress, these two strain components follow a simple power function of the following form:

$$\epsilon = \epsilon_0 + m \left(\frac{t}{t_0}\right)^n \qquad (2.1)$$

where

ϵ : time-dependent creep strain (total strain),

ϵ_0 : time-independent strain (initial strain),

m : coefficient of time-dependent term, which is a function of the stress level,

t : time after loading (in hours),

t_0 : a constant taken as unity (hours),

n : a material constant, which is independent of stress.

Eq. 2.1 describes the creep behaviour of a particular material at a particular stress level and temperature, and the only unknown parameters in this equation are m and n.

To describe the creep behaviour of a material at any stress level, the general form of Findley's equation can be used. For moderate values of stress σ, Findley has shown that a hyperbolic sine function can be used to satisfactorily describe the stress

dependence of both the time-independent strain, ε_0, and the time-dependent coefficient m, as follows:

$$\epsilon_0 = \epsilon_0' \sinh \frac{\sigma}{\sigma_\epsilon}$$

$$m = m' \sinh \frac{\sigma}{\sigma_m} \qquad (2.2)$$

Replacing in Eq. 2.1:

$$\epsilon = \epsilon_0' \sinh \frac{\sigma}{\sigma_\epsilon} + m' \left(\frac{t}{t_0}\right)^n \sinh \frac{\sigma}{\sigma_m} \qquad (2.3)$$

where,

σ = constant applied stress

σ_ε = stress at time t_0

σ_m = stress at time t, and

ε'_o, σ_ε, m', n, σ_m are constants which are independent of stress, strain and time but dependent on the material, temperature, humidity and other environmental factors. Values of these creep constants can be obtained from experiments, by curve-fitting techniques. Note that Eq. 2.3 describes both the linear and nonlinear creep responses.

2.5 Viscoelastic Modulus (E_v)

A viscoelastic modulus is an expression that describes the stress-strain relationship of viscoelastic materials with time. It is the initial slope of the

isochronous stress-strain curve, as obtained under constant stress or strain (ASCE, 1984). When a linear viscoelastic behaviour is assumed, the stress is directly proportional to strain at any given time. The assumption of linear viscoelastic behaviour for plastics is usually valid under service loading where the stresses are relatively low. On the other hand, high stress levels, elevated temperatures and severe environmental conditions increase the nonlinear behaviour of plastics, and in these situations, a nonlinear viscoelastic modulus on both time and stress level is necessary.

In this case, the analysis of a simple structure will theoretically require an infinite number of viscoelastic moduli since the stresses will vary over the cross section, as well as along the length of the structure. In practice, however, a linearized modulus approach is more useful.

In order to linearize the expression of the viscoelastic modulus, some simplifications to Eq. 2.3 are introduced. For small values of σ/σ_ϵ and σ/σ_m up to 40%, the following approximations are made:

$$\sinh \frac{\sigma}{\sigma_\epsilon} \simeq \frac{\sigma}{\sigma_\epsilon} \qquad (2.4)$$

$$\sinh \frac{\sigma}{\sigma_m} \simeq \frac{\sigma}{\sigma_m} \qquad (2.5)$$

which imply a linear relationship between the stress, σ, and both ϵ_0 and m. Replacing the above expressions in Eq. 2.3 gives

$$\epsilon = \epsilon'_o \frac{\sigma}{\sigma_\epsilon} + m' \left(\frac{t}{t_o} \right)^n \frac{\sigma}{\sigma_m} \qquad (2.6)$$

Dividing both sides of Eq. 2.6 by σ, gives

$$\frac{\epsilon}{\sigma} = \frac{\epsilon'_0}{\sigma_\epsilon} + \left(\frac{m'}{\sigma_m} \right) \left(\frac{t}{t_0} \right)^n \qquad (2.7)$$

or

$$\frac{1}{\mathbf{E}_v} = \frac{1}{\mathbf{E}_0} + \left(\frac{1}{\mathbf{E}_t} \right) \left(\frac{t}{t_0} \right)^n \qquad (2.8)$$

where

E_0 is the elastic, time-independent component of the viscoelastic modulus which is also independent of the strain rate and is defined by $\sigma_\epsilon/\epsilon'_0$,

E_t is the time-dependent component of the viscoelastic modulus and is defined by σ_m/m',

E_v is the viscoelastic modulus which describes both the instantaneous elastic and time-dependent responses of the material, and is defined by $\sigma(t)/\epsilon(t)$

By rearranging Eq. 2.8, the following expression for E_v is obtained:

$$\mathbf{E}_v = \frac{E_0 \, E_t}{E_t + E_0 \left(\frac{t}{t_0} \right)^n} \qquad (2.9)$$

2.6 Rate of Creep and Creepocity

It is often convenient in practice to evaluate the percentage increase in strain

for a given time interval:

$$\epsilon\,(\%) = \frac{\epsilon(t) - \epsilon(t_0)}{\epsilon(t_0)} \times 100 \qquad (2.10)$$

This percentage increase in strain is called "creepocity", ϕ_c (Findley and Khosla, 1956). It has been used in the Structral Plastic Design Manual (1984) for comparing of the creep behaviour of various plastics and composites.

An expression for creepocity from t_0 to any time t can be obtained by replacing the expression of $\varepsilon(t)$ from Eq.2.1 in Eq 2.10:

$$\phi_c = \frac{(\epsilon_0 + m t^n - \epsilon_0)}{\epsilon_0} \times 100 = \frac{100\, m\, t^n}{\epsilon_0} \qquad (2.11)$$

or,

$$\phi_c = \frac{m\,\psi}{\epsilon_0} \qquad (2.12)$$

where ψ is a constant independent of stress level and equal to 100 t^n. The general expression for creepocity from $t=t_i$ to $t=t_{i+1}$ can be written as:

$$\phi_c = \frac{100\, m}{\epsilon_i} \left[t_{i+1}^n - t_i^n \right] \qquad (2.13)$$

where ε_i is the total strain at time $t=t_i$.

2.7 Boltzman Superposition Principle

was later successfully applied to plastics by Findley and Khosla (1955). The superposition principle states that if a stress σ_1 is applied at time $t=t_1$ to a linear viscoelastic material, and if at time $t=t_f>t_1$ another stress σ_f is applied, then the total strain at any time $t \geq t_f$ is assumed to be equal to the summation of the two strains which would have been produced independently by the two stresses σ_1 and σ_f (See Fig. 2.5). In the application of this principle, materials are assumed to behave linearly and the change in deformation is independent of the initial stress level σ_1. This assumption is valid in this work since the specimens are loaded in their linear viscoelastic range.

To apply this principle in a general case, a modified superposition principle was suggested by Findley and Khosla (1955) to account for the general nonlinear behaviour of plastics. This modified principle when specialized to the problem of creep is stated as follows: When a material is subjected to a constant load P_1 from time t_0 to time t_1 and subsequently subjected to a load P_2 from time t_1 to t_2, the total creep strain is given by the sum of the creep strain that would occur under a constant load P_1 applied from $t=t_0$ to $t=t_2$ and the creep which would occur under a constant load (P_2-P_1) applied from $t=t_1$ to $t=t_2$.

Let σ_1 the stress produced by the initial load P_1, and σ_f the stress produced by the final load P_2. Using Eq. 2.3, the superposition rule can be expressed as:

$$\epsilon = \epsilon_0' \sinh \frac{\sigma_i}{\sigma_\epsilon} + m' \, t_2^n \sinh \frac{\sigma_i}{\sigma_m} + [\, \epsilon_0' \sinh \frac{\sigma_f - \sigma_i}{\sigma_\epsilon} +$$

$$m' \, (\, t_2 - t_1 \,)^n \sinh \frac{\sigma_f - \sigma_i}{\sigma_m} \,] \qquad (2.14)$$

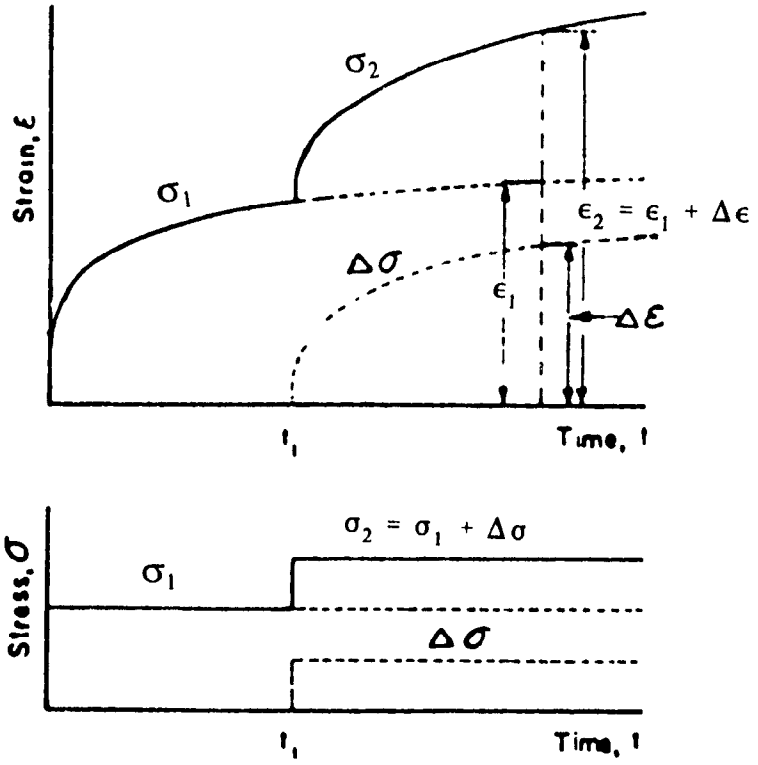

Fig. 2.5. The Superposition Principle as applied to creep when the stress is incremented by $\Delta\sigma$ at time t_1

The linearized form of the superposition principle is used in this work to predict the creep recovery of FRP materials. The creep recovery, according to this theory, is equal to the algebraic sum of the strain at the end of the loading period of the test,

and the strain that would result at a given time from a stress equal in magnitude but with opposite sense to the original stress, applied to a non-loaded specimen at the time of unloading. This can be expressed using Eq. 2.1. as,

$$\epsilon = \{ \epsilon_0 + m\, t^n \} - \{ \epsilon_0 + m\, (t - t_u)^n \} \qquad (2.15)$$

or

$$\epsilon = m \{ t^n - (t - t_u)^n \} \qquad (2.16)$$

2.8 Evaluation of creep parameters

In Eq. 2.1 the variation of the creep strain with time is usually nonlinear. Using a log-log scale, however, the nonlinear portion plots as a straight line. In order to determine the values of creep parameters m and n for a particular stress level, Eq. 2.1 is rearranged in the form:

$$\log (\epsilon - \epsilon_0) = \log m + n \log \left(\frac{t}{t_0} \right) \qquad (2.17)$$

This is the equation of a straight line of slope n and intercept m (at unit time) when $\log(\varepsilon-\varepsilon_0)$ is plotted against $\log(t/t_0)$. Such a graphical representation is used for all creep data obtained in this research.

2.9 Summary

This chapter has presented an overview of the literature published in the field

of composite materials with reference to the creep properties. The papers reviewed cover the works done since the early 1960's to date. Simple creep mechanisms are discussed and Findley's theory is presented in detail since it can predict very well the viscoelastic behaviour of composites.

The Boltzman principle of superposition, which was modified by Findley's and Khosla (1955) to account for the general inelastic behaviour of plastics, was also reviewed and presented in detail. The principle best predicts the creep recovery of FRP materials.

CHAPTER 3

EXPERIMENTAL CHARACTERIZATION OF MATERIAL PROPERTIES

3.1 Introduction

The mechanical properties of materials are usually determined from specimens tested under simple loading states from which the elastic constants, the onset of damage, and the ultimate strength can be determined. If enough tests are conducted, the variability of these parameters can be established. All material properties are normally confirmed by an appropriate test, as data given in the various handbooks and manufacturer's catalogues represent average or "obtainable" values and are often not truly representative.

The properties of materials such as composites show large variability from one sample to another. Such variability is a consequence of the anisotropic and non-homogeneous nature of these materials, the mechanical incompatibility of the constituent phases, the effect of interfacial bonding, and particular nonlinear stress-

strain behaviour of the constituents. These factors and properties are also significantly dependent on the type, shape, and size of the specimen and the rate of loading.

3.2 Destructive Tests

All the destructive tests performed for this research were carried out in the Jamieson Structural Laboratory of McGill University, Canada. The temperature and humidity have remained relatively constant for all tests. These characterization tests were conducted in May and June 1992. An Instron machine, model No. KRD-212-260, with a loading range of 0 to 223 kN (50 kips) was used for crushing compression and tension tests.

All coupons were tested in both tension and compression, while the angle stubs were tested in compression only. These tests enabled comparison of the material properties of the composite with the values given by the manufacturer (Technical Pultrusion, Inc. of St. Bruno, Quebec). For creep testing, a loading apparatus was specifically designed and constructed to meet the requirements of the test. The results obtained from both the compression and tension tests for all coupons and stubs confirmed that in the angle stub, one leg was stronger and stiffer than the other. After discussion with the manufacturer, it was concluded that this asymmetric behaviour was due to positioning of the mold during the pultrusion process itself.

3.2.1 Tension Test

Eight coupons were tested for mechanical properties on the Instron testing

machine at a 1.27 mm (0.05") per minute jaw speed using a loading scale of 0 to 44.8 kN (10000 lb). All coupons were cut from the middle of the pultruded angle section legs. All of them had a dumb-bell shape in accordance with ASTM standard D638-89 Type 1 as shown in Fig. 3.1. Dimensions of the tensile coupon were 12.7 mm (1/2") x 6.35 mm (1/4") with 50.8 mm (2") gauge length, measured at three points on the narrow section of the coupon using a vernier calliper.

The dial gauges used to measure the specimen's elongations had a sensitivity of 0.025 mm (0.001"). Stress-strain curves for the eight coupons are plotted in Fig. 3.2 and results are summarized in Table 3.1.

T = 6.35 mm (0.25")

W = 13 mm (0.5")

L = 57 mm (2.25")

W_0 = 19 mm (0.75")

L_0 = 165 mm (6.5")^{min}

G = 50 mm (2.00")

D = 115 mm (4.5")

R = 79 mm (3.00")

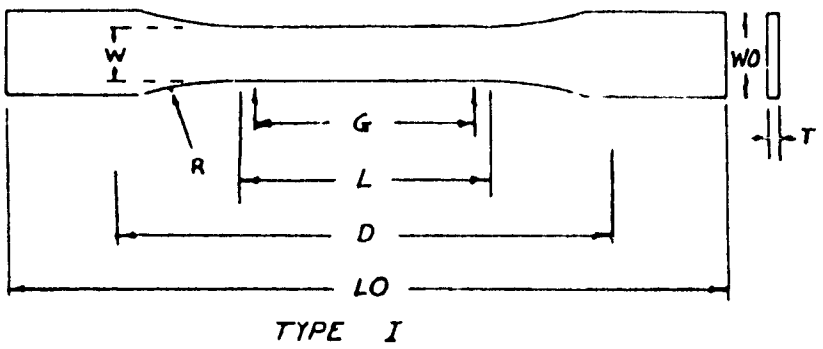

Fig. 3.1. Tension coupon geometry

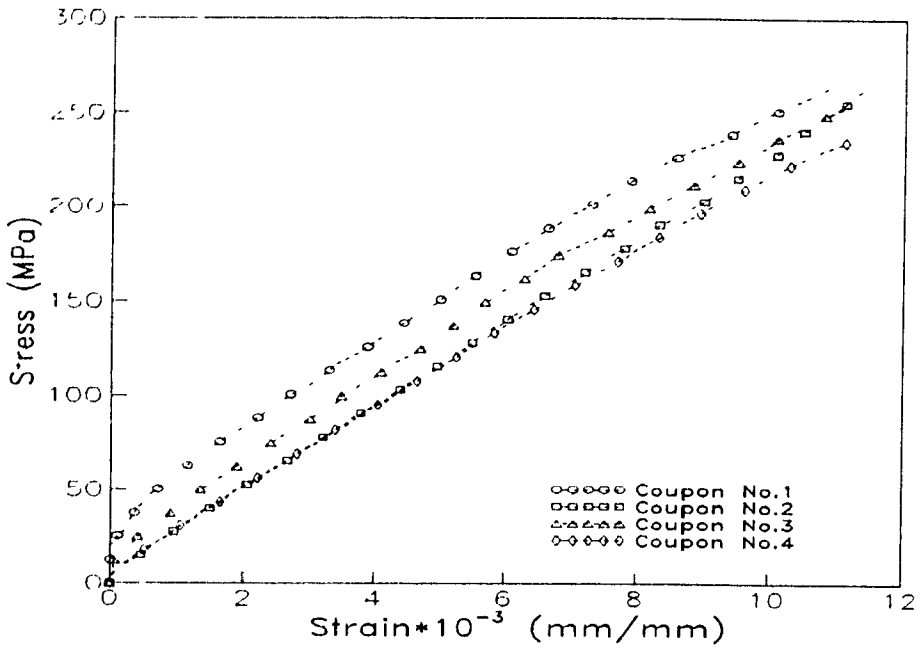

(a) Tension Coupon Test (Coupon cut from strong Leg)

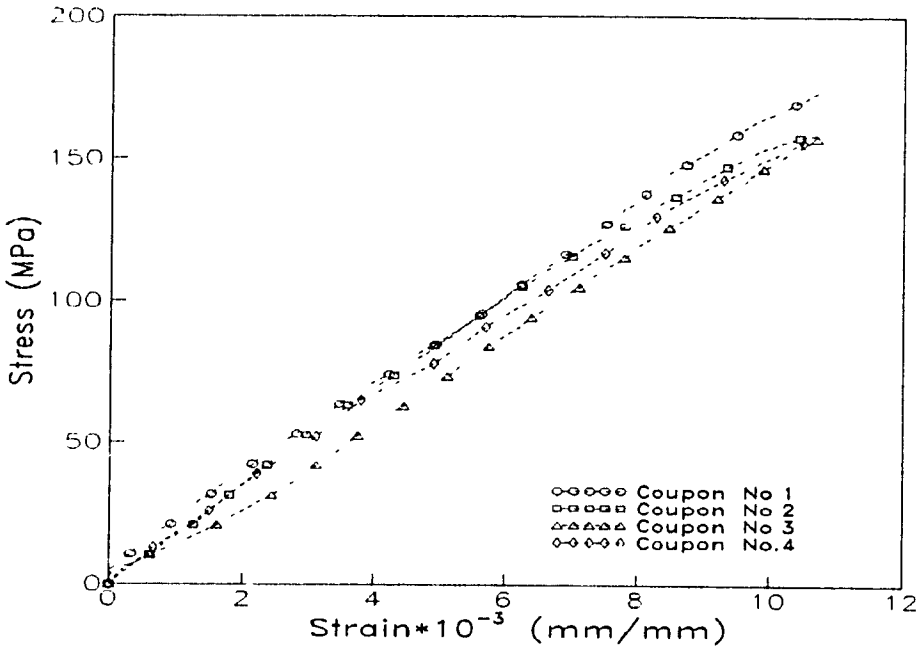

(b) Tension Coupon Test (Coupon cut from weak Leg)

Fig. 3.2. Stress-strain curves for coupons in tension

Table 3.1 Summary of uniaxial tension material properties (Coupons cut from strong and weak legs)

Property	Leg No	Coupon No				Average	Total Average
		1	2	3	4		
Modulus of Elasticity (GPa)	1	22 9	22 2	22 1	21 8	22 3 ±0 4	19 ±3
	2	16 0	15 5	15 9	15 4	15 7 ±0 3	
Ultimate Stress (MPa)	1	271	262	253	234	255 ± 14	209 ±44
	2	174	159	157	156	162 ±7	
Ultimate Strain ($X10^{3}$)	1	11 2	11.4	11 1	11 1	11 2 ±0 1	11 0 ±0 3
	2	10.8	10 8	10 7	10 5	10 7 ±0 1	

It was observed that the stress-strain relationship of the tested specimens was approximately linear. The average modulus of elasticity was 20% larger than the manufacturer's value of 15.8 GPa. Generally, the ultimate stress and strain values of Leg 1 were higher than those of Leg 2: the stress was 60% higher and the strain 10% higher, which clearly indicates that Leg 1 was stronger than Leg 2. Due to the important differences between the two legs, results will be presented separately for each of them throughout this thesis.

3.2.2 Compression Test

The provision for pure centric compression is a major consideration in buckling experiments. Care must be taken to minimize eccentricity of the loading and non-uniformity of its distribution over the cross-section of the specimen. The use of

a ball joint between the machine loading head and the specimen eliminates any eccentricity of the loading which might be caused by imperfect contact between the machine loading head and the loading plates. Stress-strain curves obtained from this series of tests were almost the same as those at the initial reading of long-term tests, as will be discussed in Chapters 5 and 6

3.2.2.1 Compression Stub Test

End plates were used to ensure uniform load transfer to the stub cross section. Also in order to minimize localized stress concentration during testing, both ends of the angle stubs were cut parallel, milled smooth, and braced. A wood end plate was used for bracing; due to its workability, the angle could be fitted snugly without damaging the composite material. Since the angle legs were not perfectly perpendicular and the thicknesses of the two legs were not exactly identical, the wood section was easy to adjust to the proper shape. A 17.46 mm (11/16") thick plywood plate was cut to 152.4 mm (6") x 152.4 mm (6") dimensions and the contour of an angle section was cut into the wood with its centroid coinciding with the centre of the plate. The wood plate was then fixed to a 25.4 mm (1") thick steel plate with high-strength epoxy glue. Care was taken not to glue the portion of steel that was to be in contact with the angle section. Fig. 3.3 illustrates an angle stub with its wood end plates.

Angle stubs of 152.4 mm (6") length and cross-sectional dimensions of 50.8 mm (2") x 50.8 mm (2") x 6.35 mm (1/4") with two different testing configurations were

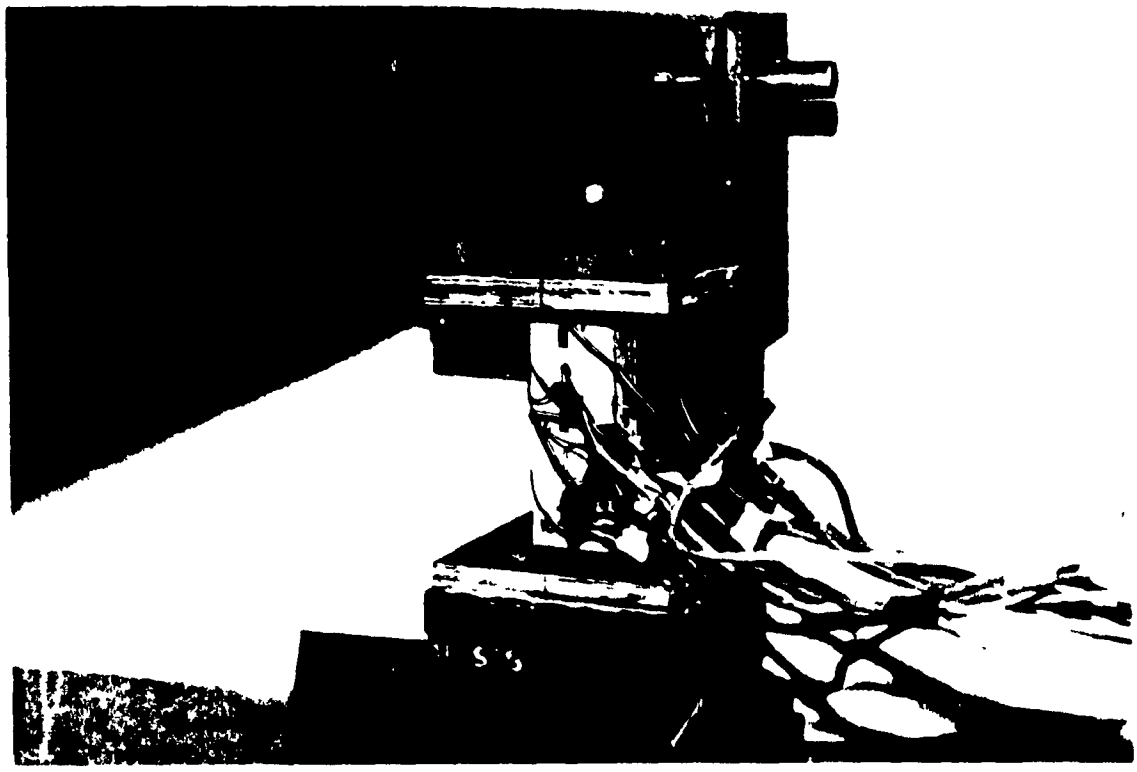

Fig. 3.3. Angle stub with steel and wood end plates

initially considered, in order to determine the practicality of the loading arrangement. The first set-up consisted of a single angle stub restrained at the top and bottom ends by wood and steel plates as described above The second set-up had two angles placed back-to-back with a small spacing, also constrained at the top and bottom ends by wood and steel plates.

Each angle stub was instrumented with six strain gauges located at mid-height as shown schematically in Fig. 3.4(a). Two gauges were placed on the outside of one leg with one gauge on the inside, while the other leg had two gauges placed on the

inside with one gauge on the outside. After testing both angle stub configurations, it was decided that the configuration consisting of a single angle would be more appropriate for the compression and creep tests. Stress-strain curves and results from this series of tests are presented in Figs. 3.5(a,b) and Tables 3.2(a,b). The "Final Stress" tabulated is the maximum applied load divided by the .verage cross sectional area of the specimen.

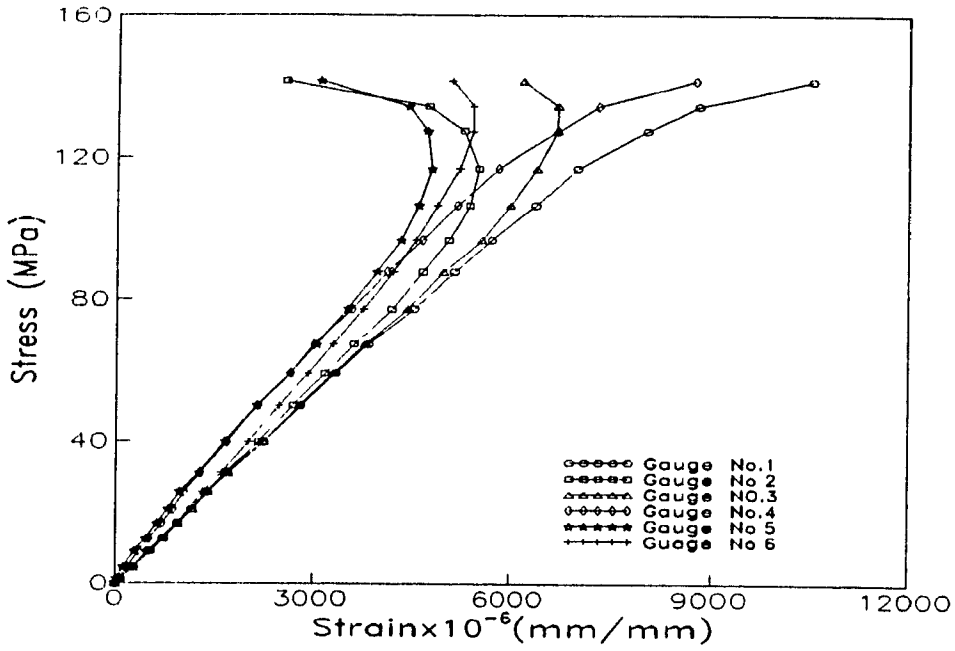

Fig. 3.5(a). Stress-strain curves for angle stubs in compression (Single angle)

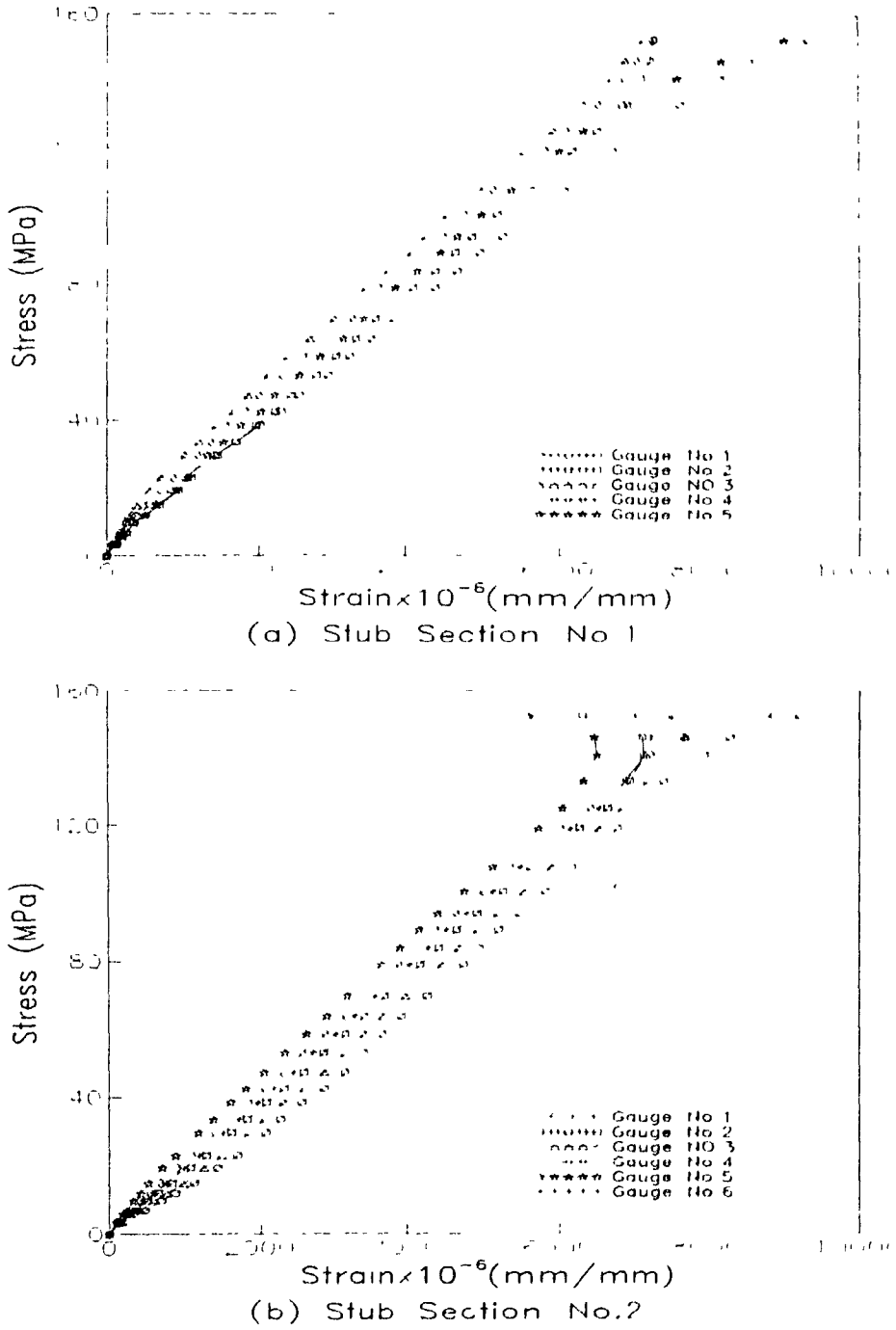

Fig. 3.5(b). Stress-strain curves for angle stubs in compression (Two angles back-to-back)

Table 3.2(a) Summary of mechanical properties of angle stubs with six strain gauges at mid-height (Two angles back-to-back)

Property	Angle Section No	Gauge No						
		1	2	3	4	5	6	Average
Modulus of Elasticity up to σ=100 MPa (GPa)	1	17.2	18.9	----	21.5	20.5	20 0	19 6 ±1 5
	2	17 3	18.9	18.1	20.1	20.9	19.8	19 2 ±1 2
Strain @ σ=100 MPa ($X10^{-6}$)	1	5574	5205	----	4537	4767	4986	4180 ±360
	2	5821	5280	5551	5010	4761	5145	5260 ±350
Final Strain ($X10^{-6}$)	1	9350	7280	7139	7300	9042	1888	7000 ±2450
	2	9240	6308	7500	8875	562+	7022	7430 ±1300
Final Stress	-------	153						

Table 3.2(b) Summary of mechanical properties of angle stub with six strain gauges at mid-height (Single angle)

Leg No.	Gauge No.	Modulus of Elasticity up to σ=100 MPa (GPa)	Strain @ σ=100 MPa ($X10^{-6}$)	Final Strain ($X10^{-6}$)	Final Stress (MPa)
1	1	17.1	6042	10558	142
	2	19.0	5172	2565	
	3	17.6	5766	6193	
Average		17.9±0.8	5660±360	6440±3270	
2	4	21.1	4881	8744	
	5	21.7	4428	3096	
	6	21.3	4678	5049	
Average		21.4±0 3	4660±190	5630±2300	
Total Average		20.3±1.8	4960±580	5910±2900	

It was observed that the stress-strain curves of the two tests were almost linear up to a stress of about 100 MPa. This corresponds to the limit of proportionality of the angle stubs. On increasing the load further, the stress distribution changed pattern. An increase and decrease in strain from the external gauge and internal gauges were respectively recorded. This indicates a buckling phenomenon.

Three single angle stub specimens were used for compression testing, and twelve electrical strain foil gauges were used for each angle stub. These gauges were located on the middle longitudinal line of each angle leg and on each face, as shown schematically in Fig. 3.4(b). The length of the strain gauges was 5 mm, and the distance between two consecutive gauges was 53.66 mm (2.11 in.). In all tests, the

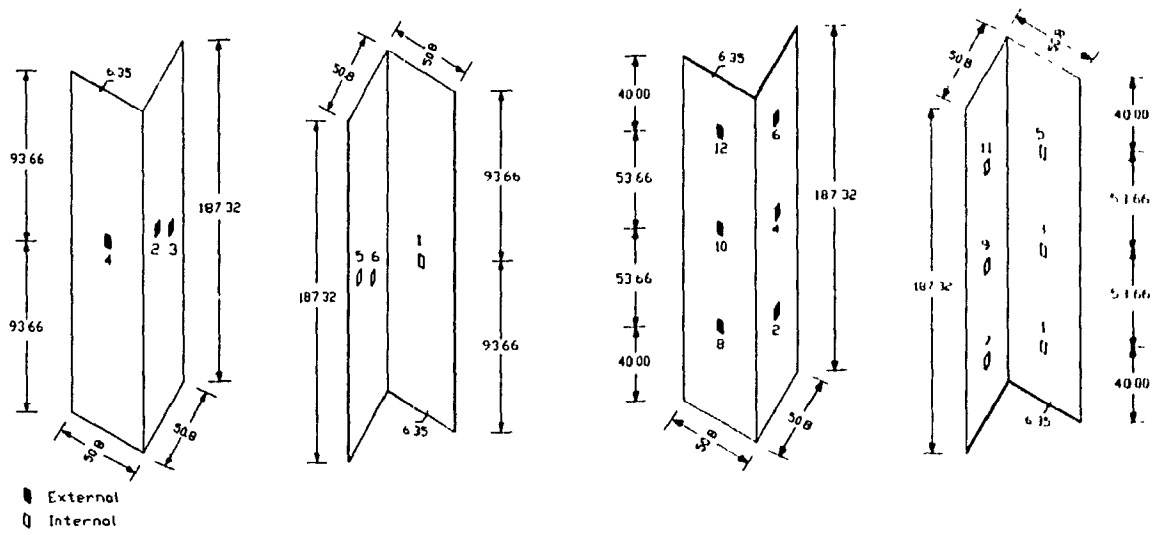

Fig. 3.4. Position of the short strain gauges on the angle section

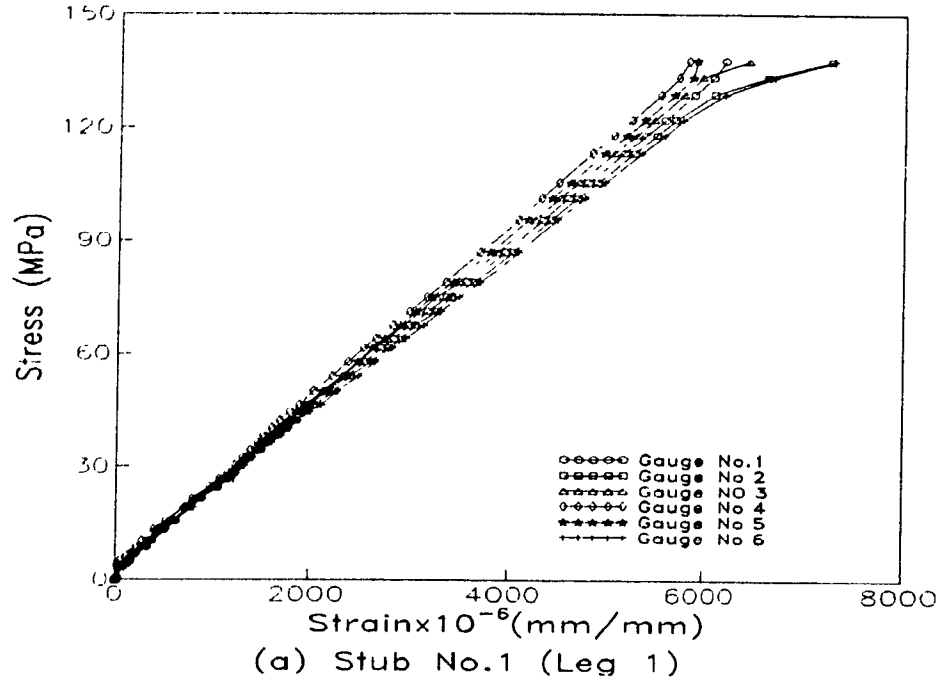

(a) Stub No.1 (Leg 1)

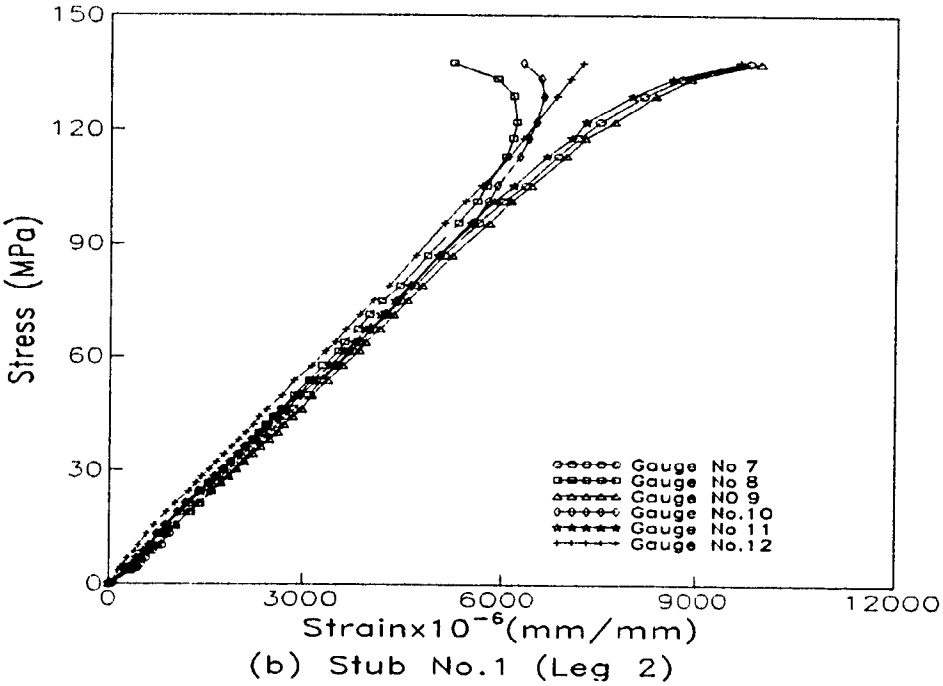

(b) Stub No.1 (Leg 2)

Fig. 3.6. Stress-strain curves for single angle stub No.1 in compression

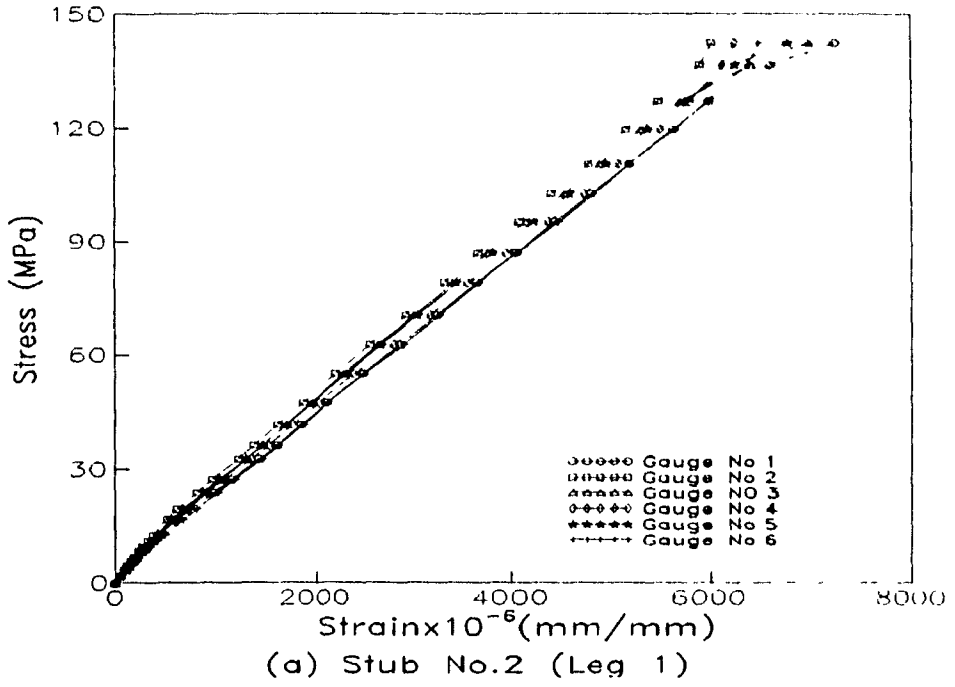

(a) Stub No.2 (Leg 1)

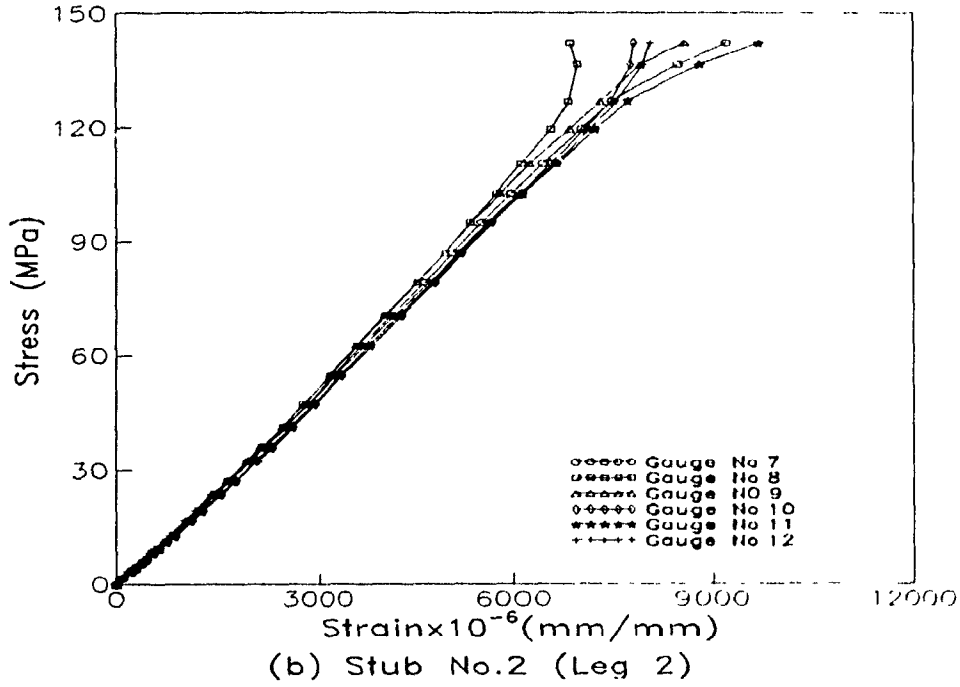

(b) Stub No.2 (Leg 2)

Fig. 3.7. Stress-strain curves for single angle stub No.2 in compression

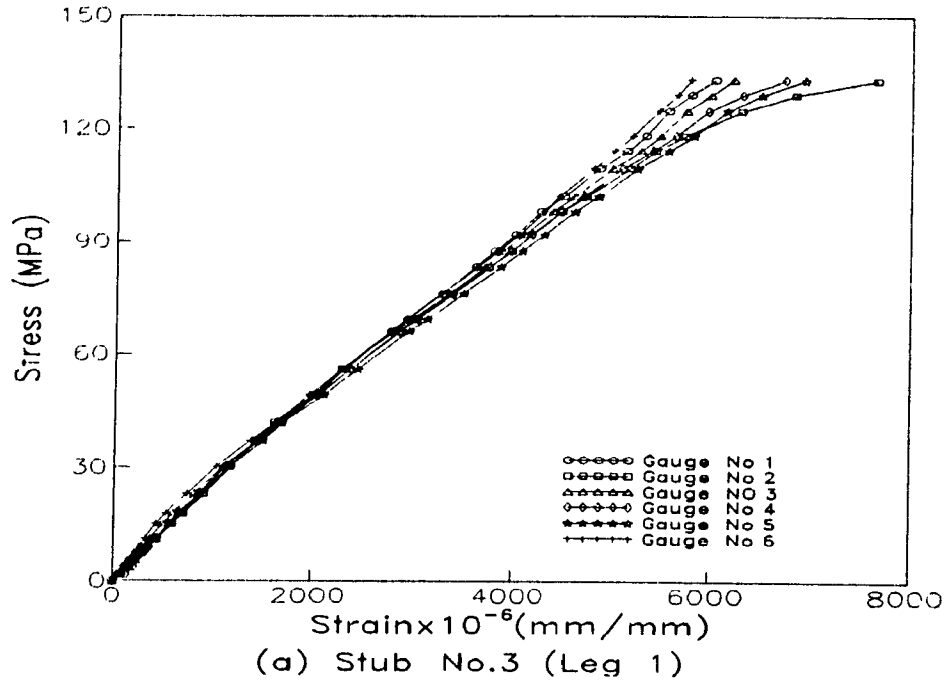

(a) Stub No.3 (Leg 1)

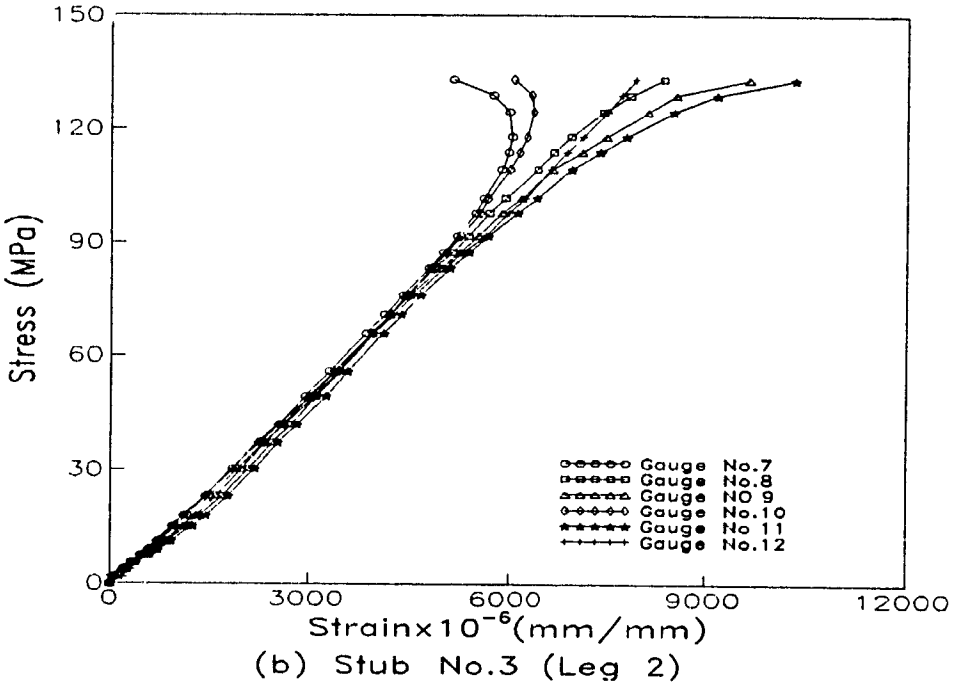

(b) Stub No.3 (Leg 2)

Fig. 3.8. Stress-strain curves for single angle stub No.3 in compression

Table 3.3 Summary of the mechanical properties of angle stubs in compression with twelve strain gauges

Property	Angle Stub No	Leg No 1						
		Gauge No						
		1	2	3	4	5	6	Average
Modulus of Elasticity up to σ=100 MPa (GPa)	1	21 8	21 6	22 0	22 7	22 5	21 4	22 0 ±0 5
	2	21 0	22 7	22 6	22 4	21 2	21 1	21 8 ±0 7
	3	22 5	21 4	21 5	21 7	20 8	21 9	21 6 ±0 5
Strain @ σ=100 MPa ($X10^{-6}$)	1	4615	4705	4526	4337	4447	4773	4570 ±150
	2	4795	4385	4517	4721	4570	4829	4640 ±160
	3	4530	4745	4633	4722	4864	4481	4660 ±130
Final Strain ($X10^{-6}$)	1	62'2	7280	6456	5812	5896	7310	6490 ±600
	2	7198	6002	6952	6240	6761	6491	6610 ±410
	3	6024	7660	6202	6727	6931	5786	6560 ±630
Final Stress (MPa)	1	138						
	2	142						
	3	133						

Property	Angle Stub No	Leg No 2						
		Gauge No						
		7	8	9	10	11	12	Average
Modulus of Elasticity up to σ=100 MPa (GPa)	1	17 4	18 2	16 8	17 2	17 3	18 2	17 5 ±0 5
	2	17 3	17 8	17 7	16 8	16 9	16 7	17 2 ±0 4
	3	17 7	17 4	16 8	17 5	16 4	16 5	17 1 ±0 5
Strain @ σ=100 MPa ($X10^{-6}$)	1	6006	5642	6131	5801	5873	5482	5820 ±220
	2	5969	5756	5815	6117	6129	6088	5980 ±150
	3	5603	5934	6176	5674	6425	6233	6010 ±300
Final Strain ($X10^{-6}$)	1	9847	5295	10000	6334	9695	7247	8070 ±1870
	2	9211	6831	8594	7848	9708	8100	8380 ±940
	3	5142	8354	9624	6061	10320	7905	7900 ±1830
Final Stress (MPa)	1	138						
	2	142						
	3	133						

strain gauges were connected to the Doric 245 data acquisition system. The stress- strain curves are shown in Figs 3.6 to 3.8 and results also are summarized in Table 3.3.

Again, the stress-strain curves for the three angle stub tests with 12 strain gauges were similar to those obtained for the two previous tests, they were linear up to about 100 MPa, and their pattern changed after further increasing the load.

An important observation from the compression tests on angle stubs is the large difference in longitudinal elastic moduli obtained for the two legs. This causes eccentricities between the centroid of the section and its centre of rigidity. A detailed calculation of the effect of these eccentricities on the normal stresses developed on the cross section when loaded at the centroid was done, using average values of the moduli obtained for the two legs Results have indicated differences in the order of $\pm$ 4-14% with the pure compression case. No attempt was made to compensate for these eccentricities in the experimental set-up. It is recognized that these eccentricities do occur in reality when such a section is used in a truss structure.

3.2.2.3 Compression Coupon Test

The compression coupons were cut in a prismatic shape, according to the ASTM standard D695-89, with a cross-section of 12.7 mm (1/2 in) x 6.35 mm (1/4 in.) and a length such that the slenderness ratio lies between 11 and 16. A length of approximately 31.75 mm (1.15 in.) was chosen, corresponding to a slenderness ratio of 12.5.

The cross-sectional dimensions were measured at three points along the coupon

length using a vernier calliper. The length was measured along each of the four edges in order to obtain a representative value for suitable strain calculations.

Difficulties were encountered during the compression tests as some specimens buckled before a compression failure occurred, which delayed the determination of the true compressive strength of the material. In order to eliminate buckling and undesirable end effects, the special apparatus described in Section 4.2 was used. The apparatus was specially designed to ensure coupon stability during creep testing.

Twelve specimens were cut from the middle of each leg of the pultruded angle section, using an electric saw. The coupons were ground to have uniform width, and the ends were milled to be parallel. All the specimens tested were instrumented with two strain gauges to measure longitudinal strains on both surfaces. The gauges were positioned at the centre of the coupon. Strains were measured by a Doric 245 multichannel data acquisition system and recorded by a dual disc drive data logger. The strain gauges used were of type CEA-06-240UZ-120.

Before the formal tests with full readings were performed, some preliminary tests were conducted without any strain gauges to check the ultimate load level and adjust the testing parameters. The results and stress-strain curves of all tests are given in Figs. 3.9, 3.10 and Tables 3.4(a) and (b).

It was observed that the average modulus of elasticity of coupons from Leg 1 and Leg 2 was respectively 37% and 2.5% higher than the nominal values guaranteed by the manufacturer. The average strain values on the internal faces of the legs were also observed to be 6% higher than the values on the external faces. This difference arises as

a result of the positioning of the mold in the pultrusion process, as discussed in Section 3.2.

3.3 Summary

This chapter has described the laboratory tests conducted in order to establish the mechanical characteristics of the composite material under consideration. The tests are destructive in nature and they involve both compression and tension tests on coupons and only compression tests on angle stubs. The detailed results were reported.

The results showed that for the weaker legs, the properties were close to those supplied by the manufacturer while for the stronger legs, the properties are much higher than the manufacturer's: Differences of the order of 30% and 37% were observed for the modulus of elasticity in both tension and compression, respectively. Stress-strain curves obtained were linear in all compression and tension coupon tests, unlike in the angle stubs where the curves were linear only up to 100 MPa.

Table 3.4(a) Summary of compression material properties (Coupon cut from Leg 1)

Property	Gauge No	Coupon No						Average	Total Average
		1	2	3	4	5	6		
Modulus of Elasticity (GPa)	1	22 4	22 6	21 3	22 1	23 2	22 6	22 4 ± 0 6	21 9 ± 0 7
	2	22 2	21 5	20 8	21 1	21 7	20 9	21 4 ± 0 5	
Ultimate Stress (MPa)	1	303 9	320 4	315 7	311 1	320 1	305 2	314 ± 7	314 ± 7
	2								
Ultimate Strain	1	12696	14210	14846	14102	13708	13518	13850 ± 660	14280 ± 740
	2	13676	15016	15416	14738	14732	14680	14710 ± 530	

Table 3.4(b) Summary of compression material properties (Coupon cut from Leg 2)

Property	Gauge No	Coupon No						Average	Total Average
		1	2	3	4	5	6		
Modulus of Elasticity (GPa)	1	16 7	16 0	17 0	16 6	16 1	16 8	16 5 ± 0 4	16 3 ± 0 7
	2	16 3	15 9	16 2	16 0	15 6	16 1	16 0 ± 0 2	
Ultimate Stress (MPa)	1	211 9	195 1	219 8	198 8	214 6	201 7	207 ± 9	207 ± 9
	2								
Ultimate Strain ($X10^{-6}$)	1	12698	12218	12952	11930	13372	11928	12520 ± 540	12840 ± 640
	2	12698	13054	13546	12998	14210	12501	13170 ± 570	

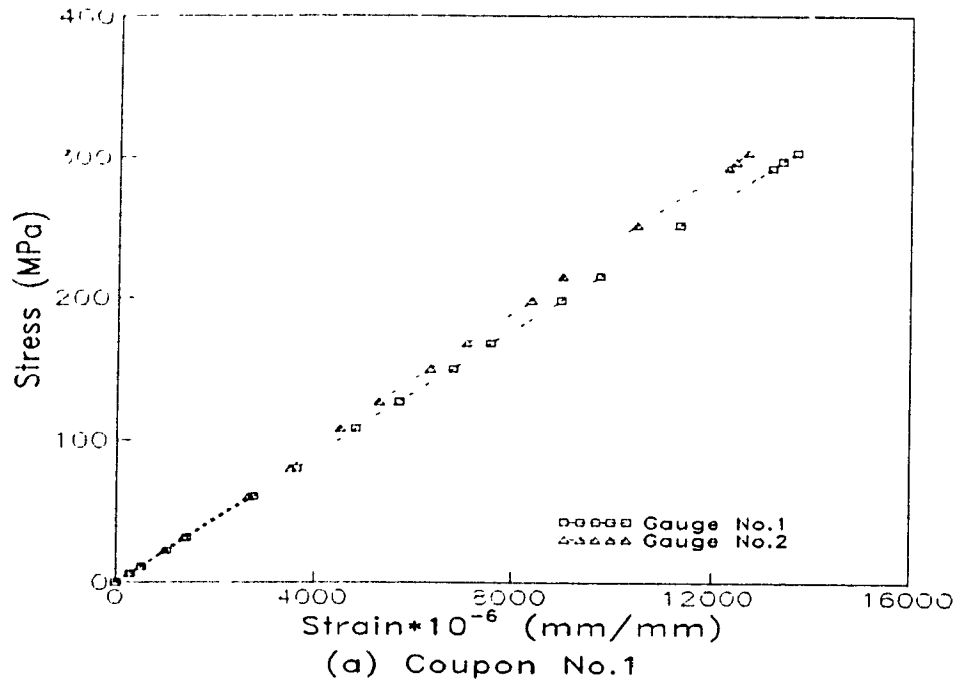

(a) Coupon No.1

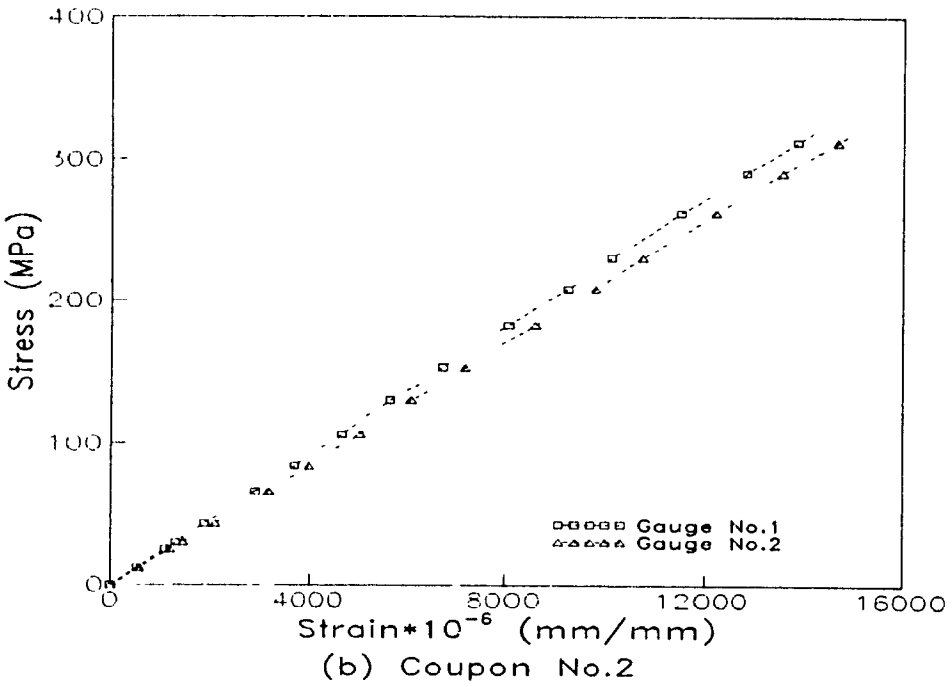

(b) Coupon No.2

Fig. 3.9. Stress-strain curves for coupons in compression (Coupon cut from strong leg)

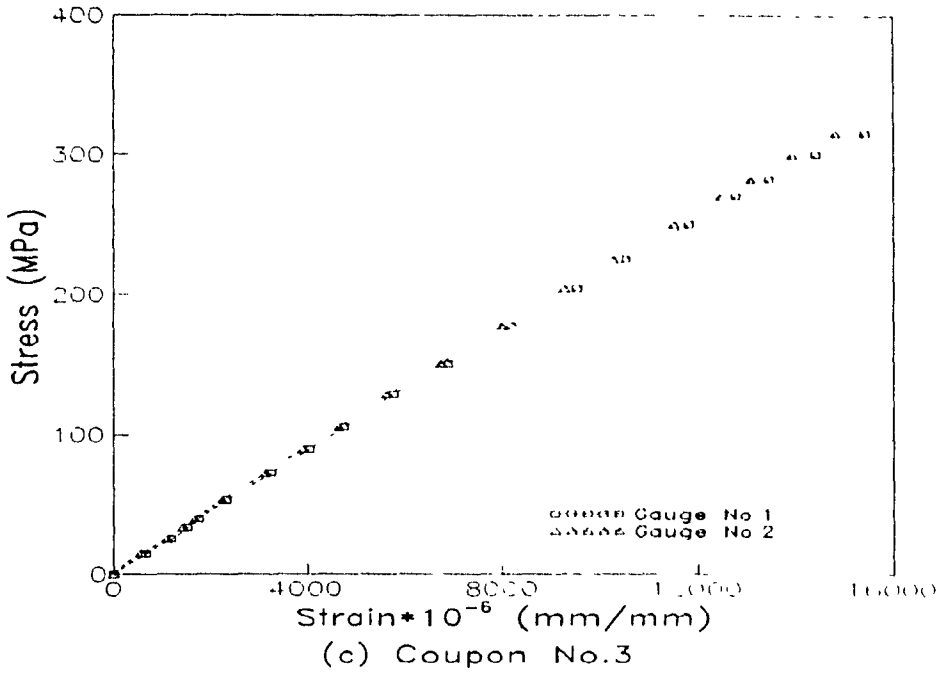

(c) Coupon No.3

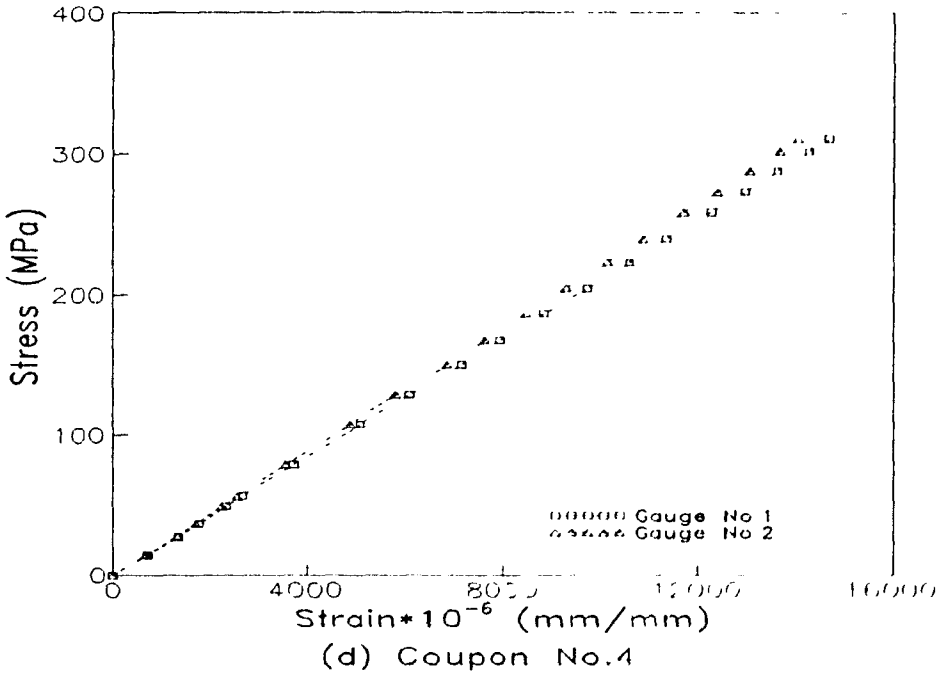

(d) Coupon No.4

Fig. 3.9. Stress-strain curves for coupons in compression (Coupon cut from strong leg)

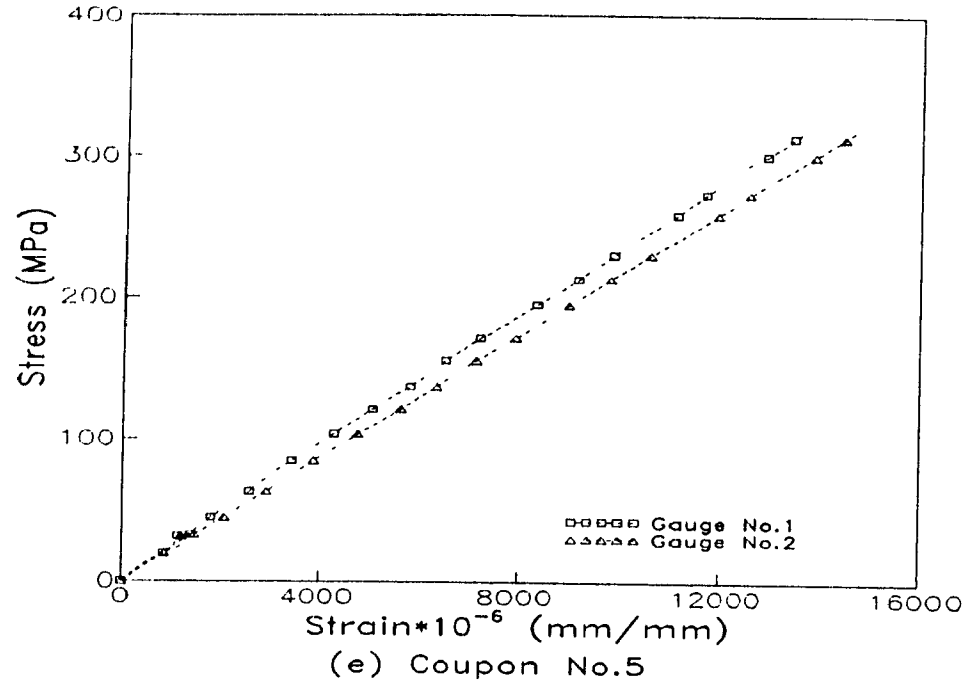

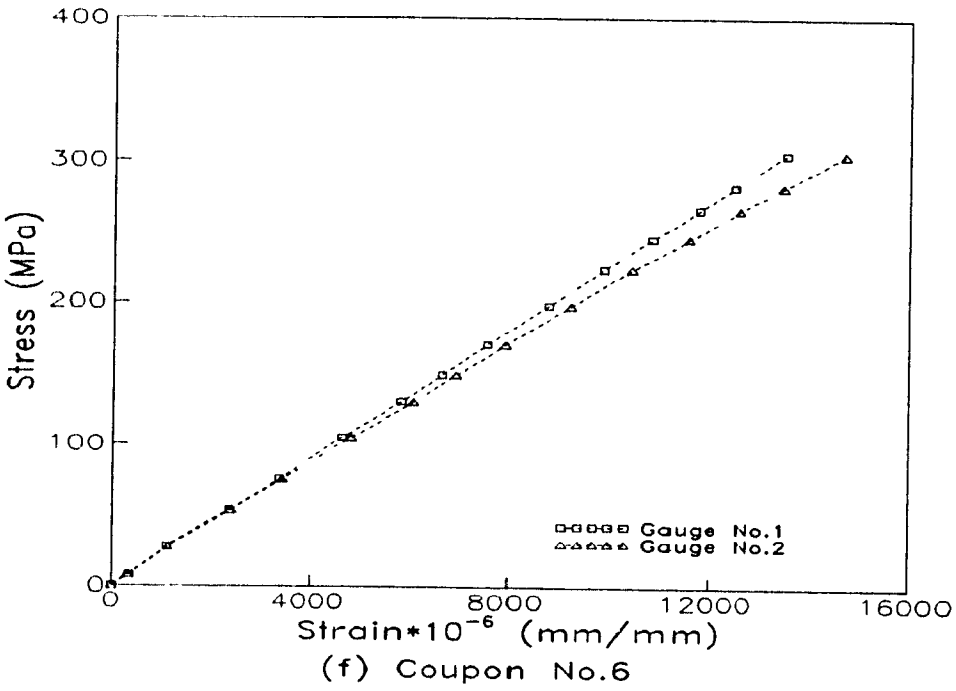

Fig. 3.9. Stress-strain curves for coupon in compression (Coupon cut from strong leg)

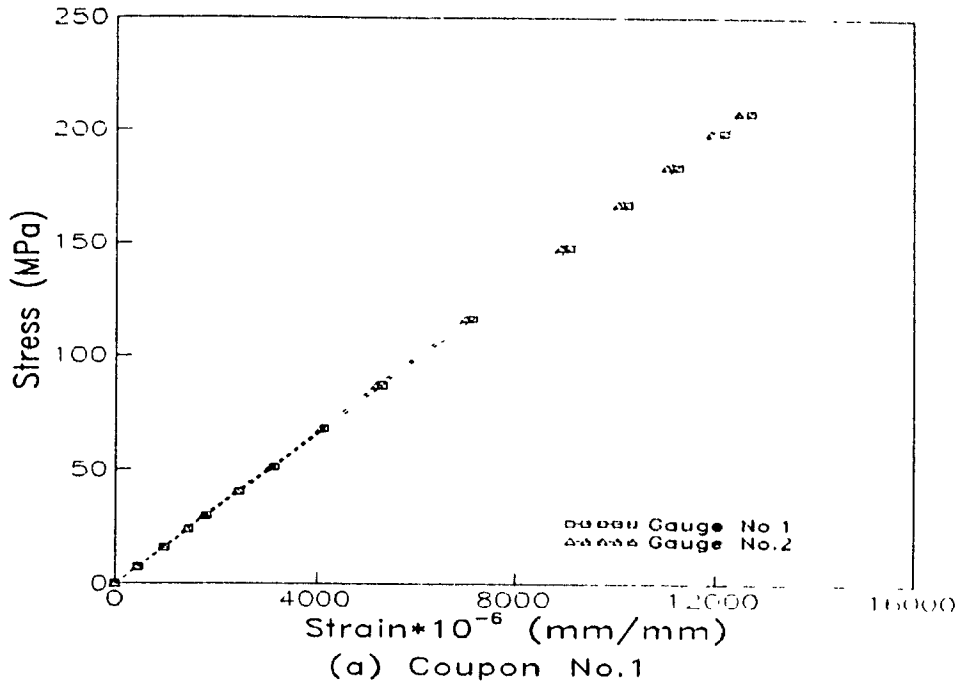

(a) Coupon No.1

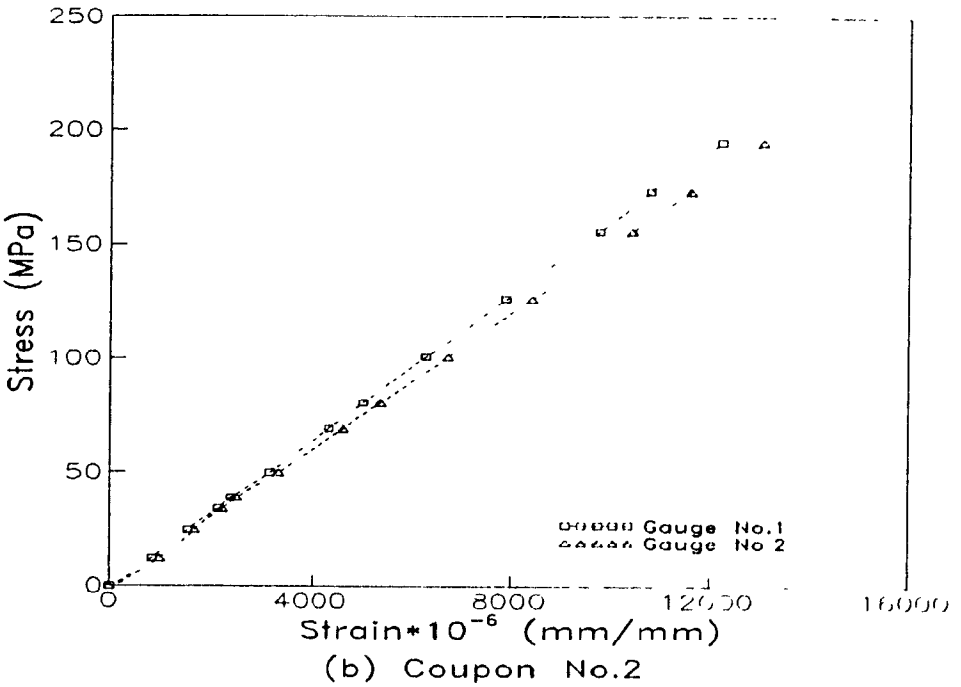

(b) Coupon No.2

Fig. 3.10. Stress-strain curves for coupon in compression (Coupon cut from weak leg)

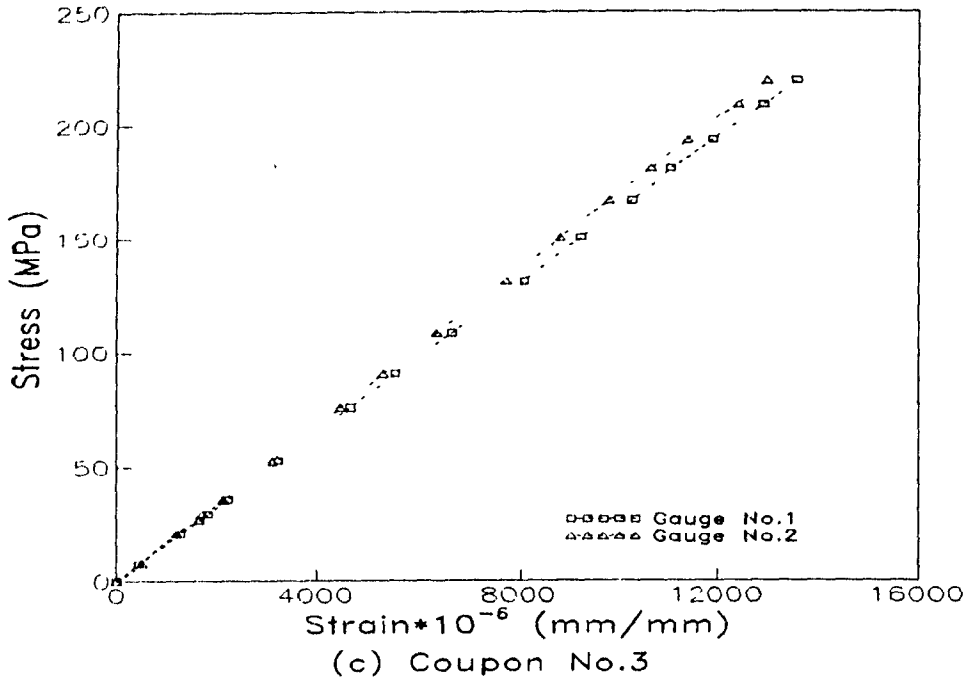

(c) Coupon No.3

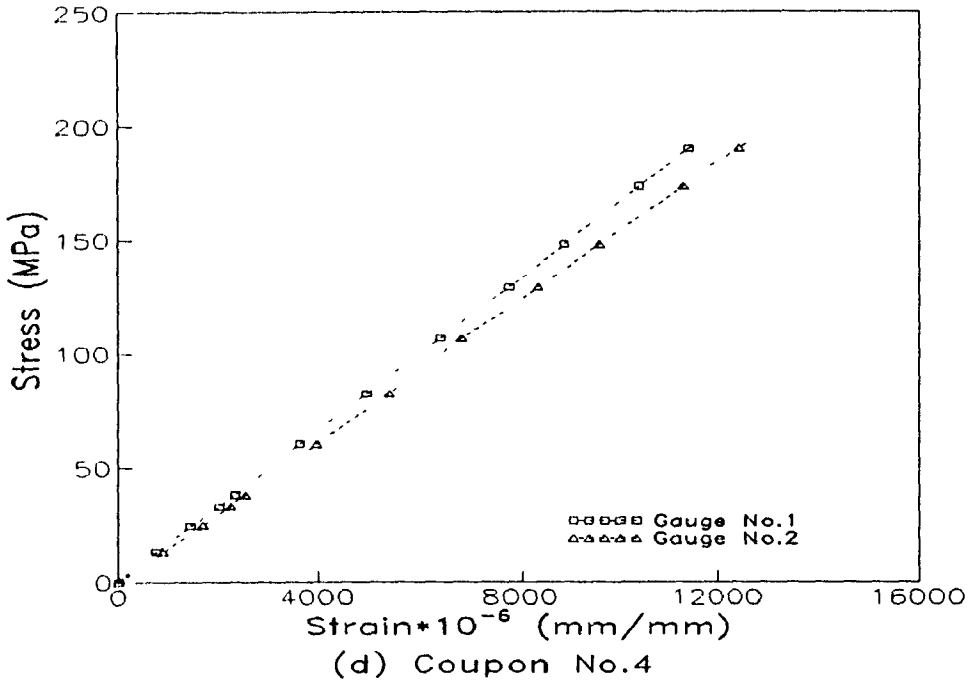

(d) Coupon No.4

Fig. 3.10. Stress-strain curves for coupon in compression (Coupon cut from weak leg)

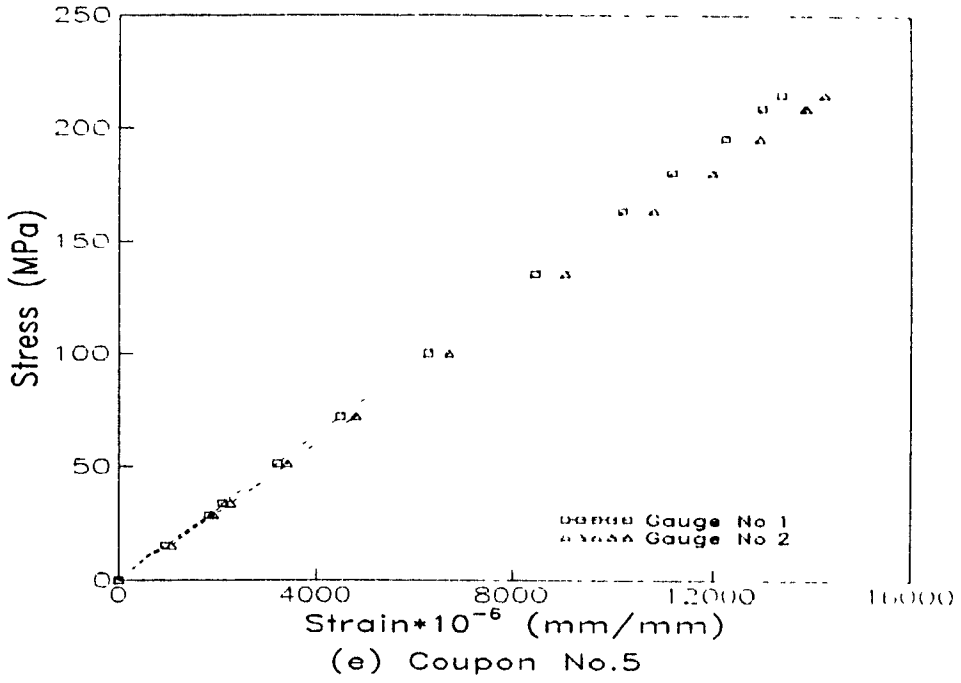

(e) Coupon No.5

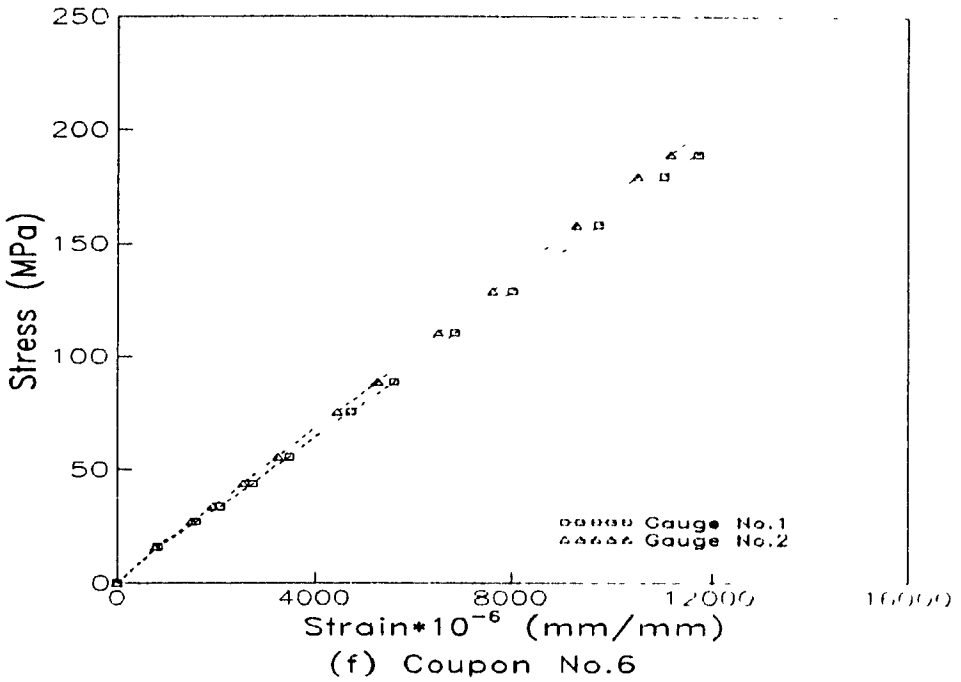

(f) Coupon No.6

Fig. 3.10. Stress-strain curves for coupon in compression (Coupon cut from weak leg)

CHAPTER 4

DESCRIPTION OF EXPERIMENTAL APPARATUS

4.1 Introduction

When testing advanced composite materials in compression, certain problems of buckling and end effects are normally encountered. In some cases, the specimen collapses without reaching the true ultimate strength of the material. One simple solution is to use a shorter specimen, but this does not necessarily yield good results. What then often happens is that end effects dominate the response so that good data is very difficult, if not impossible, to obtain. Therefore, solutions that minimize end effects while eliminating buckling at the same time are required.

4.2 Compression Fixture

Only a few references were found discussing compression creep testing of composite materials. Some of them reported the use of a hollow, solid and short specimen (Smith, 1966; Thomas, 1969; Simonovskaya, 1975), which seemed to work

well with polyvinylchloride (PVC) and polytetrafluoroethylene (PTFE). Such a coupon shape, however, cannot practically be used in the case of fibre reinforced plastics.

The sandwich beam test is considered by some investigators the best method for determining the compressive strength of composites (Hofar and Rao, 1977; Shuart and Herakovich, 1978). In this method, the specimen is loaded in flexure through a four-point concentrated load fixture, which can be accomplished either through loading pads and blocks on the surfaces of the beam, or imbedded in the honeycomb core of the beam. However, the application of this method would be difficult for creep measurements. The ASTM D695-69 compression test uses flat specimens stabilized by a supporting fixture, but exhibits problems with end-brooming, and introduces frictional forces that sometimes produce misleadingly high elastic moduli (Shart, 1978).

The fixture used in this work is similar to that built by Irion and Adams (1981), but some modifications have been made to apply a sustained load. The fixture can be easily modified to accommodate almost any width, length or thickness of specimen, and it will be possible to reuse it for further experimental studies. Fig. 4.1 shows a specimen installed in this fixture and a dimensional drawing can be found in Fig. 4.2.

This fixture is quite simple, consisting basically of four small blocks of steel, each with a rectangular slot milled in the long direction on one face. Two of these blocks make up one side of the fixture. Each side has a 12.7 mm (1/2") diameter hole

drilled in the middle of the block, to receive a solid rod that keeps the blocks lined up and the fixture square. Each block has two threaded holes, and four small rods join the two sides together, with a coupon fitting into the slot created by the two halves. The specimen fits into the fixture such that the embedment length is 25.4 mm (1 in.) at the top end and 38.1 mm (1.5 in.) at the bottom end. This arrangement allows failure to occur at the centre of the specimen. The side supports prevent buckling and can accommodate larger specimen lengths. They also reduce end effects resulting in brooming, splitting and other potential problems. Figure A.8 in appendix shows a photograph of the end fixture disassembled.

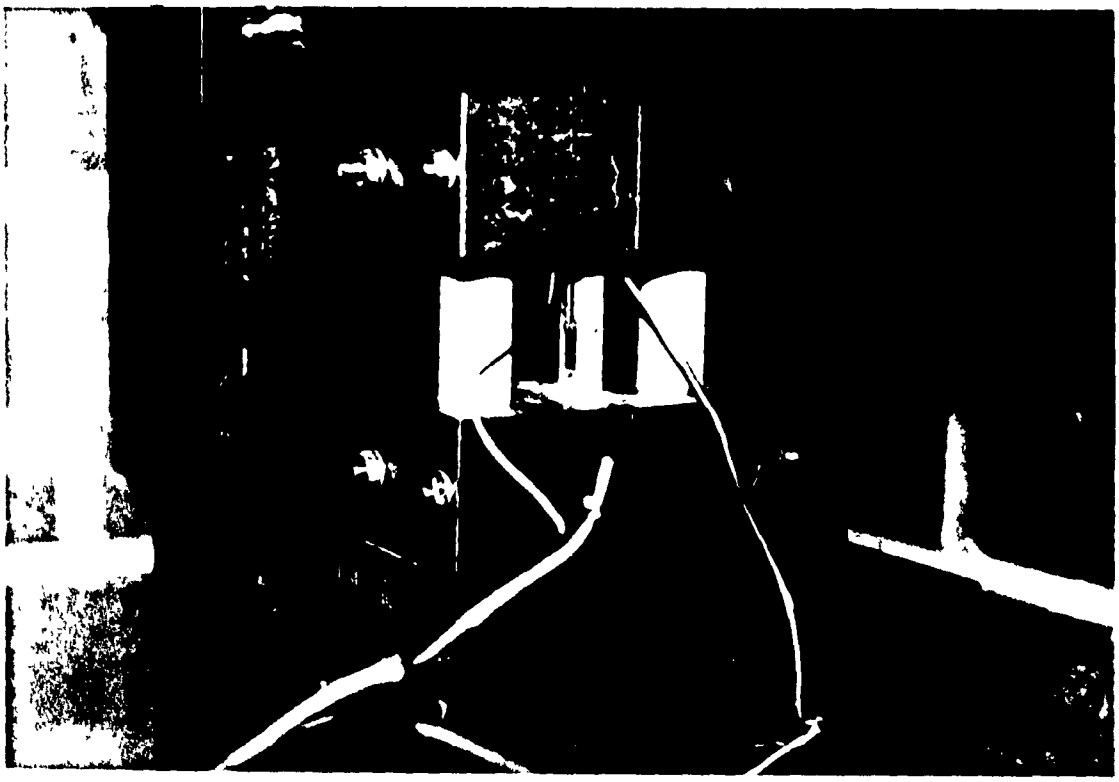

Fig. 4.1 Coupon creep fixture with specimen

Accurate machining was crucial for this fixture to ensure its alignment and to prevent offsets between halves when a specimen is installed. In addition to its simple design, another advantage is that the specimens are end-loaded, so the gauge length is the total length of the specimen. This compression fixture was used for all coupons in the compression and creep tests described in Chapters 3 and 6.

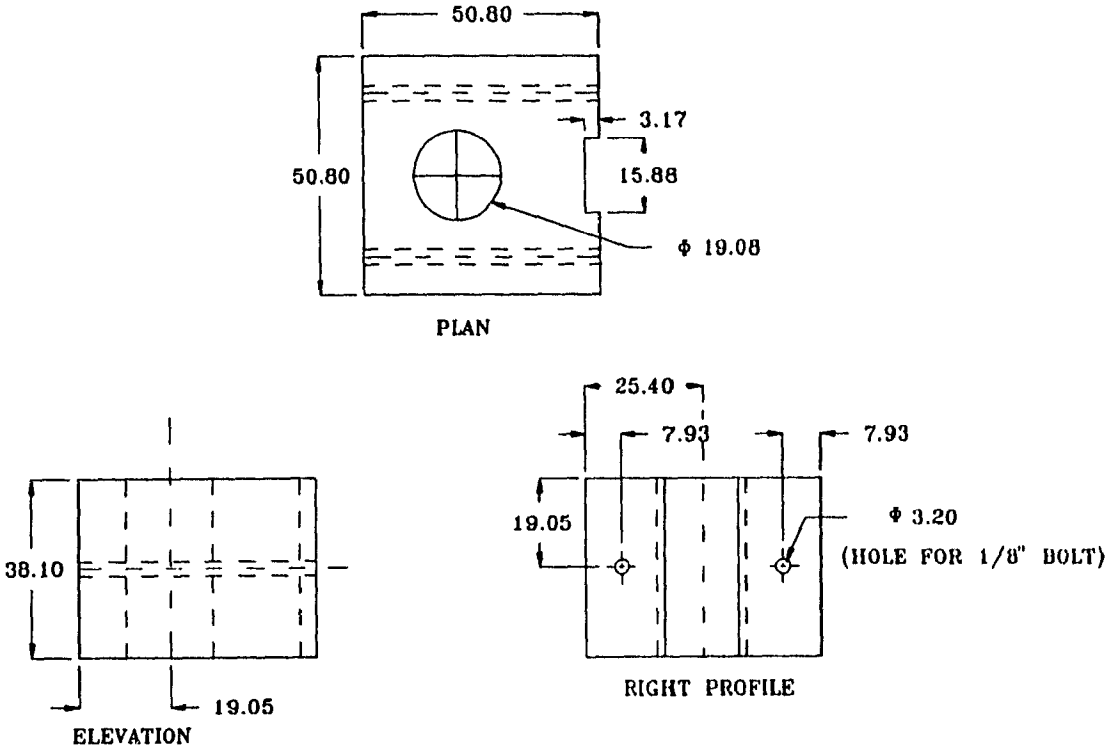

Fig. 4.2 Details of compression creep fixture

4.3 Cantilevered Creep Apparatus

The common tests used for determining the creep and stress-rupture properties of materials involve the application of a constant compressive load to the specimen maintained at a constant temperature. Generally, the corresponding dead loads required are too large to be practical, and a lever arm is introduced to multiply the effect of the applied gravity loads. It is also difficult to achieve the alignment required while applying axial loads to small specimens, and for these reasons, most creep studies in compression have used constant compressive loads either directly or through a lever arm system. Note also that hydraulic jacks exhibit load relaxation over time, and hence, are not suited for this type of experiment, and a mechanism using gravity loads is indicated.

In order to test the angle sections for compressive creep behaviour, a special cantilever loading device was then constructed for this study. It was decided that a lever arm apparatus of practical dimensions would generate high compressive loads, with a multiplying factor of the order of ten between the applied dead weights and the compression force transferred to the specimen. Using steel HSS square sections 101.6 X 101.6 X 9.37 mm, a mechanism consisting of three pin-ended lever arms, each 1600 mm in length, was constructed as illustrated in Fig. 4.3. Each cantilever arm was attached to a short steel post of identical cross section, the tensile reaction load being transferred by a pin into two side plates that were fillet-welded to the post. The three reaction posts rested on a common member from which three 1500 mm legs ran directly beneath and parallel to the cantilever arms. All three legs and

the base beam to which they were attached were made from the same HSS tubing as the cantilever arms and the posts.

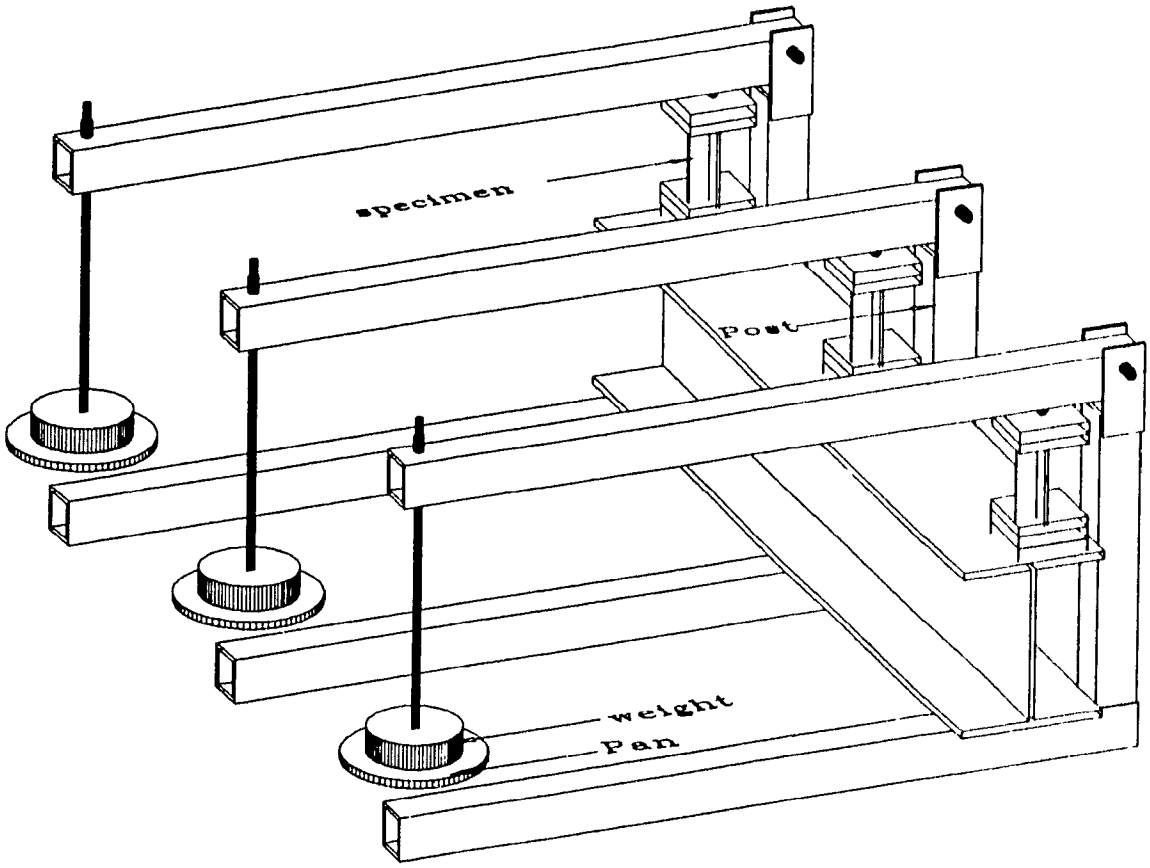

Fig. 4.3. Cantilevered apparatus for creep testing

Three weight pans were hung from the cantilever end of the three lever arms, and consisted simply of a circular plate with a threaded rod bolted to the cantilever.

A steel washer was welded to the underside of the cantilever in order to place a ball bearing that transferred the compressive load precisely at the centroid of the angle stub. A specimen in position with end plates and ball bearing is shown in Fig. 3.3.

The testing cantilever apparatus was calibrated in order to ensure accurate load transfer The side plates that transfer the dead weight from the cantilever end into the reaction post were ground to reduce frictional resistance. The lateral faces of the cantilever tube were also ground at the pinned end, and the pin was lubricated as well to minimize the occurrence of any frictional moment.

A load cell of range of 0 to 22.25 kN was used to calibrate the apparatus. The reaction of the cantilever arm on the load cell was registered for each arm, as the loading of the weight pan was increased. Load increments of approximately 98 N to 147 N were used, up to a maximum load of 22.25 kN. Calibration was repeated three times for each arm. The apparatus performed very well under the calibration loads and was considered satisfactory for testing. The load cell was applied before the test on each arm in order to obtain identical loading on each specimen. Fig. 4.4. shows a photograph taken during calibration of a cantilever arm.

4.4 Summary

The experimental apparatuses used in this research and their set-ups were fully described in this chapter. The coupon fixture used in this work is similar to that built by Irion and Adams (1981), but some modifications were done to facilitate the application of a sustained load. A cantilever arm apparatus was constructed to

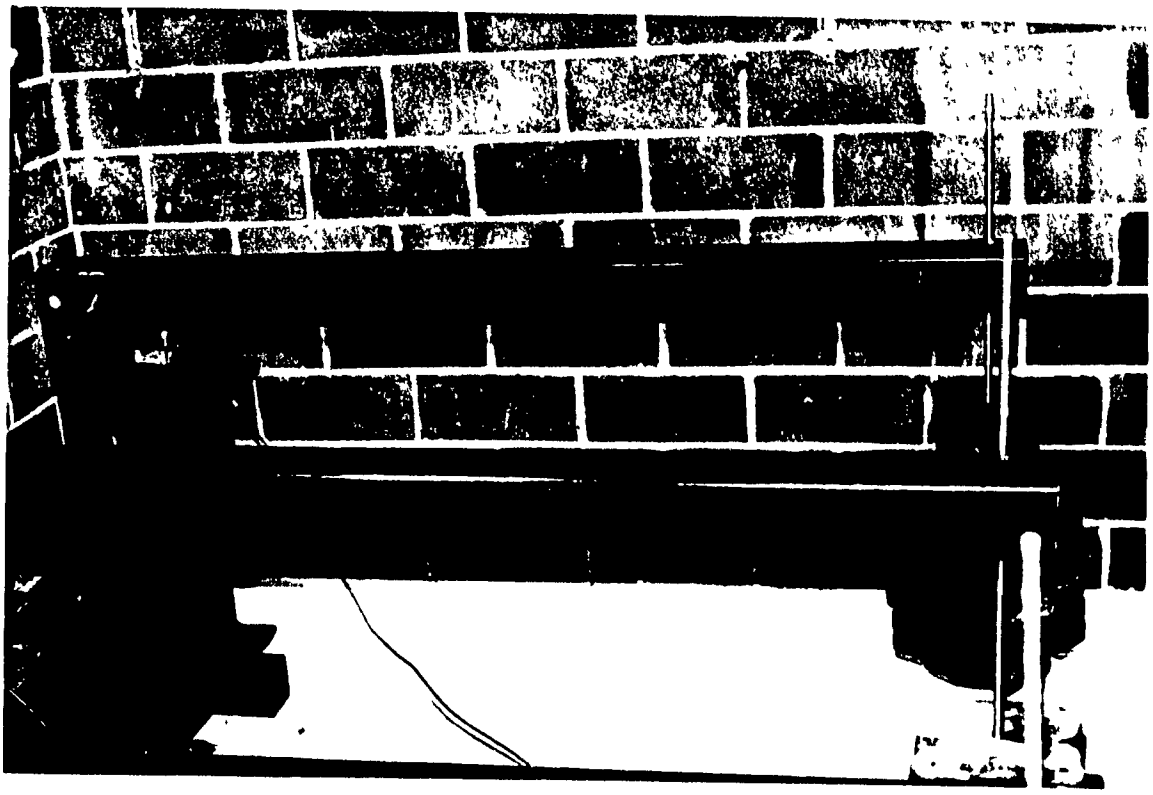

Fig. 4.4 Load cell for calibration of cantilevered creep apparatus

multiply the applied dead loads by a factor of 10, and was used for creep tests on both coupons and angle stubs. The whole experimental set-up was designed to remove some of the limitations of the methods used by previous researchers in order to maximize the accuracy of the measurements.

CHAPTER 5

PRELIMINARY INVESTIGATION

5.1 Introduction

In order to finalize the details of the apparatus and adjust the testing parameters of the creep test on angle stubs, a preliminary compression creep test was performed. The lever arm system described in Section 4.3 was used to load three angle stubs for a duration of 350 hours in creep and 150 hours in creep recovery. The main purpose of this preliminary test was to decide on the loading arrangement and type of strain gauges for the longer duration test. The following details were checked: the strain gauge arrangement on the specimen, the load level to be used on the angles, and the efficiency of the steel/wood end plates.

5.2 Compression Creep and Relaxation Test Procedure on Angle Stubs

Due to the moulded nature of pultruded composite shapes, non-homogeneity can occur locally in the angle section. Since earlier crushing tests on angle stubs had shown that one leg was systematically stronger than the other, a strain gauging pattern identical in both legs was needed. Three different arrangements were examined in the preliminary test, as described below.

The earlier strain gauges were of the foil type commonly used for crushing testing, short (5 mm) and easy to apply to the surface. These gauges were arranged on the angle surface such that three gauges were placed in a vertical line on each of the four faces of the specimen, for a total of 12 gauges for each angle. This gauge configuration was used for one angle only in the preliminary test. The other two angles were fitted with polyester strain gauges. These gauges were available in various lengths, and lengths of 90 mm and 120 mm were chosen. One angle was fitted with the 90 mm gauges, one on each face, while the other had the 120 mm gauges in the same pattern (Fig. 5.1). The reason for using these long gauges was to obtain a larger strained length that would eventually average out the local imperfections or disparities of the material. Note that the polyester gauges were much more fragile than the smaller foil gauges and were very difficult to apply to the surfaces

The load level used for the preliminary test was 20% of the theoretical buckling load of an angle section as determined by a commercial design aid (MMFG, 1990). This low load level did not significantly strain the angles and a higher load level, approximately 50% of the theoretical buckling load (45% of the failure load determined from experimental compression angle stub tests), was subsequently used for the formal creep tests.

Strain readings were taken at the following time intervals during the test. for the first one hour every minute, afterwards every five minutes for up to 24 hours, and finally 18 minutes up to the completion of 350 hours Readings for the "unloading" recovery portion of the test were recorded at the same time intervals. Experimental results obtained are shown in Figs. 5.2 and 5.3 for the three angle stubs tested. These results are further

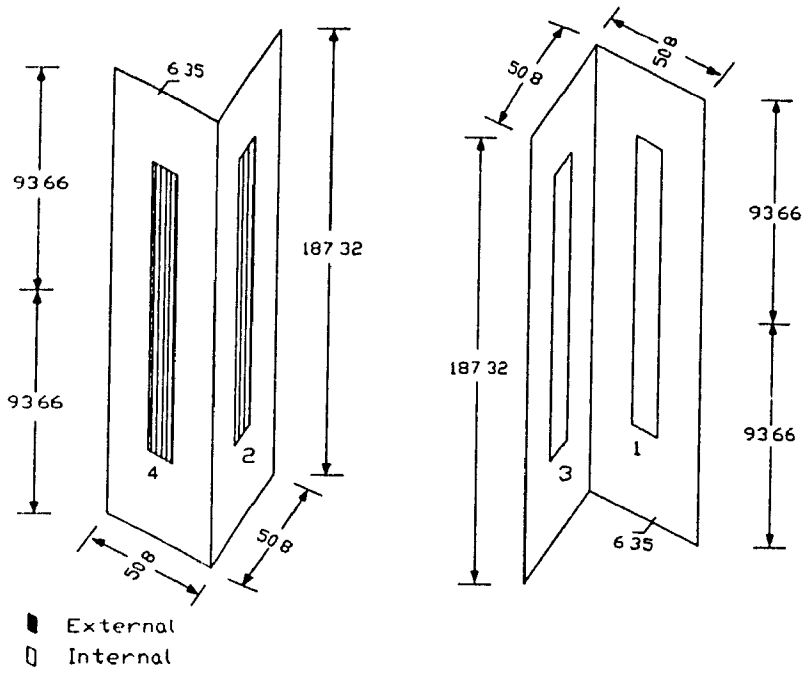

Fig. 5.1. Position of long strain gauges

discussed in the next section.

5.3 Test Results

5.3.1 Evaluation of creep parameters

The creep parameters of Findley's model were evaluated by curve fitting using the following expression:

$$\log (\epsilon - \epsilon_0) = \log m + n \log (t/t_0) \qquad (2.17)$$

which represents a straight line of slope n and intercept m (at unit time), if log $(\epsilon-\epsilon_0)$ is

plotted versus log (t/t_0). Four plots are given in Fig. 5.4, which correspond to the strain measurements of Fig. 5.2. The values of the creep parameters m and n obtained by fitting

Table 5.1 Summary of creep parameters in angle stubs

Condition	Gauge No.	Creep Parameters		Initial Strain ($X10^{-6}$)	Creepocity @ 350 Hours ($X10^{-6}$)
		m	n		
Angle Stub with 5 mm Strain Gauges	1	15 8	0 368	912	102
	3	11 5	0 366	907	84
	4	8.5	0.359	820	61
	5	14.4	0.354	905	99
	6	9.9	0 360	783	72
	7	9 7	0.361	915	74
	8	7.8	0.341	769	64
	9	8.3	0.378	909	69
	10	7.9	0.355	788	61
	11	9.4	0.384	948	78
Average		10 3±2.6	0 363±0.012	866±64	76±14
Angle Stub With 90 mm Strain Gauges	1	8 4	0.332	658	62
	3	7.4	0.321	741	53
	4	6 2	0 302	847	47
Average		7.3±0.9	0.318±0 012	749±77	54±6
Angle Stub With 120 mm Strain Gauges	1	13 9	0 212	800	56
	2	4.82	0.358	657	42
	3	8.5	0 304	888	57
Average		9.1±3 7	0 291±0.060	782±95	52±7

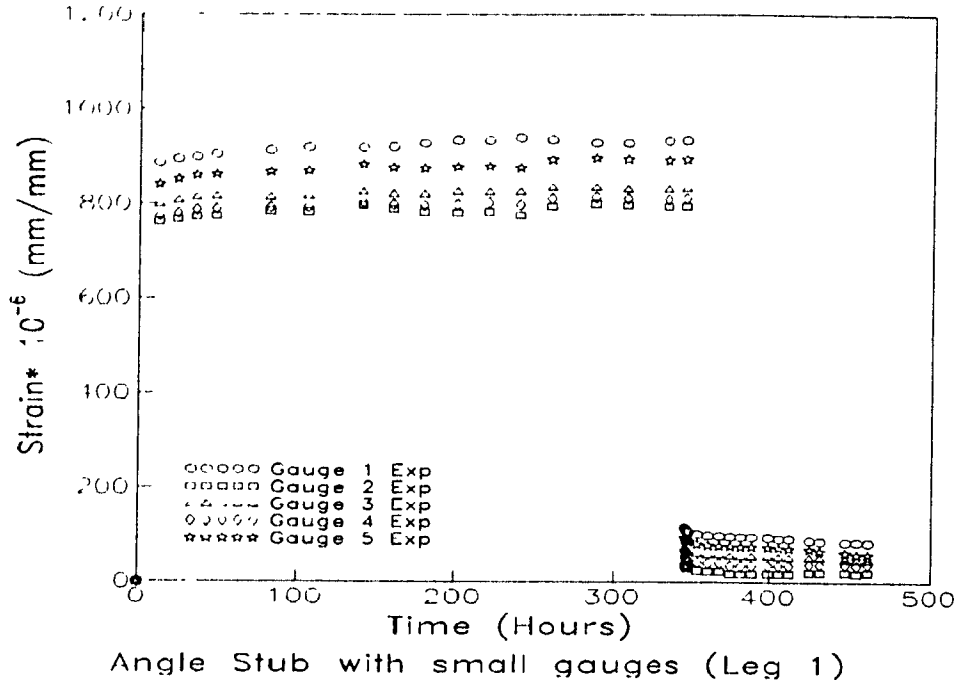

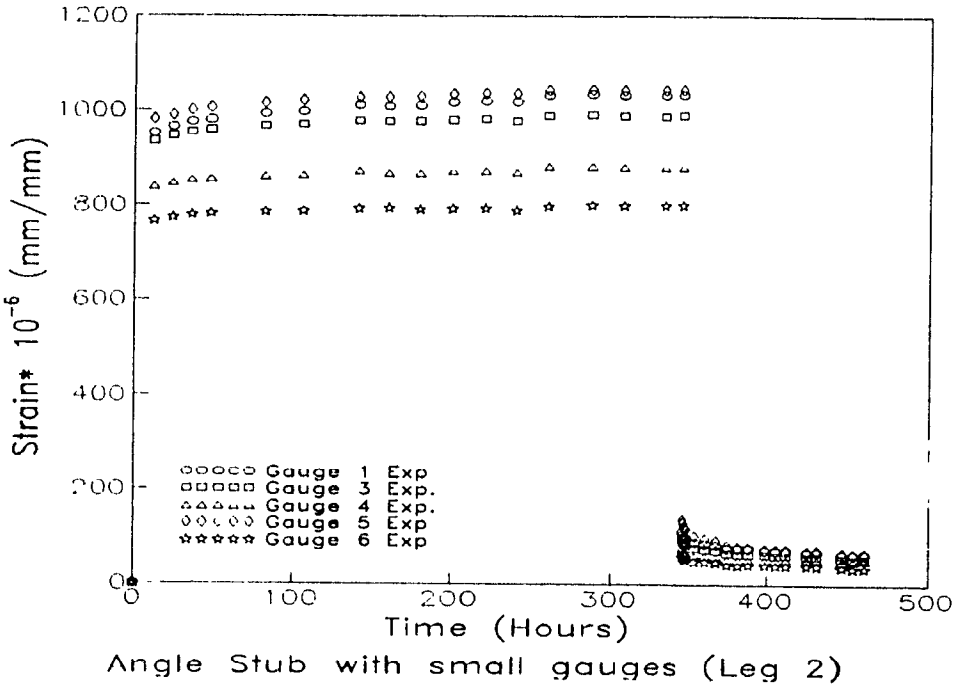

Fig. 5.2(a). Creep and creep recovery of angle stub with short gauges

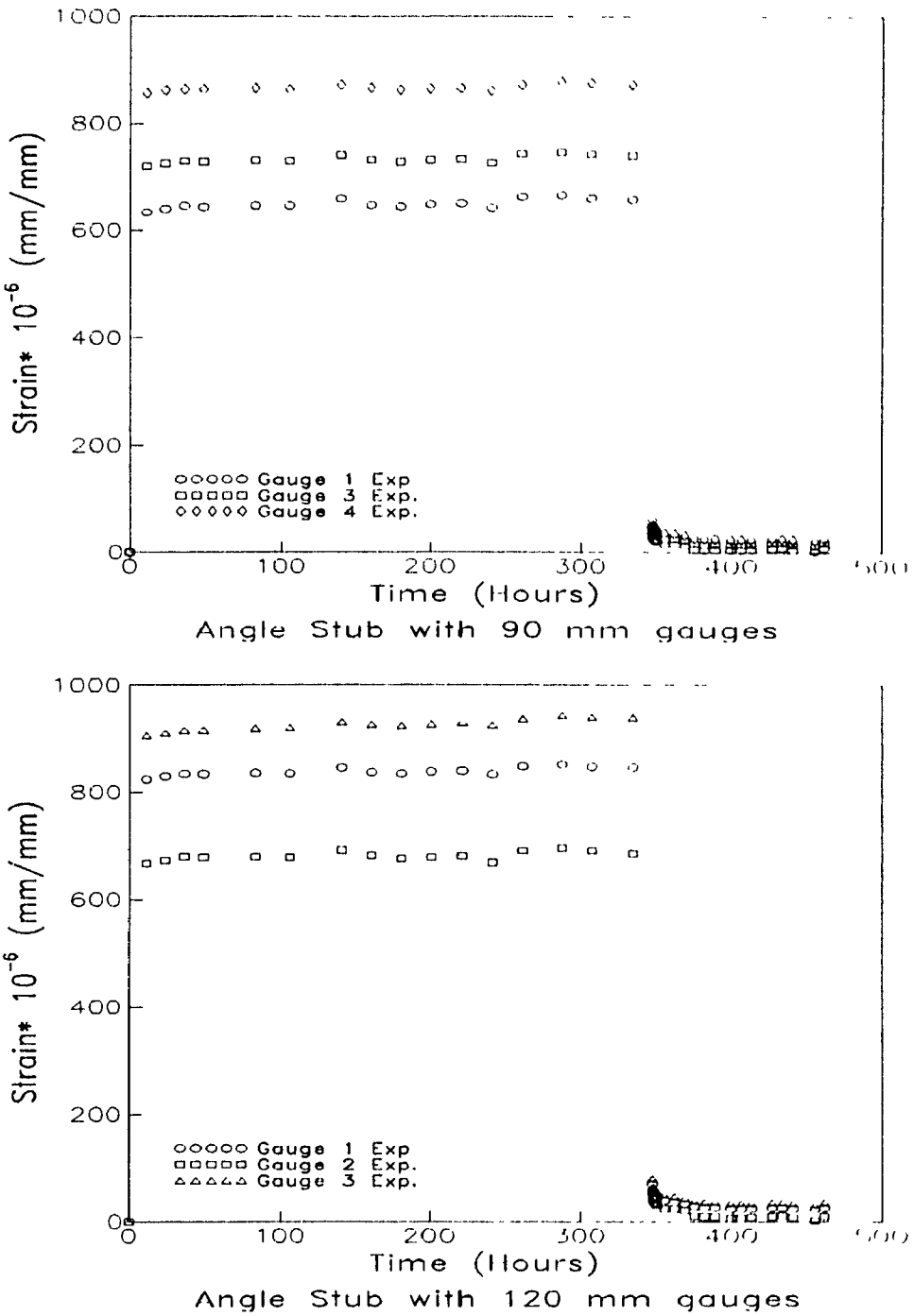

Fig. 5.2(b). Creep and creep recovery of angle stubs with long gauges

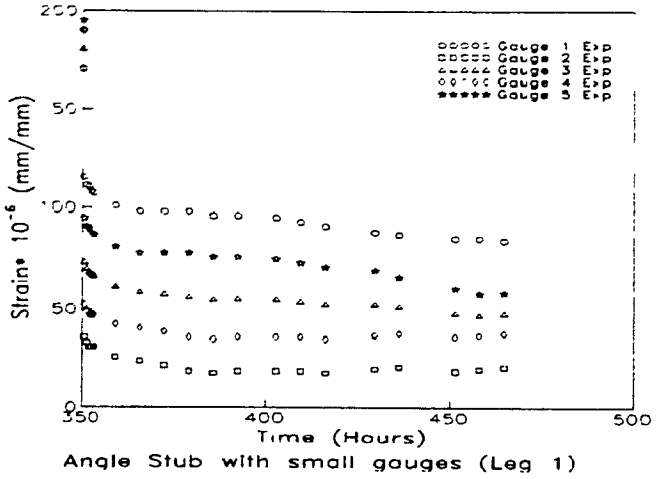

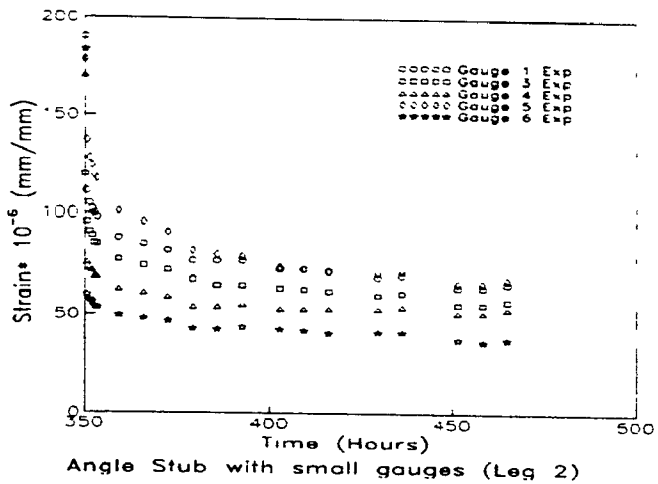

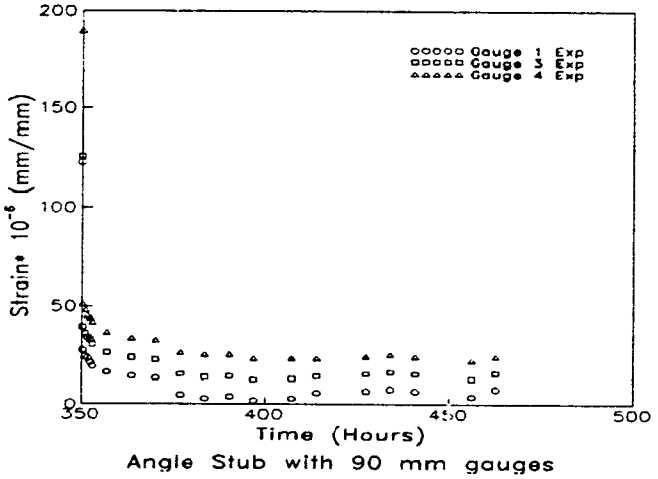

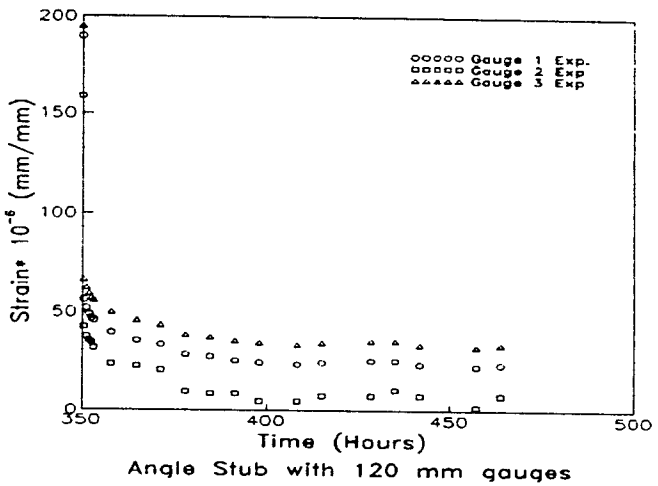

Fig. 5.3. Creep recovery of angle stubs

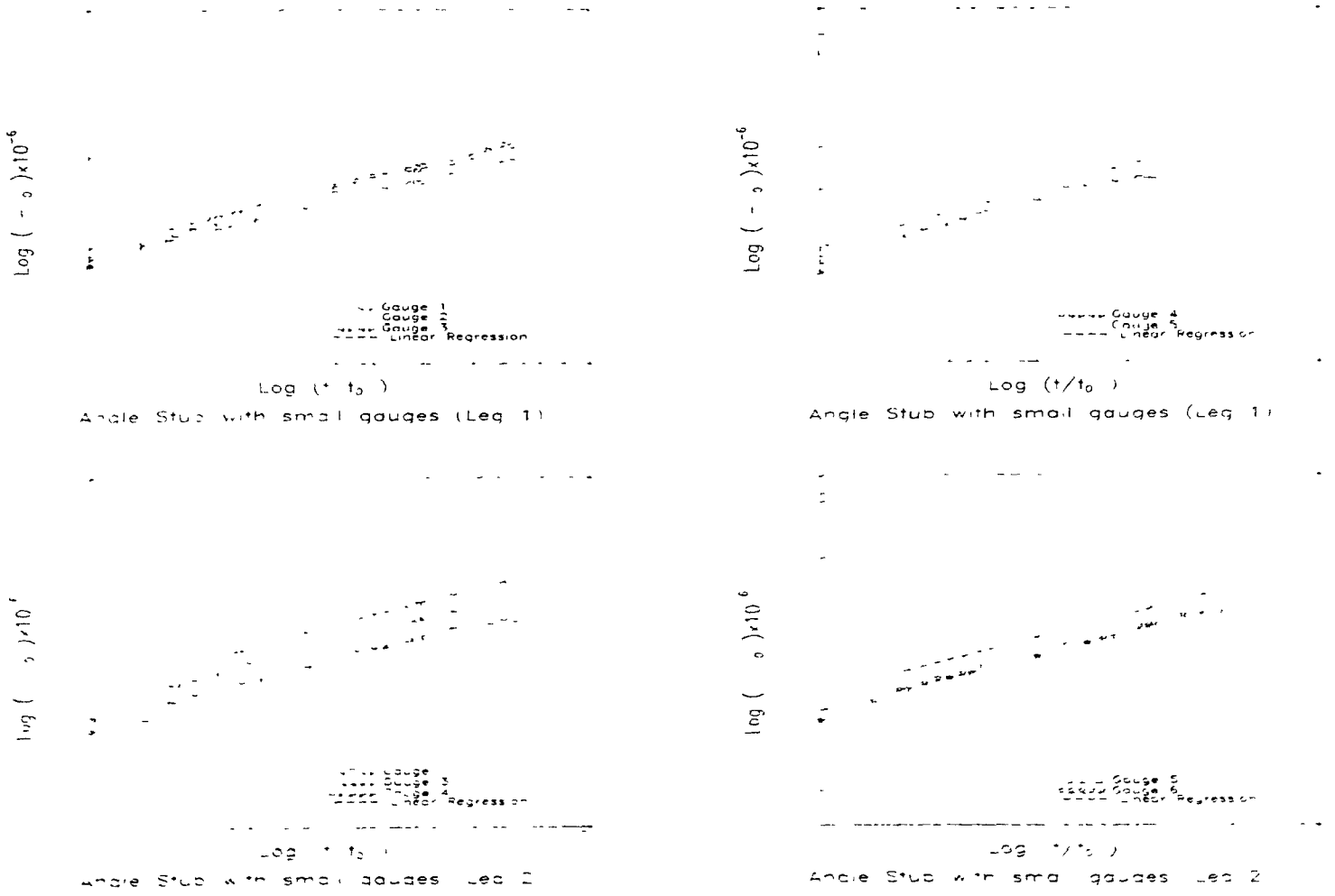

Fig. 5.4(a). Evaluation of compression creep parameters for angle stubs with short gauges

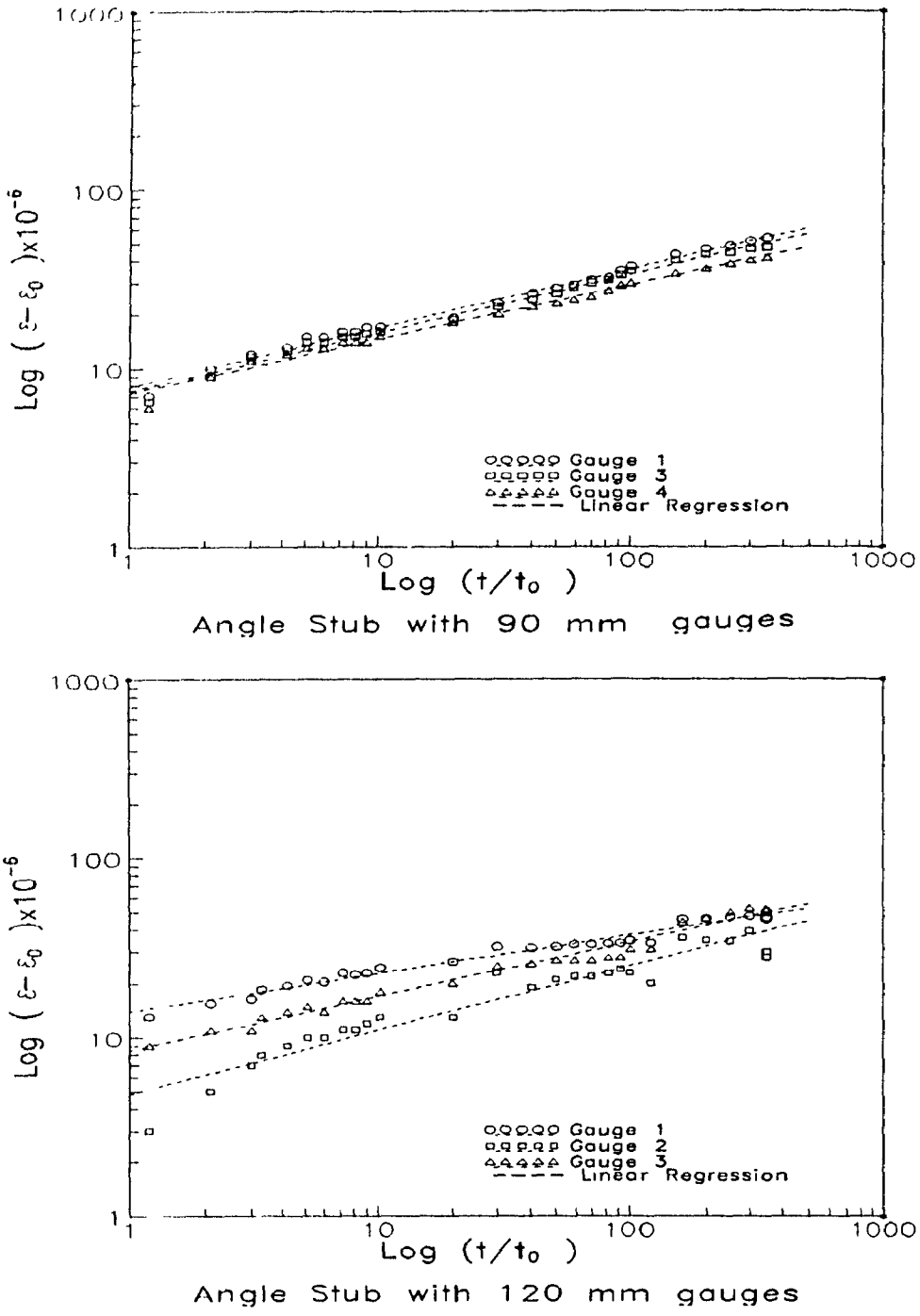

Fig. 5.4(b). Evaluation of compression creep parameters for angle stubs with long gauges

a straight line are listed in Table 5.1. Note that the creep parameter n is independent of the stress level which explains its smaller variability when compared to that of parameter m.

5.3.2 Comparisons of Experimental Results and Predictions Using Findley's Model

The theoretical predictions and experimental results for the three angle stubs tested are compared in Figs. 5.5(a) and (b) where generally good agreement is shown between theory and experiment. Results using small 5 mm gauges were less scattered than those obtained from the 90 mm and 120 mm gauges. This is because the specimen with small gauges allowed strain reading at more locations. The strain variation with time is higher in the longer gauges, and, since only one long gauge fits on each face of the angle stub, the effect of cumulative creep deformation in a single gauge is more severe than in the smaller gauges, which adds to the scatter of the measurements.

5.4 Summary

Preliminary investigations to select the best loading set-up and type of strain gauges for the tests were discussed in this chapter. Three different strain gauge arrangements were used in the tests: one using 12 short 5 mm strain gauges and two others using four 90 mm and 120 mm gauges, respectively.

The experimental results were compared with the predictions of Findley's model using creep parameters obtained by curve fitting. It was found that the results using the 5 mm strain gauges were better than those obtained from the 90 mm and 120 mm gauges, the reason being that the smaller gauges allow strain measurement at more location and show less variability than the two other types of gauges.

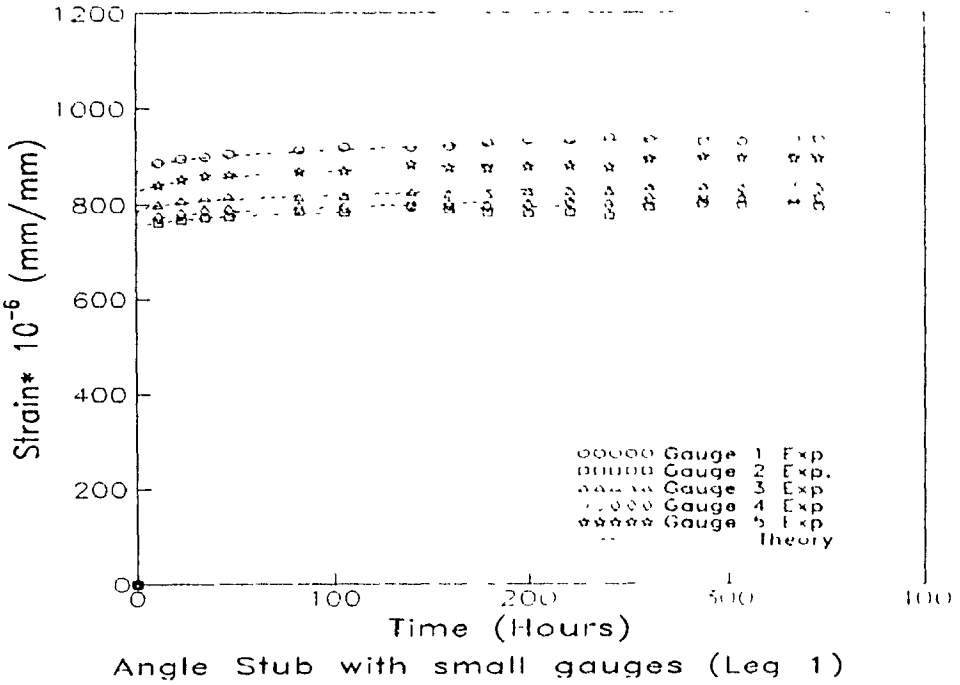

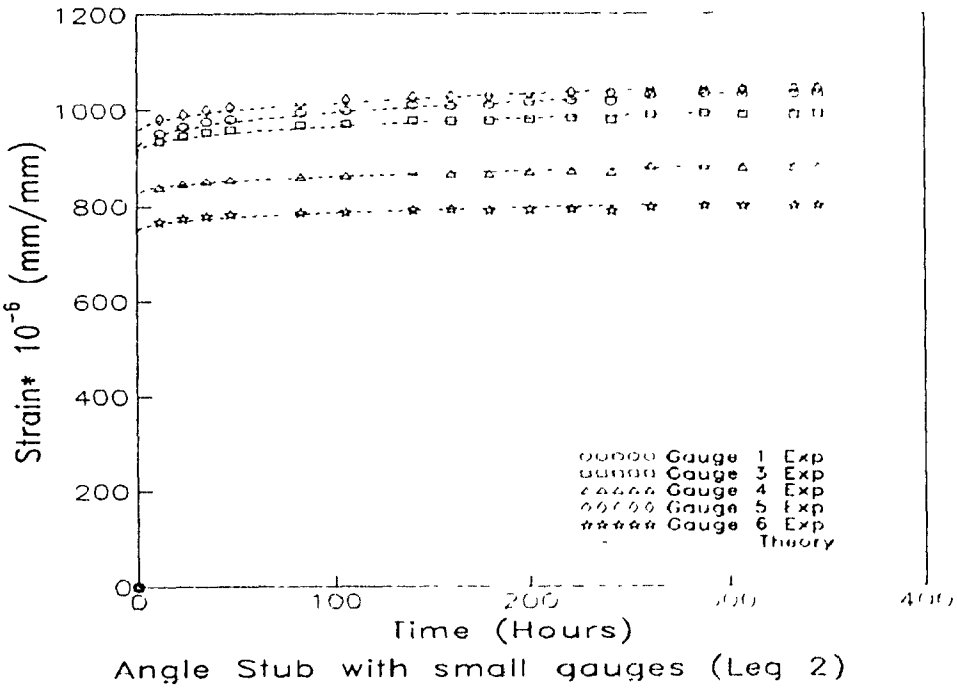

Fig. 5.5(a). Creep measurements and predictions for angle stub with short gauges

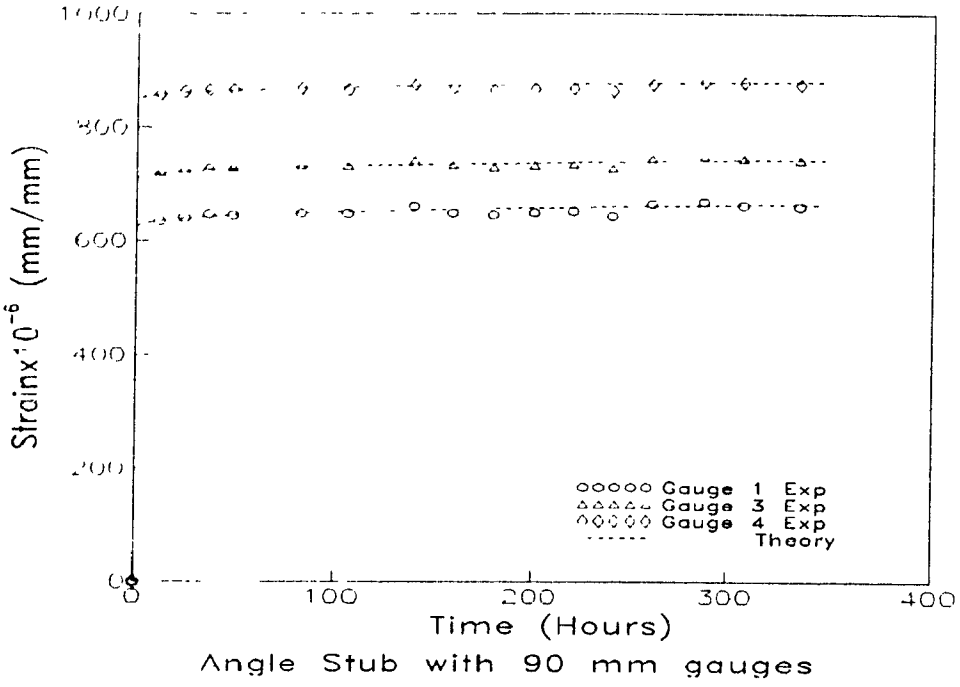

Angle Stub with 90 mm gauges

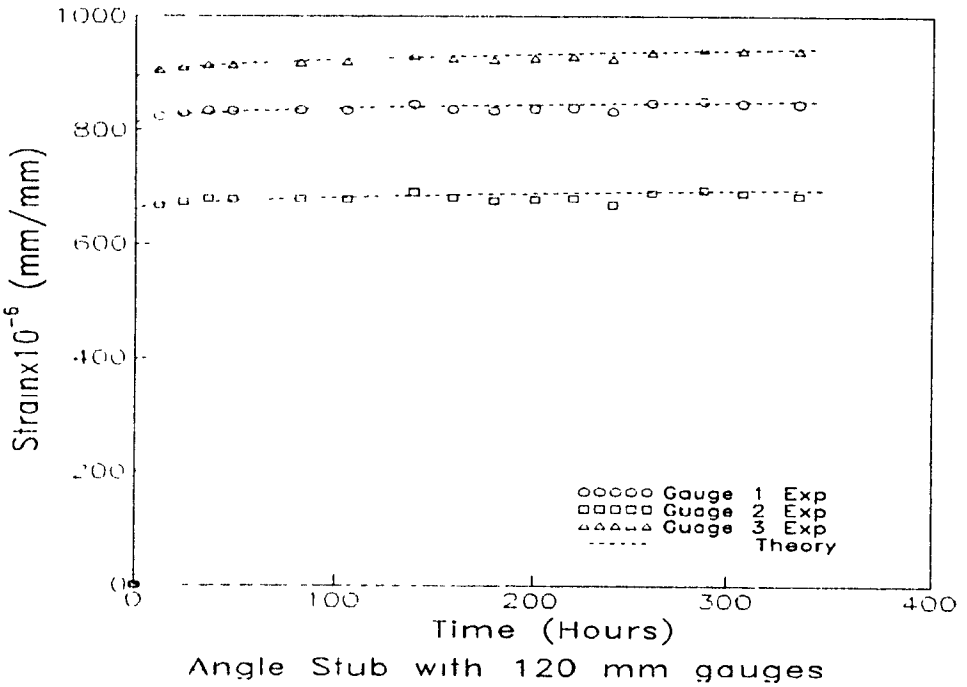

Angle Stub with 120 mm gauges

Fig. 5.5(b). Creep measurements and predictions for angle stubs with long gauges

CHAPTER 6

EXPERIMENTAL PROCEDURE

6.1 Introduction

In this chapter, the time-dependent (long-term) behaviour of the angle stubs and coupons is investigated. Six creep tests were performed in this study; three on angle stubs and three on coupons. A description of these tests is presented in the following sections.

6.2 Specimen Creep and Creep Recovery Tests

The creep tests were conducted from September 1992 to February 1993 in a closed room of the Solid Mechanics Laboratory where the temperature and humidity variations were minimal. The average room temperature and relative humidity were 24°C (69°F) and 25%, respectively. Results on an unloaded reference specimen have indicated that no significant corrections were needed to account for environmental conditions. The creep tests were performed on angle stubs and coupons identical to those used in the time-independent study (Section 3.2.2).

6.2.1 Tests on Angle Stubs

Sustained loads were applied to the angle stubs using steel plates suspended from the lever arms (see Fig. 3.3). The loads were transferred using a ball joint, as in the time-independent study. The total load applied on each angle stub was of 23.2 kN (5.225 kips), which is approximately 45% of the initial buckling load of 51.6 kN (11.6 kips), as previously discussed in Chapter 3. Small differences (2%) were observed between the time-independent strain and the time-dependent initial creep strain for a given load. Strain data were recorded with 120-ohm strain gauges (CEA-06-250UW-350), and read from a Doric 245 acquisition system. The locations of the strain gauges were identical to those used in the time-independent and preliminary time-dependent stub tests (Fig. 3.4 b). Each angle stub had 12 strain gauges on it, but due to the limited number of channels of the data acquisition system, a total of five gauges had to be disconnected.

At the beginning of the test, readings for all strain gauge channels were set to zero. The load was then applied centrically at the middle point of the steel plate. The total duration of the loading in the stub tests was of 2500 hours. Readings were taken at the following time intervals: every five seconds for the first hour, followed by readings every minute for the next 23 hours, then every 10 minutes for two weeks (350 hours) and finally, every hour until completion of the test. The angle stubs were unloaded upon completion of the 2500-hour period, and creep recovery data was recorded for 250 hours thereafter. Readings for the "unloading" recovery portion of

the test were recorded in time intervals similar to those used for the "loading" portion The compression creep set-up for the angle stubs is shown in Fig. 6.1.

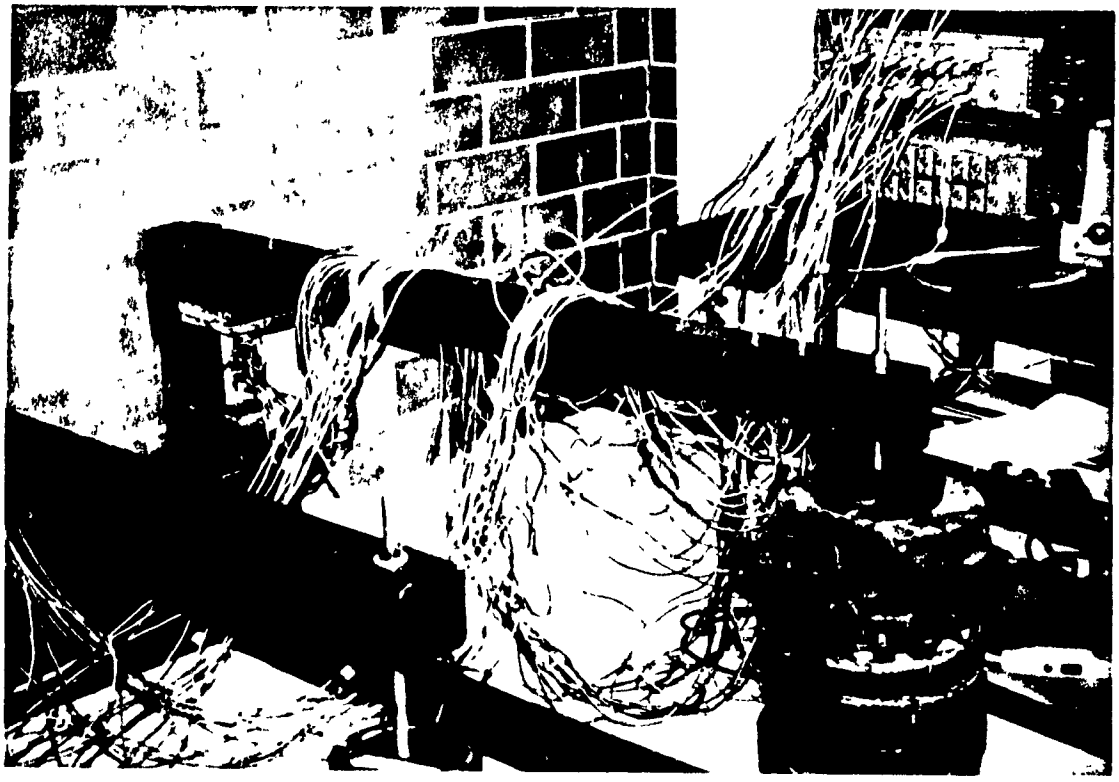

Fig. 6.1 Compression creep set-up for angle stubs

6.2.2 Tests on Coupons

The compression coupon tests were performed using a 31.75 mm (1.15") x 12.7 mm (0.50") x 6.35 mm (0.25") coupon cut from the middle of the angle stub strong leg, of the same size as in the creep test described previously, namely 50.8 mm (2") x 50.8 mm (2") 6.35 mm x (0.25"). The coupons were subjected to an axial load of

14.2 kN (2567 lbs), corresponding to 45% of their ultimate compressive load, as in the angle stub tests. The loads were applied through a lever system. The compression strain data was recorded using two strain gauges mounted on the centre line of opposing faces of the specimen and along the longitudinal fibre direction. The duration of the tests was 2500 hours of loading (the same as for angle stubs), and 250 hours of creep recovery. The intervals between strain readings for loading and unloading parts were the same as those for the compression creep tests on angle stubs. Fig. 6.2 shows the set-up for the compression creep test on coupons.

6.3 Experimental Results

6.3.1 Tests on Angle Stubs

The test results are presented in Figs. 6.3 to 6.6. Strain readings were taken at different locations on the angle stubs, and the lowest strains were measured on Leg 1 and the largest on Leg 2; the average stress was approximately equal to 44 MPa. Tables 6.1 and 6.2 contain a summary of the creepocity and creep recovery values in the angle stubs.

Table 6.1 Summary of the creepocity of the angle stubs

Stub No.	Initial Strain ϵ_0 ($X10^{-6}$)	Creep Values @ 2500 Hours ($X10^{-6}$)	Creepocity (%) @ Time t (Hours)		
			1	24	2500
1	2137	344	4.3	6.9	14.1
2	2159	329	4.0	7.0	15.2
3	2164	304	4.0	6.7	13.9
Total Average	2153±233	325±53	4.1±0.7	6.6±1.0	14.4±2.2

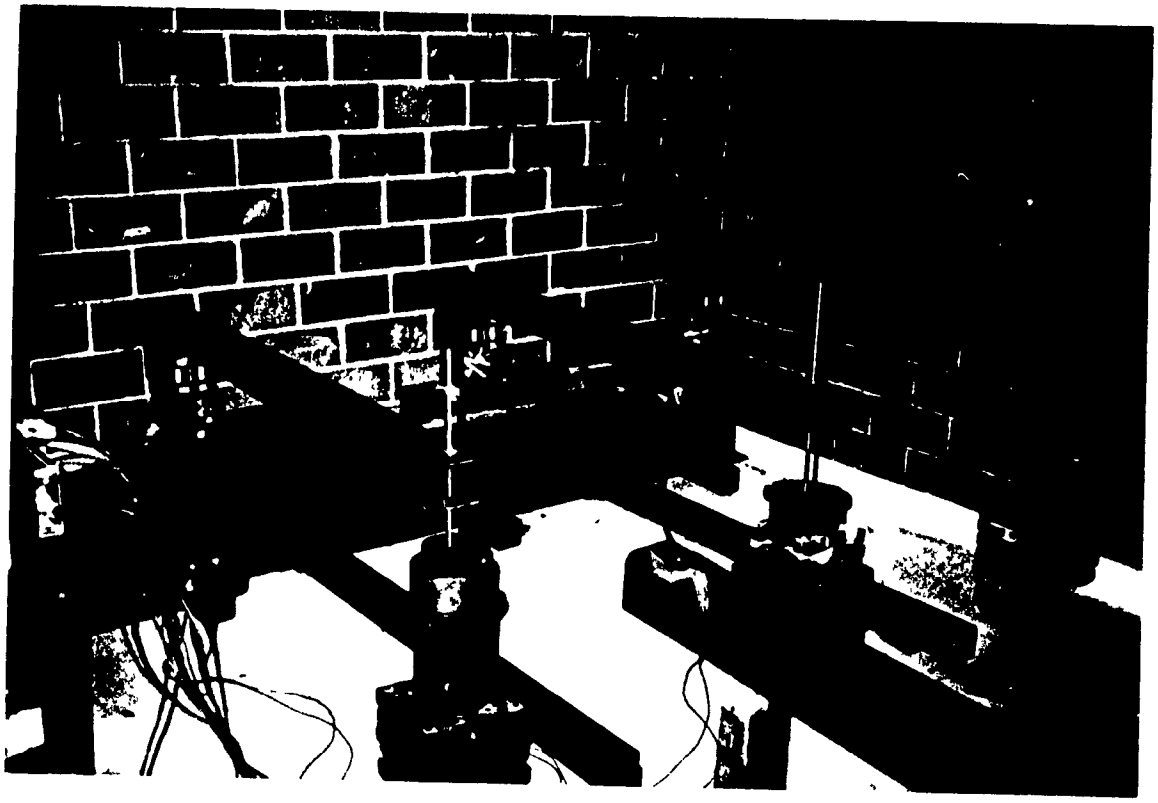

Fig. 6.2. Compression creep coupon test set-up

It was observed that approximately 26% of the total creep strain occurred in the first hour and 45% in the first 24 hours. Note that the rate of creep is different in the two legs; the lowest rate being observed in Leg 1, the strongest and stiffest of the two.

Table 6.2 Summary of the creep recovery values of the angle stubs

Stub No.	Initial Recovery ($X10^{-6}$)	Recovery Values @250 Hours ($X10^{-6}$)	Recovery Rate (%) @ Time t (Hours)			
			1 Min	1	24	250
1	-2137	228	10.4	24.3	42.3	66.2
2	-2154	223	12.5	25.5	44.9	67.0
3	-2184	208	15.3	28.1	46.6	67.4
Total Average	-2158±235	220±29	13±3	26±3	45±4	67±2

The strain recovery was achieved in both Leg 1 and Leg 2 after only a few minutes of unloading, for all the angle stubs tested. Tables 6.3 to 6.5 contain data for creepocity and Tables 6.6 to 6.8 show measurements of creep recovery at selected times.

Table 6.3 Summary of data for creepocity at selected times on Angle Stub No.1

Time t (Hours)	Leg No	No 1						No 2						Total Average
	Gauge No	1	2	3	4	6	Average	7	8	9	11	12	Average	
	Initial strain	1893	1894	2181	2041	1714	1945±157	1953	2484	2195	2599	2411	2328±229	2137±275
1	Strain Creepocity at Time t	74	100	90	70	100	87±13	80	111	92	104	82	94±12	91±13
24		138	173	157	136	176	156±17	135	170	158	174	133	154±17	155±17
100		176	228	214	167	222	201±25	166	220	204	226	176	198±24	200±24
500		219	300	280	221	284	261±34	215	297	265	292	223	258±34	260±34
1000		243	339	325	247	327	296±42	239	339	299	331	252	292±40	294±41
2000		277	378	366	283	365	334±44	264	372	335	380	277	326±48	330±46
2500		280	394	376	292	389	346±50	274	395	352	391	291	341±50	344±50
1	Strain Creepocity at Time t to Initial Strain (%)	3 9	5 3	4 1	3 4	5 8	4 5±0 9	4 1	4 5	4 2	4 0	3 4	4 0±0 4	4 3±0 7
24		6 8	8 4	6 7	6 3	9 4	7 5±1 2	6 4	6 4	6 7	6 3	5 2	6 2±0 5	6 9±1 1
100		8 6	11 0	9 1	7 7	11 8	9 6±1 5	7 9	8 2	8 6	8 1	6 8	7 9±0 6	8 8±1 4
500		10 5	13 8	11 4	9 9	14 3	12±1 8	10 0	10 7	10 9	10 2	8 5	10 1±0 8	11 1±1 7
1000		11 5	15 3	13 1	10 8	16 2	13 4±2 1	11 0	12 1	12 1	11 4	9 5	11 2±1 0	12 3±2 0
2000		13 0	16 8	14 6	12 3	17 8	14 9±2 1	12 3	13 2	13 5	13 0	10 4	12 5±1 1	13 7±2 1
2500		12 8	17 4	14 8	12 6	18 8	15 3±2 5	12 4	13 9	14 0	13 2	10 9	12 9±1 1	14 1±2 3
1	Strain Creepocity at Time t to Total Creepocity (%)	26 4	25 4	23 9	24 0	25 7	25 1±1 0	29 2	28 1	26 1	26 6	28 3	27 7±1 1	26 4±1 7
24		49 9	43 9	41 8	46 6	45 2	45 5±2 7	49 3	43 0	44 9	44 5	45 9	45 5±2 1	45 5±2 4
100		62 9	57 9	56 9	57 2	57 1	58 4±2 3	61 0	55 7	58 0	57 8	61 7	58 8±2 2	58 6±2 3
500		78 2	76 1	74 5	75 7	67 1	74 3±3 8	78 5	75 2	75 3	74 7	76 9	76 1±1 4	75 2±3 0
1000		86 8	86 0	86 4	84 6	84 1	85 6±1 0	87 2	85 3	85 2	84 6	86 6	85 8±1 0	85 7±1 0
2000		99 3	96 2	97 6	97 2	93 8	96 8±1 8	96 7	94 4	95 2	97 2	95 2	95 7±1 0	96 3±1 6
2500		100	100	100	100	100	100	100	100	100	100	100	100	100

Table 6.4 Summary of data for creepocity at selected times on Angle Stub No.2

Time t (Hours)	Leg No	1					2						Total Average
	Gauge No	2	3	5	6	Average	8	9	10	11	12	Average	
	Initial strain	1851	2027	2236	1932	2012±144	2001	2371	2414	2218	2520	2305±180	2159±220
1	Strain Creepocity at Time t	68	99	94	88	87±12	70	74	100	75	93	82±12	85±12
24		119	164	173	157	153±21	119	126	181	128	172	145±26	149±24
100		153	220	224	189	197±29	152	162	236	164	226	188±35	193±33
500		204	277	301	251	258±36	199	211	310	218	302	248±48	253±43
1000		219	314	338	269	285±45	220	228	349	239	343	276±58	281±53
2000		241	354	373	297	316±52	242	265	394	273	386	312±65	314 ±59
2500		249	367	394	312	331±56	259	272	412	289	404	327±67	329 ±62
1	Strain Creepocity at time t to Initial Strain (%)	3 7	4 9	4 2	4 6	4 4±0 5	3 5	3 1	4 1	3 4	3 7	3 6±0 3	4 0 ±0 6
24		6 4	8 1	7 7	8 1	7 6±0 7	6 0	5 3	7 5	5 8	6 8	6 3 ±0 8	7 0 ±1 0
100		8 3	10 9	10 0	9 8	9 8±0 9	7 6	6 8	9 8	7 4	9 0	8 1±1 1	9 0 ±1 3
500		11 0	13 7	13 5	13 0	12 8±1 1	9 9	8 9	12 8	9 8	12 0	10 7±1 5	11 8 ±1 7
1000		11 8	15 5	15 1	13 9	14 1±1 4	11 0	9 6	14 5	10 8	13 6	11 9±1 8	13 0 ±2 0
2000		13 0	17 5	16 7	15 4	15 7±1 7	12 1	11 2	16 3	12 3	15 3	13 4±2 0	14 6 ±2 2
2500		13 5	18 0	17 6	16 1	16 3±1 8	13 0	11 5	17 1	13 0	16 0	14 1±2 1	15 2 ±2 2
1	Strain Creepocity at Time t to Total Creepocity (%)	27 3	27 0	23 9	28 2	26 6±1 6	27 0	27 2	24 3	26 0	23 0	25 5±1 6	26 1 ±1 7
24		47 8	44 7	43 9	50 3	46 7±2 5	46 0	46 3	44 0	44 3	42 6	44 6±1 4	45 7 ±2 2
100		61 4	60 0	56 9	60 6	59 7±1 7	58 7	59 6	57 3	56 7	55 9	57 6±1 3	58 7 ±1 8
500		81 9	75 5	76 4	80 4	78 6±2 7	76 8	77 6	75 2	75 4	74 8	76 0±1 1	77 3 ±2 3
1000		88 0	85 6	85 8	86 2	86 4±0 9	84 9	83 8	84 7	82 7	84 9	84 2±0 9	85 3 ±1 4
2000		96 8	96 5	94 7	95 1	95 8 ±0 9	93 4	97 4	95 6	94 5	95 5	95 3±1 3	95 6 ±1 2
2500		100	100	100	100	100	100	100	100	100	100	100	100

Table 6.5 Summary of data for creepocity at selected times on Angle Stub No.3

Time t (Hours)	Leg No	1							2						Total Average
	Gauge No	1	2	3	4	5	6	Average	7	8	9	11	12	Average	
	Initial strain	1942	1802	1787	2194	2108	2342	2029±204	2205	2374	2266	2299	2347	2298±60	2164±205
1	Strain Creepocity at Time t	80	66	98	73	77	69	77±10	75	107	84	101	105	94±13	86±14
24		137	112	163	127	135	128	134±15	128	177	130	153	166	151±19	143±19
100		175	148	220	169	169	163	174±22	167	226	172	194	213	194±23	184±25
500		231	182	263	215	222	225	223±24	213	298	213	245	269	248±33	236±31
1000		252	210	299	251	240	260	252±26	234	335	221	272	304	273±42	263±36
2000		285	238	333	274	273	285	281±28	253	366	247	291	329	297±45	289±38
2500		296	247	346	281	272	302	291±30	260	380	258	300	388	317±57	304±46
1	Strain Creepocity at time t to Initial Strain (%)	4 1	3 7	5 5	3 3	3 7	2 9	3 9±0 8	3 4	4 5	3 7	4 4	4 5	4 1±0 5	4±0 7
24		7 1	6 1	9 1	5 8	6 4	5 5	6 7±1 2	5 6	7 5	5 7	6 7	7 1	6 6±0 7	6 7±1 0
100		9 0	8 2	12 3	7 7	8 0	7 0	8 7±1 7	7 6	9 6	7 6	8 4	9 1	8 5±0 8	8 6±1 4
500		11 9	10 1	14 7	9 8	10 5	9 6	11 1±1 8	9 7	12 6	9 4	7 6	8 4	9 5±1 7	10 3±1 9
1000		13 0	11 7	16 7	11 4	11 4	11 1	12 6±2	10 6	14 1	9 8	11 8	12 9	11 8±1 5	12 2±1 8
2000		14 7	13 7	18 6	12 5	13 0	12 2	14 1±2 2	11 5	15 4	10 9	12 7	14 0	12 9±1 6	13 5±2 0
2500		15 2	13 7	19 4	12 8	12 9	12 9	14 5±2 4	11 8	16 0	11 4	13 0	14 4	13 3±1 7	13 9±2 2
1	Strain Creepocity at Time t to Total Creepocity (%)	27 0	26 7	28 3	26 0	28 3	22 8	26 5±1 9	28 8	28 2	32 6	33 7	31 7	31±2 1	28 8±3 0
24		46 3	45 3	47 1	45 2	49 6	42 4	46 ±2 2	49 2	46 6	50 4	51 0	49 1	49 3±1 5	47 7±2 5
100		59 1	60 0	63 6	60 0	62 1	54 0	59 8 ±3	64 2	60 3	66 7	64 7	63 0	63 8±2 1	61 8 ±3 3
500		78 0	73 7	76 0	76 5	81 6	74 5	76 7 ±2 6	81 9	78 4	82 6	81 7	79 6	80 8±1 6	78 8 ±3 0
1000		85 1	85 0	86 4	89 3	88 2	86 1	86 7 ±1 6	90 0	88 2	85 7	90 7	89 9	88 9±1 8	87 8 ±2 0
2000		96 3	96 4	96 2	97 5	100 0	94 4	96 8 ±1 7	97 3	96 3	95 7	97 0	97 3	96 7±0 6	96 8 ±1 3
2500		100	100	100	100	100	100	100	100	100	100	100	100	100	100

Table 6.6 Summary of data for creep recovery at selected times on Angle Stub No.1

Time t (Hours)	Leg No	1						2						Total Average
	Gauge No	1	2	3	4	6	Average	7	8	9	11	12	Average	
	Initial Recovery	282	380	390	302	405	352 ±50	282	380	331	400	280	335 ±49	344 ±50
1 Min	Strain Recovery at Time t	35	26	48	49	16	35 ±13	45	19	39	35	30	34 ±9	35 ±11
1		77	72	99	80	72	80 ±10	87	73	80	101	76	83 ±10	82 ±10
24		112	142	161	120	164	140 ±21	142	146	143	170	141	148 ±11	144 ±17
50		133	163	186	141	188	162 ±23	151	174	160	197	151	167 ±17	165 ±20
100		166	189	229	176	218	196 ±24	164	201	182	224	164	187 ±23	192 ±24
200		175	215	234	189	252	213 ±28	180	231	207	253	190	212 ±27	213 ±27
250		187	232	252	203	273	229 ±31	196	245	219	268	202	226 ±27	228 ±29
1 Min	Strain Recovery at Time t to Initial Strain (%)	1 8	1 4	2 2	2 4	0 9	1 8 ±0 5	2 3	0 8	1 8	1 3	1 2	1 5 ±0 5	1 7 ±0 5
1		4 1	3 8	4 5	3 9	4 2	4 1 ±0 3	4 5	2 9	3 6	3 9	3 2	3 6 ±0 5	3 9 ±0 5
24		5 9	7 5	7 4	5 9	9 6	7 2 ±1 3	7 3	5 9	6 5	6 5	5 8	6 4 ±0 5	6 8 ±1 1
50		7 0	8 6	8 5	6 9	11 0	8 4 ±1 5	7 7	7 0	7 3	7 6	6 3	7 2 ±0 5	7 8 ±1 3
100		8 8	10 0	10 5	8 6	12 7	10 1 ±1 5	8 4	8 1	8 3	8 6	6 8	8 0 ±0 6	9 1 ±1 5
200		9 2	11 4	10 7	9 3	14 7	11 1 ±2 0	9 2	9 3	9 4	9 7	7 9	9 1 ±0 6	10 1 ±1 8
250		9 9	12 2	11 6	9 9	15 9	11 9 ±2 2	10 0	9 9	10 0	10 3	8 4	9 7 ±0 7	10 8 ±2 0
1 Min	Strain Recovery at Time t to Final Recovery (%)	12 3	6 8	12 3	16 2	4 0	10 3 ±4 4	16 0	5 0	11 7	8 8	10 7	10 4 ±3 6	10 4 ±4 0
1		27 0	18 9	25 4	26 5	17 8	23 1 ±3 9	30 9	19 2	24 0	25 6	27 1	25 4 ±3 8	24 3 ±4 0
24		39 3	37 4	41 3	39 7	40 5	39 6 ±1 3	50 4	38 4	43 0	42 5	50 4	44 9 ±4 7	42 3 ±4 4
50		46 7	42 9	47 7	46 7	46 4	46 1 ±1 6	53 4	45 8	48 0	49 3	53 9	50 1 ±3 1	48 1 ±3 2
100		58 2	49 7	58 7	58 3	53 8	55 7 ±3 5	58 2	52 9	54 7	56 0	58 6	56 1 ±2 1	55 9 ±2 9
200		61 4	56 6	60 0	62 6	62 2	60 6 ±2 2	63 8	60 8	62 2	63 3	67 9	63 6 ±2 4	62 1 ±2 7
250		65 6	61 6	64 6	67 2	67 4	65 3 ±2	65 9	64 8	65 8	67 1	72	67 ±2 5	66 2 ±2 5
1 Min	Strain Recovery at Time t to Total Recovery (%)	18 7	11 2	19 0	24 1	5 9	15 8 ±6 4	23 0	7 8	17 8	13 1	14 9	15 3 ±5 0	15 6 ±5 8
1		41 2	31 0	39 3	39 4	26 4	35 5 ±5 7	44 4	29 8	36 5	25 6	37 6	34 8 ±6 5	35 2 ±6 2
24		59 9	61 2	63 9	59 7	60 1	57 0 ±8 7	72 4	59 6	65 0	62 4	69 8	66 ±4 6	6 6 ±8 3
50		71 1	70 7	73 8	69 5	68 9	70 7 ±1 7	77 3	71 0	73 0	73 5	74 6	73 8 ±2 0	72 3 ±2 4
100		88 9	81 5	90 9	86 9	79 9	85 6 ±4 2	83 7	82 0	82	83 6	81 2	82 7 ±1 0	84 2 ±3 4
200		93 6	92 7	92 9	93 1	92 3	92 9 ±0 4	95 8	94 3	94 5	94 4	96	95 ±0 1	95 4 ±0 9
250		100	100	100	100	100	100	100	100	100	100	100	100	100

Table 6.7 Summary of data for creep recovery at selected times on Angle Stub No.2

Time t (Hours)	Leg No.	1					2						Total Average
	Gauge No.	2	3	5	6	Average	8	9	10	11	12	Average	
	Initial Recovery	262	370	395	318	336 ±51	262	277	413	283	419	331 ±70	334 ±62
1 Min	Strain Recovery at Time t	32	40	46	40	40 ±5	36	39	50	33	60	44 ±10	42 ±8
1		68	86	100	83	84 ±11	66	79	106	75	97	85 ±15	85 ±13
24		121	164	164	153	151 ±18	133	123	170	124	184	147 ±25	149 ±22
50		139	186	190	171	172 ±20	141	140	191	145	195	162 ±25	167 ±23
100		150	207	213	184	189 ±25	151	161	223	158	228	184 ±34	187 ±30
200		171	236	244	210	215 ±28	173	182	255	183	260	211 ±38	213 ±34
250		179	244	256	215	224 ±30	184	190	267	193	271	221 ±39	223 ±35
1 Min	Strain Recovery at Time t to Initial Strain (%)	1 7	2 0	2 1	2 1	2 0 ±0 1	1 8	1 6	2 1	1 5	2 4	1 9 ±0 3	2 0 ±0 3
1		3 7	4 2	4 5	4 3	4 2 ±0 3	3 3	3 3	4 4	3 4	3 8	3 7 ±0 4	4 0 ±0 5
24		6 5	8 1	7 3	7 9	7 5 ±0 6	6 6	5 2	7 0	5 6	7 3	6 4 ±0 8	7 0 ±0 9
50		7 5	9 2	8 5	8 9	8 5 ±0 6	7 0	5 9	7 9	6 5	7 7	7 0 ±0 7	7 8 ±1 0
100		8 1	10 2	9 5	9 5	9 3 ±0 8	7 5	6 8	9 2	7 1	9 0	7 9 ±1 0	8 6 ±1 1
200		9 2	11 6	10 9	10 9	10 7 ±0 9	8 6	7 7	10 6	8 3	10 3	9 1 ±1 1	9 9 ±1 3
250		9 7	12 0	11 4	11 1	11 1 ±0 9	9 2	8 0	11 1	8 7	10 8	9 5 ±1 2	10 3 ±1 3
1 Min	Strain Recovery at Time t to Final Recovery (%)	12 3	10 8	11 6	12 6	11 8 ±0 7	13 7	14 1	12 1	11 7	14 3	13 2 ±1 1	12 5 ±1 1
1		25 9	23 2	25 3	26 1	25 1 ±1 1	25 2	28 5	25 7	26 5	23 2	25 8 ±1 7	25 5 ±1 5
24		46 2	44 3	41 5	48 1	45 0 ±2 4	50 8	44 4	41 2	43 8	43 9	44 8 ±3 2	44 9 ±2 9
50		50 1	50 3	48 1	53 8	50 6 ±2 1	53 8	50 5	46 2	51 2	46 5	49 6 ±2 9	50 1 ±2 6
100		57 3	55 9	53 9	57 9	56 3 ±1 5	57 6	58 1	54 0	55 8	54 4	56 0 ±1 6	56 2 ±1 6
200		65 3	63 8	61 8	66 0	64 2 ±1 6	66 0	65 7	61 7	64 7	62 1	64 0 ±1 8	64 1 ±1 7
250		68 3	65 9	64 8	67 6	66 7 ±1 4	70 2	68 6	64 4	68 2	64 7	67 2 ±2 3	67 0 ±2 0
1 Min	Strain Recovery at Time t to Total Recovery (%)	17 9	16 4	18 0	18 6	17 7 ±0 8	19 6	20 5	18 7	17 1	22 1	19 6 ±1 7	18 7 ±1 7
1		38 0	35 2	39 1	38 6	37 7 ±1 5	35 9	41 6	39 7	38 9	35 8	38 4 ±2 2	38 1 ±2 0
24		67 6	67 2	64 1	71 2	67 5 ±2 5	72 3	64 7	63 7	64 2	67 9	66 6 ±3 2	67 1 ±3 0
50		77 7	76 2	74 2	79 5	76 9 ±1 9	76 6	73 7	71 5	75 1	72 0	73 8 ±1 9	75 4 ±2 5
100		83 8	84 3	83 2	85 6	84 2 ±0 9	82 1	84 7	83 5	81 7	84 1	83 2 ±1 1	83 7 ±1 2
200		95	96 7	95 3	97 7	96 3 ±1 0	94 2	95 8	95 5	94 8	96 0	95 3 ±0 7	95 8 ±1 0
250		100	100	100	100	100	100	100	100	100	100	100	100

Table 6.8 Summary of data for creep recovery at selected times on Angle Stub No.3

Time t (Hours)	Leg No	1							2						Total Average
	Gauge No	1	2	3	4	5	6	Average	7	8	9	11	12	Average	
	Initial Recovery	285	254	352	195	198	191	246 ±59	263	383	276	308	318	321 ±42	284 ±61
1 Min	Strain Recovery at Time t	27	42	57	37	45	49	43 ±9	34	50	63	50	33	44 ±11	46 ±10
1		66	69	105	76	87	87	82 ±13	73	104	96	96	70	92 ±14	87 ±14
24		118	120	179	132	141	134	137 ±20	125	164	143	147	145	150 ±12	144 ±18
50		135	132	197	149	160	150	154 ±21	139	193	158	170	158	170 ±18	162 ±20
100		155	144	214	163	172	167	169 ±22	151	214	171	186	180	188 ±21	179 ±22
200		176	162	238	186	188	188	190 ±23	175	241	189	209	207	212 ±22	201 ±24
250		185	170	243	195	198	191	197 ±22	180	247	196	215	217	219 ±23	208 ±24
1 Min	Strain Recovery at Time t to Initial Strain(%)	1 4	2 3	3 2	1 7	2 1	2 1	2 1 ±0 6	1 5	2 1	2 8	2 2	1 4	2 1 ±0 5	2 1 ±0 5
1		3 4	3 8	5 9	3 5	4 1	3 7	4 1 ±0 8	3 3	4 4	4 2	4 2	3 0	3 9 ±0 6	4 ±0 7
24		6 1	6 7	10 0	6 0	6 7	5 7	6 9 ±1 5	5 7	6 9	6 3	6 4	6 2	6 4 ±0 4	6 7 ±1 1
50		7 0	7 3	11 0	6 8	7 6	6 4	7 7 ±1 5	6 3	8 1	7 0	7 4	6 7	7 3 ±0 6	7 5 ±1 2
100		8 0	8 0	12 0	7 4	8 2	7 1	8 4 ±1 6	6 8	9 0	7 5	8 1	7 7	8 1 ±0 7	8 3 ±1 3
200		9 1	9 0	13 3	8 5	8 9	8 0	9 5 ±1 8	7 9	10 2	8 3	9 1	8 8	9 1 ±0 8	9 3 ±1 4
250		9 5	9 4	13 6	8 9	9 4	8 2	9 8 ±1 7	8 2	10 4	8 6	9 4	9 2	9 4 ±0 9	9 6 ±1 4
1 Min	Strain Recovery at Time t to Final Recovery (%)	9 5	16 5	16 2	12 5	15 7	16 0	14 4 ±2 6	2 9	13 1	22 8	16 2	9 4	15 6 ±4 0	15 ±3 5
1		23 2	27 2	29 8	25 7	30 3	28 3	27 4 ±2 4	27 8	27 2	34 8	31 2	22 0	28 8 ±4 3	28 1 ±3 4
24		41 4	47 2	50 9	44 6	49 1	43 6	46 1 ±2 3	47 5	42 8	5 8	47 7	45 6	47 ±2 9	46 6 ±3 2
50		47 4	52 0	56 0	50 3	55 7	48 9	51 7 ±3 2	52 9	56 4	57 2	55 2	49 7	52 ±1 8	52 4 ±3 1
100		54 4	56 7	60 8	55 1	60 0	54 4	56 9 ±2 6	57 4	55 9	62 0	60 4	56 6	58 7 ±2 3	57 5 ±2 6
200		61 8	63 8	67 6	62 8	65 5	61 2	63 8 ±2 2	66 5	62 9	68 5	67 8	65	66 1 ±2 6	65 ±2 4
250		64 9	66 9	69 0	65 9	68 9	62 2	66 3 ±2 4	68 4	64 5	71 0	69 8	68 2	68 4 ±2 2	67 4 ±2 5
1 Min	Strain Recovery a Time t to Tota Recovery %	15 1	24 7	23 5	9 0	22 7	25 7	2 8 ±2 7	8 9	21 2	22	22 7	5 7	22 9 ±5 6	22 4 ±4 7
1		36 2	41	43 2	29 0	44 0	46 2	4 4 ±3 0	46 6	42 1	49 2	45 1	22 7	42 2 ±5 4	41 8 ±4 4
24		64 3	70 6	72 6	67 7	71 2	71 2	69 6 ±2 9	69 4	66 4	77	69 6	67 2	69 9 ±2 3	69 3 ±2 7
50		77 1	77 6	81	76 4	80 4	78 5	78 ±2 6	77 2	78	85 6	74 5	72 3	77 4 ±2 5	78 ±2 6
100		84 2	84 7	88	82 6	86 9	87 4	85 8 ±1 7	82 9	86 6	87 2	87 1	82 4	85 ± 6	86 ± 7
200		95 7	95 7	98	94 4	96 2	98 4	96 2 ± 5	97 2	97 6	96 4	97 7	95 4	96 9 ± 7	96 6 ± 6
250		100	100	100	97	100	97	99	100	100	100	100	100	100	100

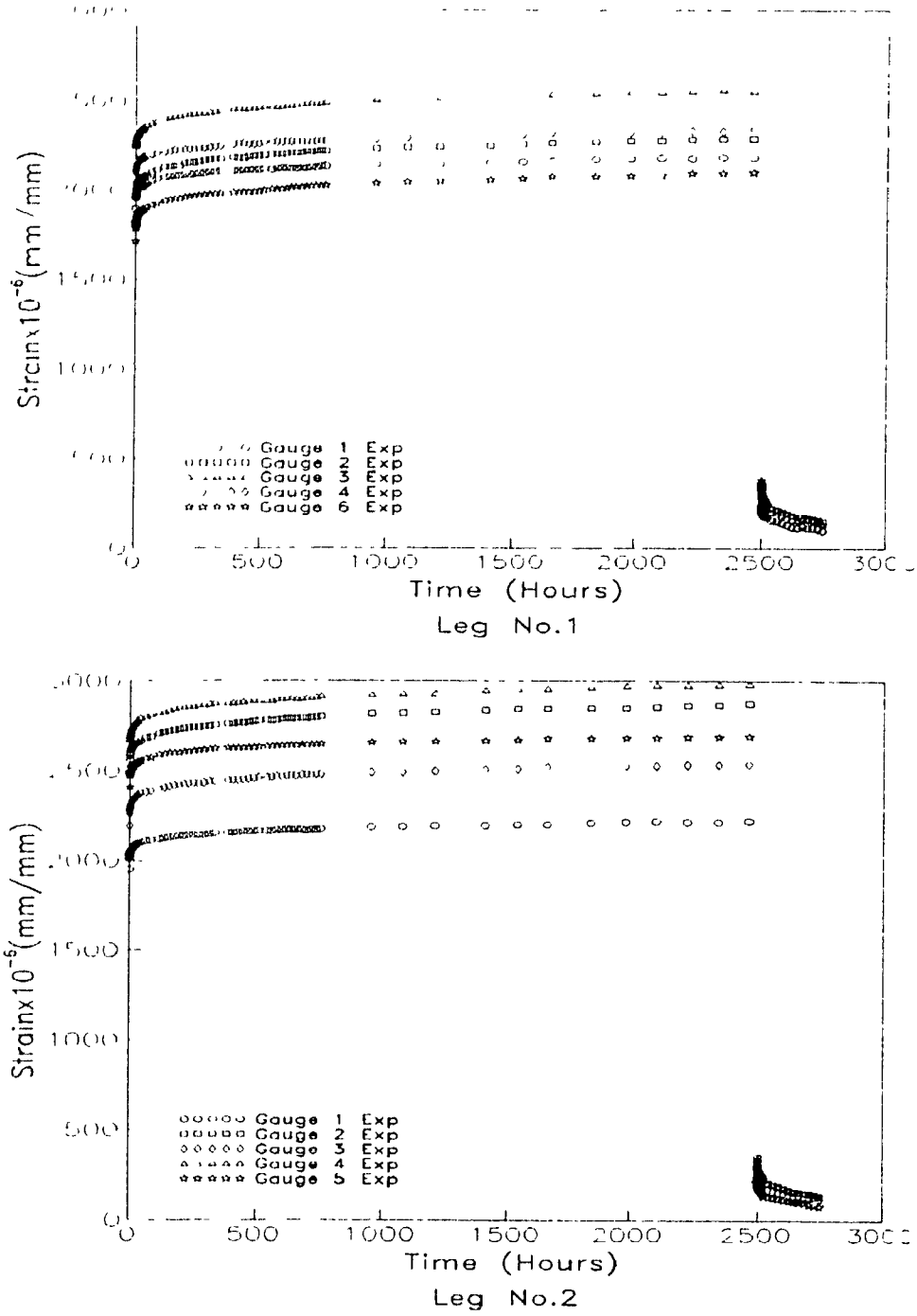

Fig 6.3. Creep and creep recovery of Angle Stub No.1

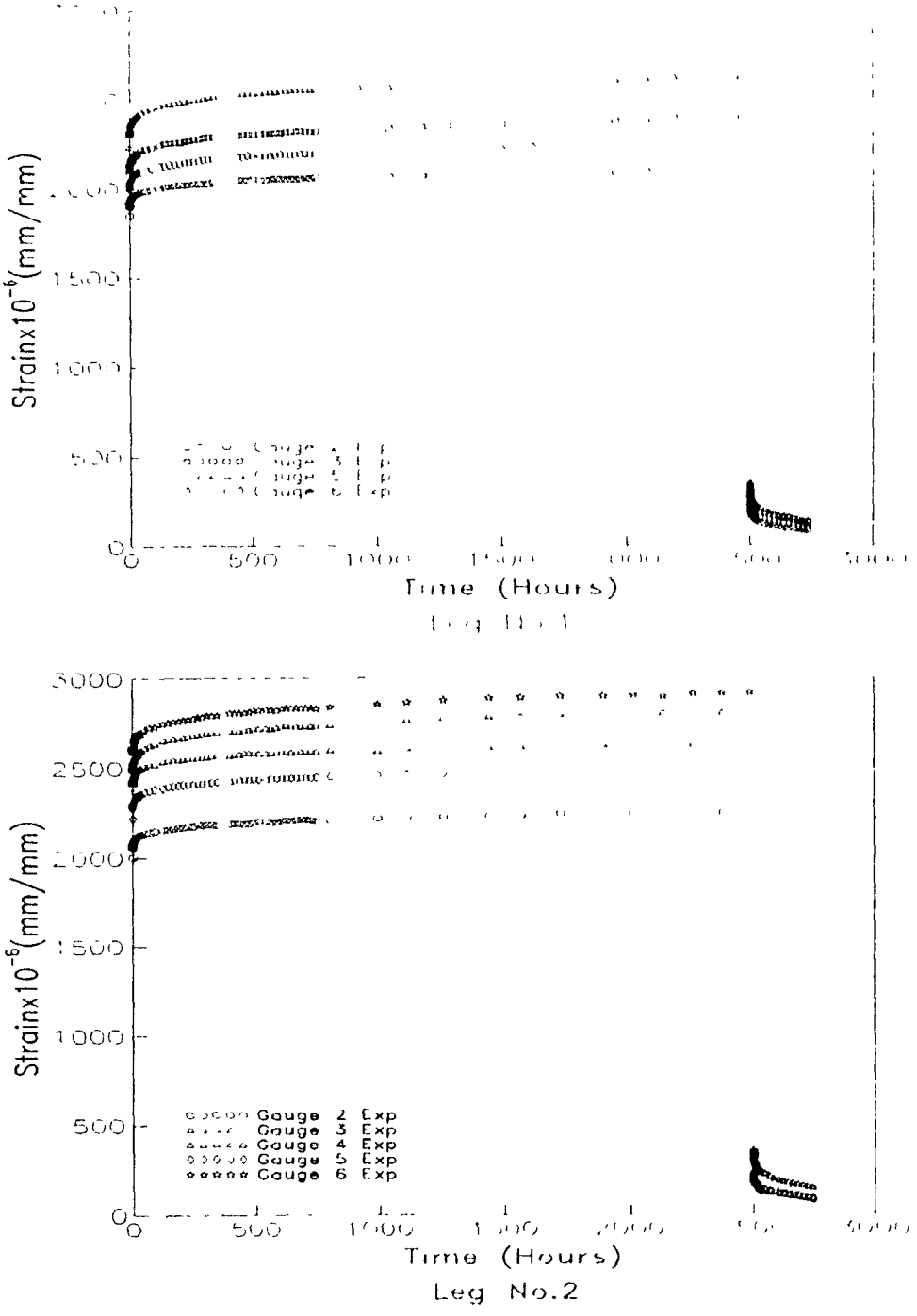

Fig. 6.4. Creep and creep recovery of Angle Stub No 2

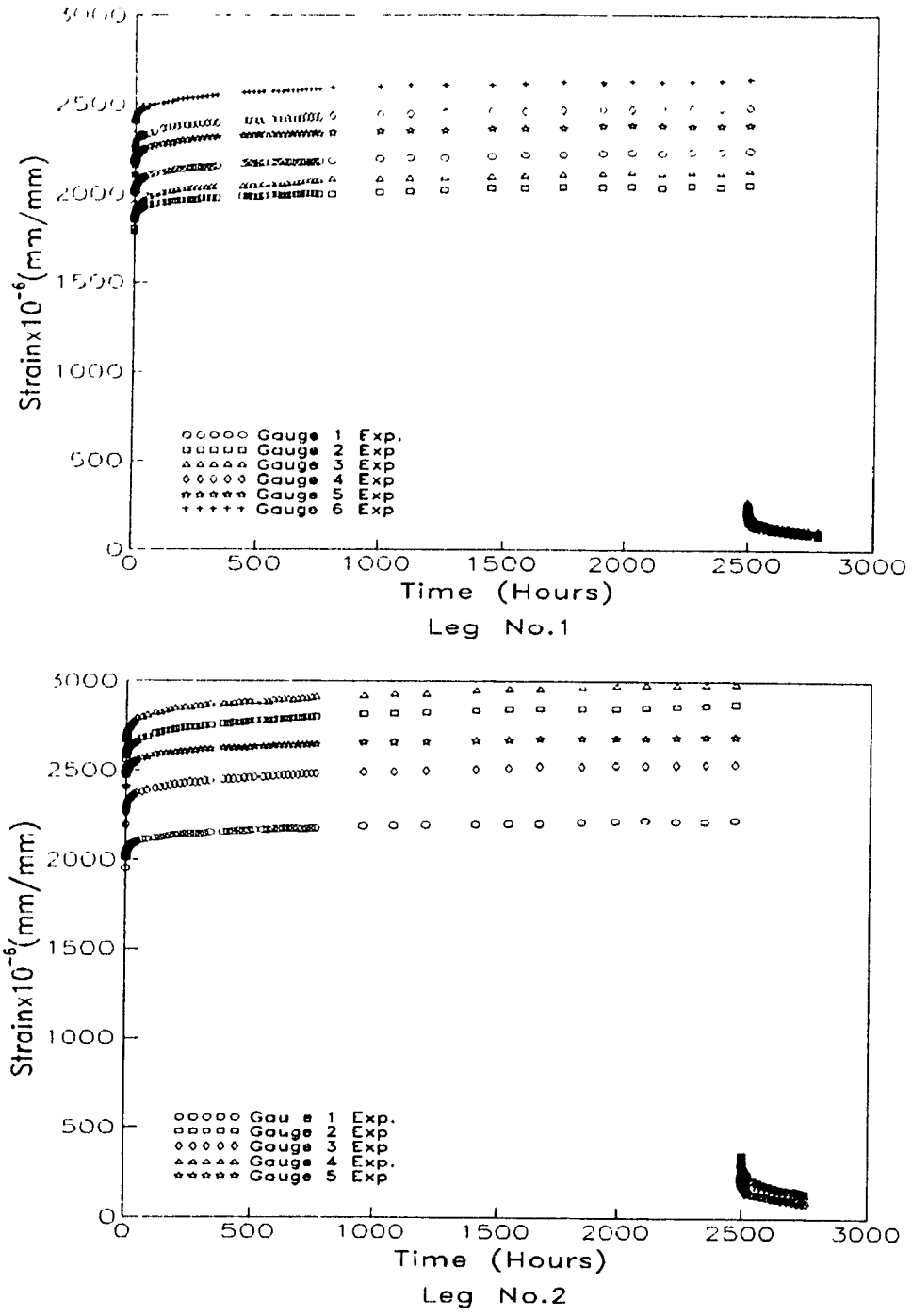

Fig. 6.5. Creep and creep recovery of Angle Stub No.3

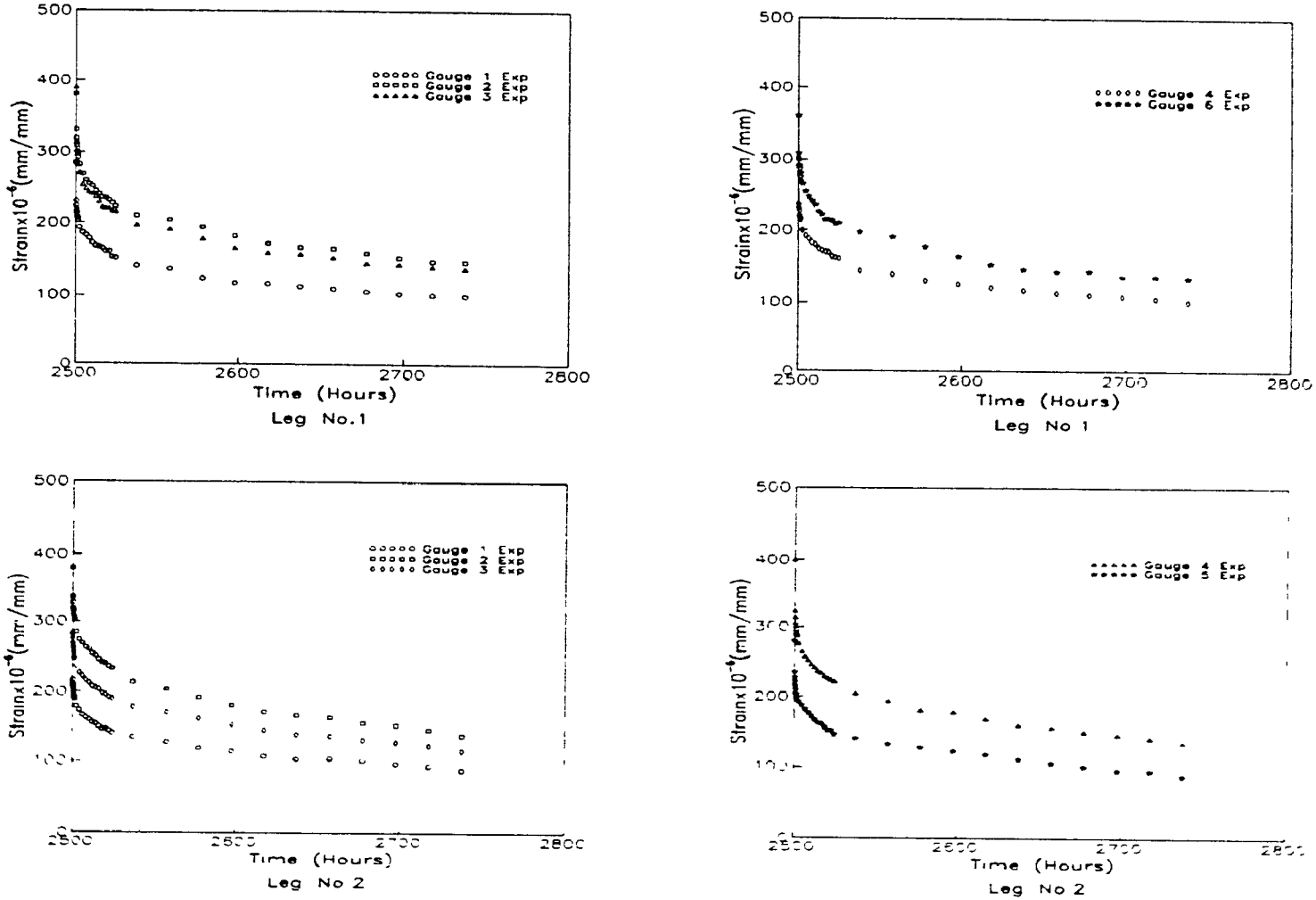

Fig. 6.6. Creep recovery of Angle Stub No.1

6.3.2 Tests on Coupons

Fig. 6 7 shows the creep and recovery curves for the two strain readings of the each coupon tested. Main results are presented in Tables 6.9 and 6.10.

Table 6 9 Summary of creepocity on coupons

Coupon No	Initial Strain ϵ_0 ($X10^{-6}$)	Creep Values @ 2500 Hours ($X10^{-6}$)	Creepocity (%) @ Time t (Hours)			
			1	24	100	2500
1	6715	958	2.0	4 3	6.1	14.3
2	6686	919	1.8	4.2	6 0	13.8
3	6674	889	2 1	4.1	6.0	13.3
Total Average	6691±172	922±101	2.0±0.2	4.2±0.3	6.0±0 6	13.8±1.2

Table 6.10 Summary of recovery values on coupons

Coupon No	Initial Recovery ($X10^{-6}$)	Recovery Values @ 250 Hours ($X10^{-6}$)	Recovery Rate (%) @ Time t (Hours)			
			1 Min	1	24	250
1	-6708	228	5 2	7.5	32	53
2	-6686	223	6.1	8.7	34	54
3	-6627	236	5.0	7 2	33	54
Total Average	-6673±34	229±5	5 4±0.6	7 8±1 2	33±1.7	54±1.3

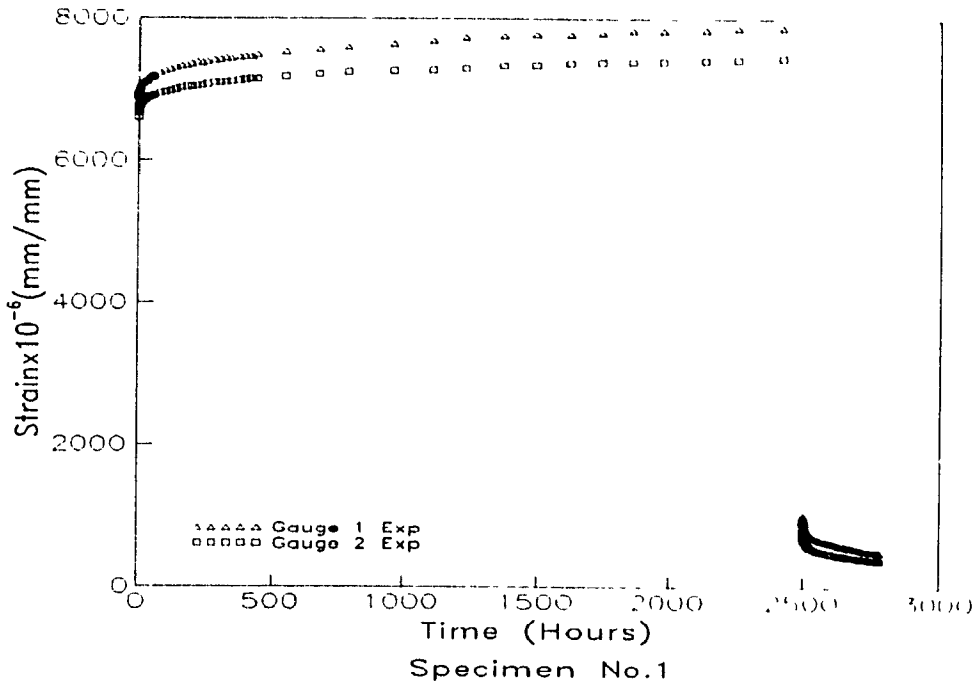

(a)

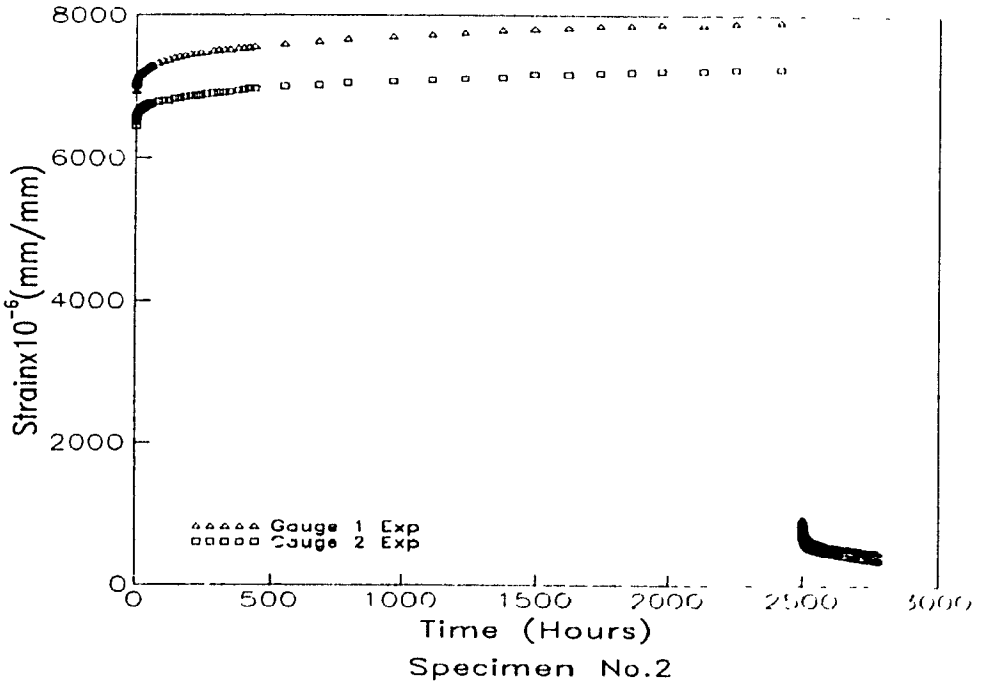

(b)

Fig. 6.7. Creep and creep recovery of coupon tests

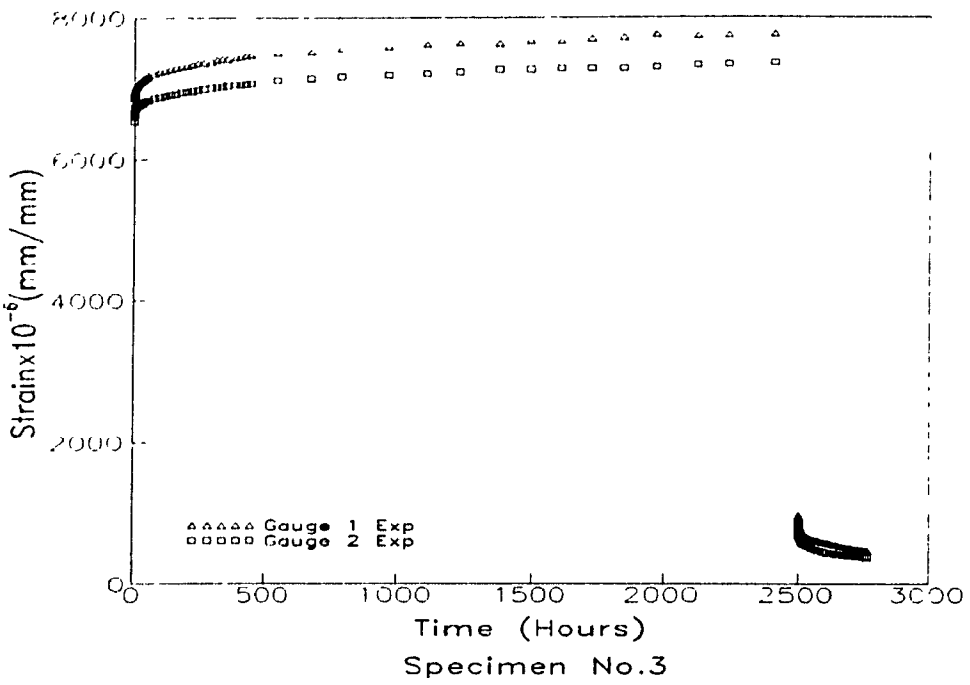

(c)

Fig. 6.7. Creep and creep recovery of coupon tests

The initial strains in coupons were approximately three times the corresponding initial elastic strains in the angle stub creep test. The reason being that the coupons have higher failure loads and the initial stress level was selected as 45 % of the average stress at failure. It was observed that approximately only 15% of the total creep strain occurred in the first hour, 30% in 24 hours and 43% in 50 hours. The creepocities after 50 hours of loading in the coupons are very close to the creepocities in the angle stubs after 24 hours.

Subsequently, a rapid rate of recovery took place for the first few minutes (95%). The recovery continued at a decreasing rate until the end of the 250 hours

of unloading. At that time, approximately only 50% of the total strain had been recovered for the coupons tested. The recovery of the initial compressive strain was achieved after a few minutes for all coupons. Tables 6 11 and 6.12 summarize data for creepocity and creep recovery strains for all coupon tests at selected times. It is interesting to note that the initial creep values and the subsequent recovery values are generally higher in Gauge No.2 (external faces) than those obtained in Gauge No.1 (internal faces).

6.4 Summary

Creep and creep recovery test procedures were fully described in this chapter. These tests are necessary to characterize the long-term behaviour of the pultruded angle stubs and coupons cut from both legs of the angle stubs.

A total of six tests, three samples each for angle stubs and coupons, were conducted in this study. The results showed that the average creepocity obtained in coupons was 13.8% of the total creep, and 14.5% in angle stubs. The stress level in the coupons was three times higher than in the angle stubs, which precludes that adjustments in the creep parameters will be necessary when results from coupons and angle stubs are compared.

Table 6.11 Summary of data for creepocity at selected times on coupons

Time t (Hours)	Coupon No.	1			2			3			Total Average
	Gauge No.	1	2	Average	1	2	Average	1	2	Average	
	Initial strain	6820	6610	6715±105	6934	6438	6686±248	6796	6552	6674±122	6692±172
1	Strain Creepocity at Time t	140	118	129±11	126	118	122±4	149	126	138±12	130±11
24		307	266	287±21	288	267	278±11	315	237	276±39	280±27
100		456	359	408±49	432	365	399±34	452	341	397±56	401±47
500		711	572	642±70	667	560	614±54	706	561	634±73	630±67
1000		847	671	759±88	785	654	720±66	814	660	737±77	739±79
2000		1027	798	913±115	936	783	860±77	936	759	848±89	874±99
2500		1068	847	958±111	1009	828	919±91	976	801	889±88	922 ±101
1	Strain Creepocity at Time t to Initial Strain (%)	2.1	1.8	2 0±0.2	1.8	1 8	1.8±0 0	2 2	1 9	2 1±0.2	2 0 ±0 2
24		4.5	4.0	4.3±0.3	4.2	4.1	4 2±0.1	4.6	3.6	4 1±0 5	4 2 ±0.3
100		6.7	5.4	6.1±0 7	6.2	5 7	6 0±0 3	6.7	5.2	6 0±0 8	6 0 ±0 6
500		10 4	8.7	9 6 ±0.9	9 6	8.7	9.2 ±0.5	10 4	8.6	9.5 ±0 9	9.4 ±0 8
1000		12.4	10 2	11.3±1 1	11.3	10.2	10 8±0 6	12.0	10 1	11 1±1.0	11.1 ±0 9
2000		15.1	12 1	13.6±1 5	13 5	12.2	12.9±0 7	13 8	11 6	12 7±1 1	13 1 ±1 2
2500		15 7	12 8	14 3±1.4	14 6	12 9	13 8±0 8	14.4	12.2	13 3±1 1	13 8 ±1 2
1	Strain Creepocity at Time t to Total Creepocity (%)	13 1	13.9	13.5±0.4	12.5	14 3	13.4±0 9	15 3	15.7	15 5±0 2	14 1 ±1.1
24		28 7	31 4	30 1±1.3	28 5	32.2	30.4±1.9	32.3	29 6	31 0±1.3	30 5 ±1.6
100		42.7	42.4	42 6±0 2	42.8	44.1	43.5±0.7	46.3	42.6	44.5±1.8	43 5 ±1 4
500		66.6	67 5	67 1±0.5	66.1	67.6	66.9±0 8	72.3	70.0	71 2±1 1	68 4 ±2 2
1000		79 3	79 2	79.3±0.0	77 8	79.0	78 4±0 6	83.4	82 4	82 9±0 5	80.2 ±2 0
2000		96 2	94 2	95.2±	92.8	94.6	93 7±0.9	95 9	94 8	95 4±0 6	94 8 ±1 1
2500		100	100	100	100	100	100	100	100	100	100

Table 6.12 Summary of data for creep recovery at selected times on coupons

Time t (Hours)	Coupon No	1			2			3			Total Average
	Gauge No	1	2	Average	1	2	Average	1	2	Average	
	Initial Recovery	1078	851	965 ±114	1009	834	922 ±88	1016	825	921 ±96	936 ±102
1 Min	Strain Creepocity at Time t	54	46	50 ±4	58	53	56 ±3	46	45	46 ±1	51 ±5
1		77	66	72 ±6	77	81	79 ±2	58	71	65 ±7	72 ±8
24		329	285	307 ±22	321	299	310 ±11	334	276	305 ±29	307 ±22
50		393	328	361 ±33	379	340	360 ±20	384	321	353 ±32	358 ±29
100		446	370	408 ±38	444	381	413 ±32	440	381	411 ±30	411 ±33
200		536	432	484 ±52	500	445	473 ±28	516	429	473 ±44	477 ±43
250		565	454	510 ±56	528	468	498 ±30	543	445	494 ±49	501 ±47
1 Min	Strain Recovery at Time t to Initial Strain(%)	0 8	0 7	0 8 ±0 1	0 8	0 8	0 8 ±0 0	0 7	0 7	0 7 ±0 0	0 8 ±0 1
1		2 1	1 8	2 0 ±0 2	2 0	2 1	2 1 ±0 1	1 8	2 0	1 9 ±0 1	2 0 ±0 1
24		4 8	4 3	4 6 ±0 3	4 6	4 6	4 6 ±0 0	4 9	4 2	4 6 ±0 4	4 6 ±0 2
50		5 8	5 0	5 4 ±0 4	5 5	5 3	5 4 ±0 1	5 7	4 9	5 3 ±0 4	5 4 ±0 3
100		6 5	5 6	6 1 ±0 5	6 4	5 9	6 2 ±0 3	6 5	5 8	6 2 ±0 4	6 2 ±0 4
200		7 9	6 5	7 2 ±0 7	7 2	6 9	7 1 ±0 2	7 6	6 5	7 1 ±0 6	7 1 ±0 5
250		8 3	6 9	7 6 ±0 7	7 6	7 3	7 5 ±0 2	8 0	6 8	7 4 ±0 6	7 5 ±0 5
1 Min	Strain Recovery at Time t to Final Recovery (%)	5 0	5 4	5 2 ±0 2	5 7	6 4	6 1 ±0 4	4 5	5 5	5 0 ±0 5	5 4 ±0 6
1		7 1	7 8	7 5 ±0 4	7 6	9 7	8 7 ±1 1	5 7	8 6	7 2 ±1 5	7 8 ±1 2
24		30 5	33 5	32 0 ±1 5	31 8	35 9	33 9 ±2 1	32 9	33 5	33 2 ±0 3	33 0 ±1 7
50		36 5	38 5	37 5 ±1 0	37 6	40 8	39 2 ±1 6	37 8	38 9	38 4 ±0 6	38 4 ±1 3
100		41 4	43 5	42 5 ±1 1	44 0	45 7	44 9 ±0 9	43 3	46 2	44 8 ± 5	44 1 ±1 6
200		49 7	50 8	50 3 ±0 6	49 6	53 4	51 5 ±1 9	50 8	52 0	51 4 ±0 6	51 1 ±1 3
250		52 4	53 3	52 9 ±0 5	52 3	56 1	54 2 ±1 9	53 4	53 9	53 7 ±0 3	53 6 ±1 3
1 Min	Strain Recovery at Time t to Total Recovery (%)	9 6	10 1	9 9 ±0 3	11 0	11 3	11 2 ±0 2	8 5	10 1	9 3 ±0 8	10 1 ±0 9
1		13 6	14 5	14 1 ±0 5	14 6	17 3	16 0 ±1 4	10 7	16 0	13 4 ±2 7	14 5 ±2 1
24		58 2	62 8	60 5 ±2 3	60 8	63 9	62 4 ±1 6	61 5	62 0	61 8 ±0 3	61 6 ±1 8
50		69 6	72 2	70 9 ±1 3	71 8	72 6	72 2 ±0 4	70 7	72 1	71 4 ±0 7	71 5 ±1 0
100		78 9	81 5	80 2 ±1 3	84 1	81 4	82 8 ±1 4	81 0	85 6	83 3 ±2 3	82 1 ±2 2
200		94 9	95 2	95 1 ±0 2	94 7	95 1	94 9 ±0 2	95 0	96 4	95 7 ±0 7	95 2 ±0 6
250		100	100	100	100	100	100	100	100	100	100

CHAPTER 7

RESULTS AND DISCUSSION

7.1 Introduction

In this chapter, comparisons between the experimental creep strains and the theoretical creep strain predictions using Findley's power law (Eq. 2.1) are presented. In addition, the output of the superposition equation is compared to the recovery data from each strain gauge.

The objective of the theoretical analysis was to obtain axial compression creep parameters from the strain gauge data and to use these creep parameters to develop creep models able to predict the long term effect in the angle stub sections. Since most creep information is usually obtained from coupon tests only, without checking the validity of the creep parameters on any shape, these results will allow this validation to be made. Finally the correlation of creep parameters between coupons and stubs is discussed.

7.2 Evaluation of Creep Parameters

To obtain the values of creep parameters m and n for a particular stress level,

Eq. 2.1 was rearranged in the form discussed earlier:

$$\epsilon = \epsilon_0 + m \left(\frac{t}{t_0} \right)^n \qquad (2.1)$$

$$\log (\epsilon - \epsilon_0) = \log m + n \log \left(\frac{t}{t_0} \right) \qquad (2.17)$$

As stated earlier, this relation represents a straight line of slope n and intercept m (at unit time) if log $(\epsilon-\epsilon_0)$ is plotted versus log (t/t_0). These plots were done for all creep data sets obtained from both the angle stub and coupon tests. Figs. 7.1 to 7.4 show the different graphs obtained. It can be seen from these graphs that all curves are nearly parallel and close to straight lines, which indicates that the value of n is constant and independent of stress level. The graphs for both angle stubs and coupons are nearly parallel, but with different intercepts varying with stress level.

Tables 7.1 to 7.3 contain the values of parameters m and n obtained from measurements on the angle stubs using data for the full 2500-hour period. The average values of m and n are 85 and 0.17, respectively. The maximum and minimum values of m were recorded in Angle Stub No.3 and are respectively 101 and 66. Parameter n has a maximum value of 0.185, recorded in Angle Stub No.1 The minimum value of n was 0.147, obtained from Angle Stub No.3.

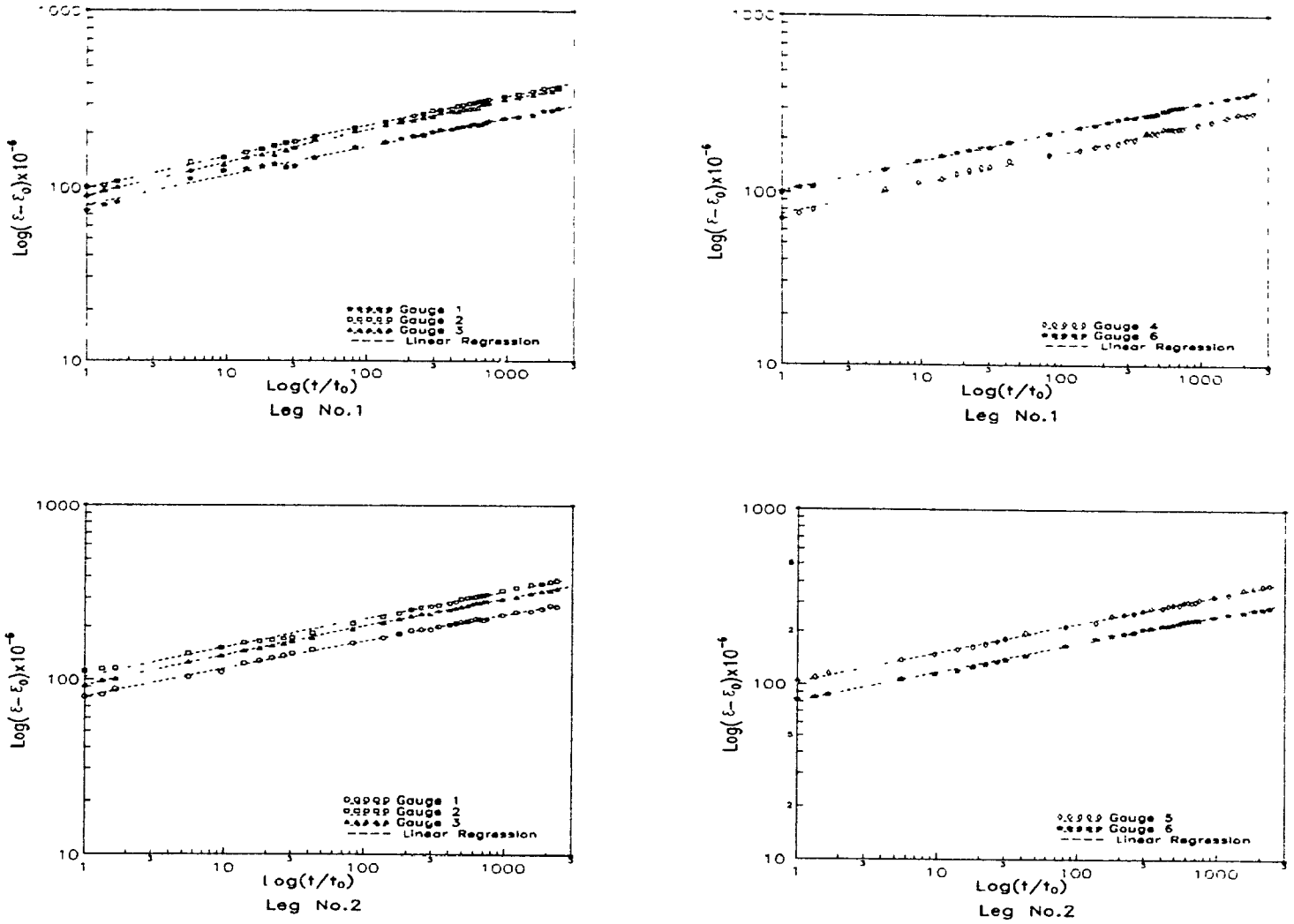

Fig. 7.1. Evaluation of compression creep parameters for Angle Stub No.1

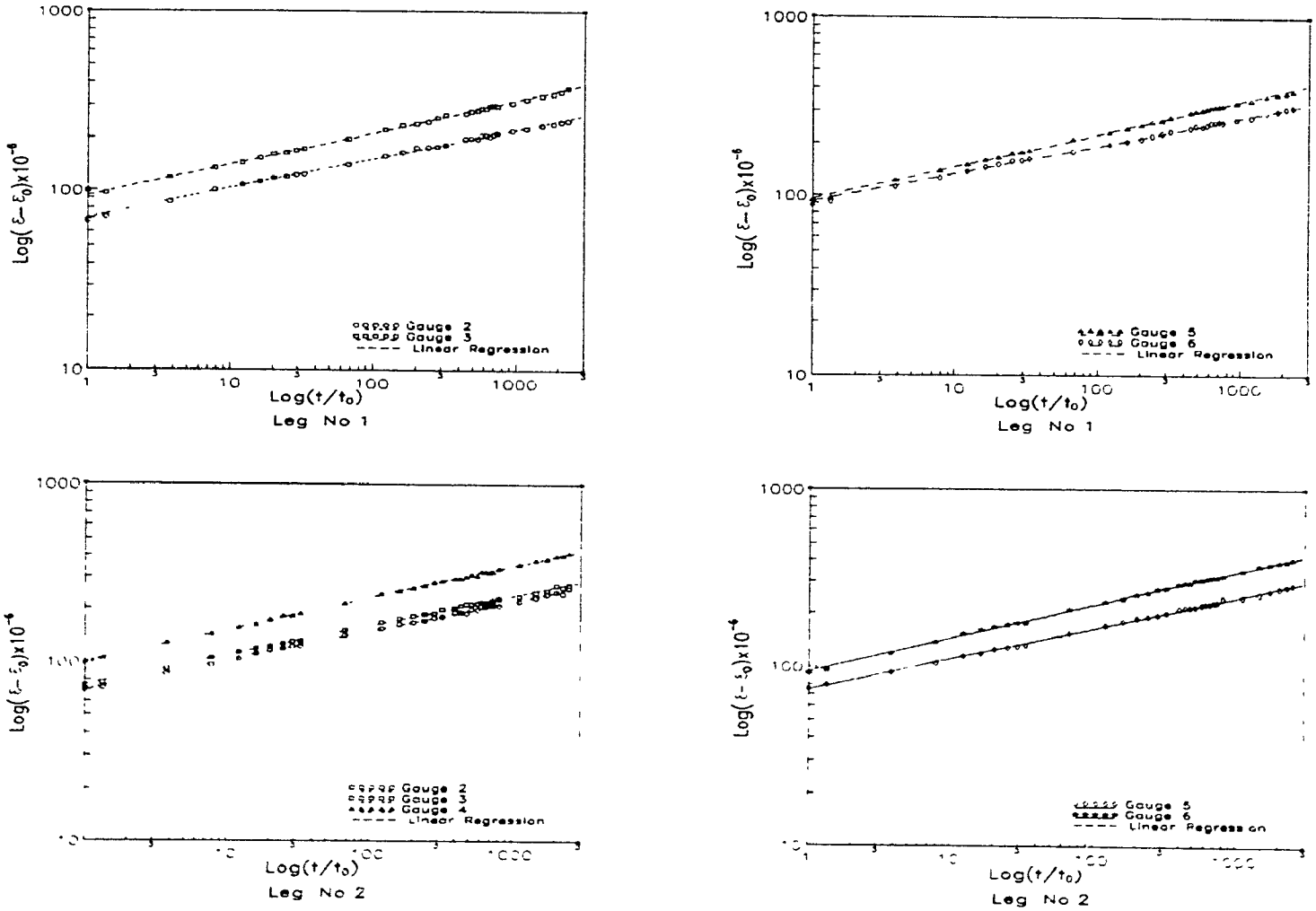

Fig. 7.2. Evaluation of compression creep parameters for Angle Stub No.2

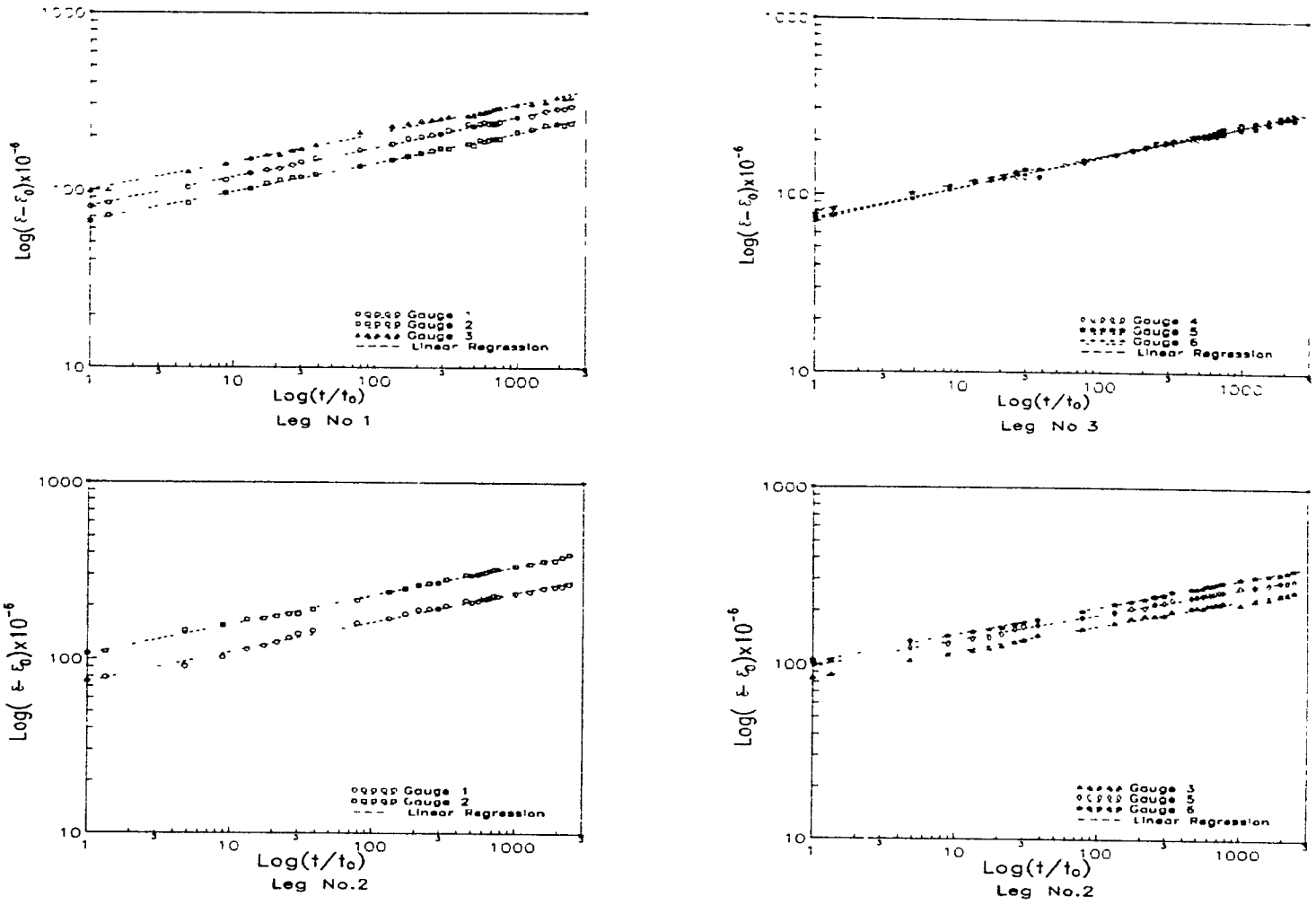

Fig. 7.3. Evaluation of compression creep parameters for Angle Stub No.3

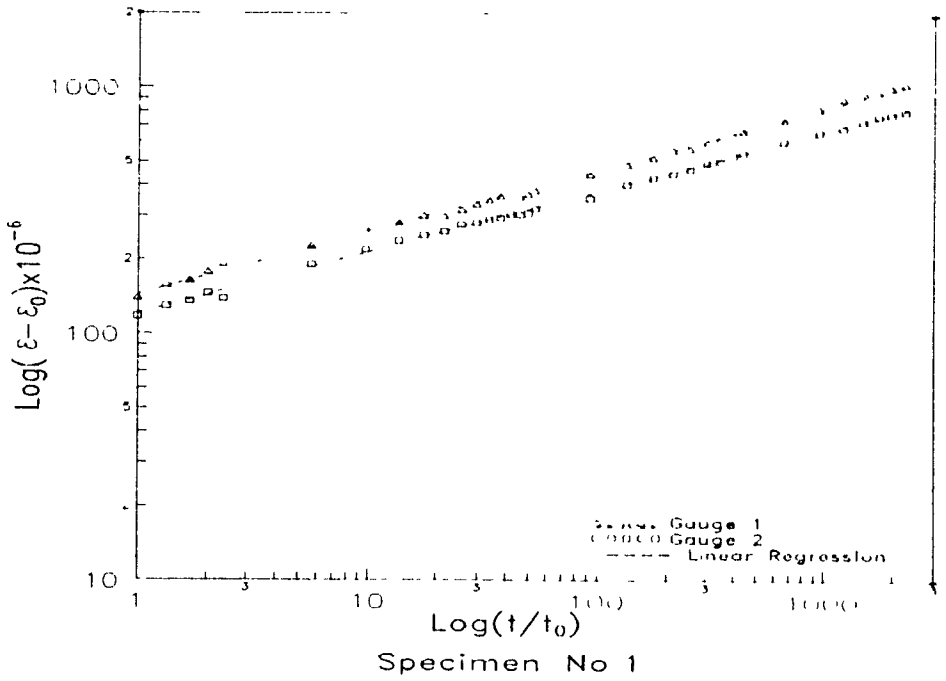

(a)

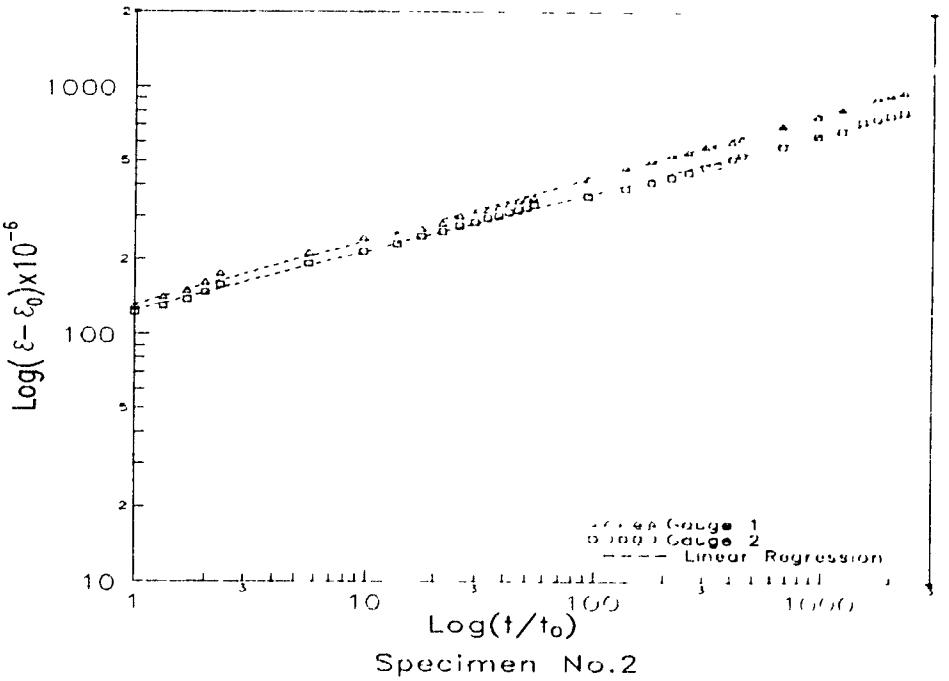

(b)

Fig. 7.4. Evaluation of compression creep parameters for coupons

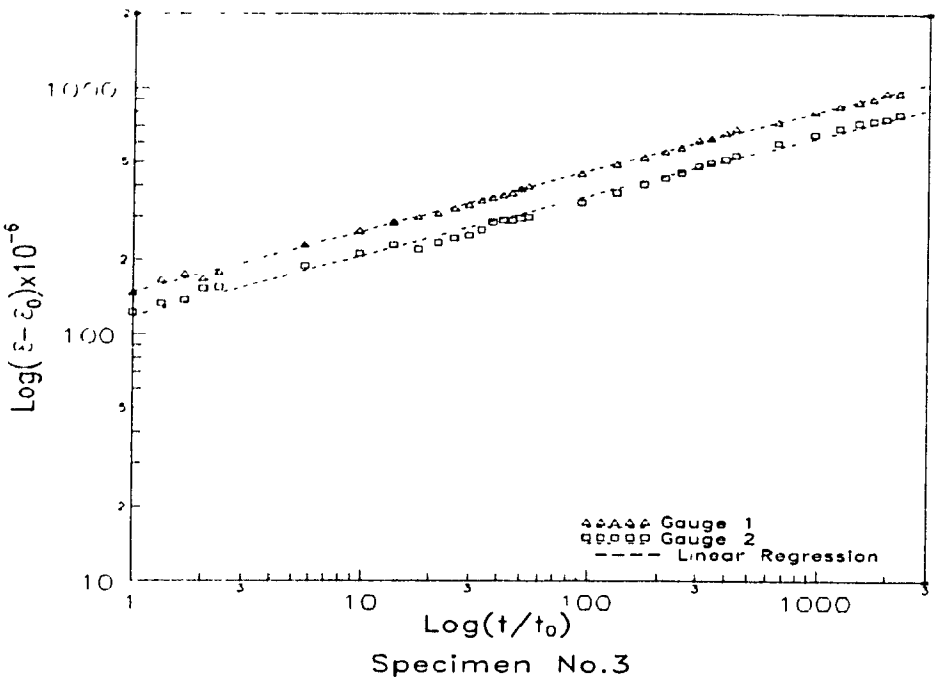

Fig. 7.4. Evaluation of compression creep parameters for coupons

The values of parameters m and n obtained from the coupon tests are also shown in Table 7.4. The maximum and minimum values of m are 132.3 and 112.5, and were obtained in specimen No.3. The variable n has a maximum value of 0.261, which was obtained in specimen No.1, and its minimum value is 0.241, which corresponds to specimen No.2.

Generally the average values of n and m in the coupon tests are 50% higher than those obtained in the stub tests. Note that because angle stubs and coupons were not loaded at the same stress level, it was expected that values would be substantially different.

7.3. Predictions of Creep and Creep Recovery on Angle Stubs

Figs. 7.5 to 7.7 show both the theoretical and experimental creep strain and creep recovery curves obtained for the angle stubs. Theoretical values are in fact predictions according to Findley's model but using creep parameters that fit the experimental measurements. It can be seen that these results are in excellent agreement with each other. The rapid increase in strain in the first 24 hours of loading is shown in Appendix B. For the unloading portion, the predicted strain recovery using the superposition principle agrees very well with the experimental results (as illustrated in Fig. 7.8 and in Appendix B).

Experimental creep values were observed to be slightly higher than theoretical values for upto about 1000 hours, but this trend changed after 1000 hours, as indicated in Tables 7.1 to 7.4.

Table 7.1 Summary of data for creep parameters on Angle Stub No.1

Condition	Leg No	1						2						Total Average
	Gauge No	1	2	3	4	6	Average	7	8	9	11	12	Average	
Creep Parameters	m	79.0	94.3	89.5	73.7	99.8	87±10	78 9	92 6	88.4	96.7	81.3	88±7	87 5±8.3
	n	0.163	0 182	0.182	0.174	0.171	0.17±0 01	0 158	0 184	0.175	0 178	0.162	0.17±0.01	0.17±0 01
Findley's Model	1	79	95	90	74	100	88±10	79	93	89	97	82	88±7	88±8
	500	218	292	278	217	289	259±34	211	291	262	293	223	256±34	258±34
	1000	244	333	316	246	326	293±40	236	331	297	332	250	289±40	291±40
	2500	283	392	372	288	380	343±47	272	391	348	389	289	338±50	341±49
Direct Measurements	1	74	100	90	70	100	87±13	80	111	92	104	82	94±12	91±13
	500	219	300	280	221	284	261±34	215	297	265	292	223	258±34	260±34
	1000	243	339	325	247	327	296±42	239	337	300	331	251	292±40	294±41
	2500	277	394	376	292	389	346±50	274	395	352	391	291	341±50	344±50

Table 7.2 Summary of data for creep parameters on Angle Stub No.2

Condition	Leg No.	1					2						Total Average
	Gauge No.	2	3	5	6	Average	8	9	10	11	12	Average	
Creep Parameters	m	68.3	92.7	93.8	88.8	86±10	68	70	96.2	72.6	90.9	80±12	83±12
	n	0.169	0.181	0 185	0.161	0.17±0.01	0.167	0.172	0.184	0 174	0.190	0.18±0.01	0 18±0.01
Findley's Model	1	68	93	94	89	86 ±11	68	70	96	73	91	80 ±12	83 ±12
	500	195	286	297	242	255 ±40	192	204	302	214	296	242 ±47	249 ±45
	1000	220	325	338	271	289 ±47	216	230	344	242	339	274 ±56	282 ±52
	2500	256	382	399	313	338 ±57	251	269	406	283	402	322 ±68	330 ±64
Direct Measurements	1	68	99	94	88	87 ±12	70	74	100	75	93	82 ±12	85 ±12
	500	204	277	301	251	258 ±36	199	211	310	218	302	248 ±48	253 ±43
	1000	219	314	338	269	285 ±45	220	228	349	239	343	276 ±58	281 ±53
	2500	249	367	394	312	331 ±56	259	272	412	289	404	327 ±67	329 ±62

Table 7.3 Summary of data for creep parameters on Angle Stub No.3

Condition	Leg No	1							2						Total Average
	Gauge No	1	2	3	4	5	6	Average	7	8	9	11	12	Average	
Creep Parameters	m	80 3	65 9	100 9	72 3	79 2	70 1	78±11	78 2	98 1	82 7	92 9	100	90±9	84±12
	n	0 167	0 168	0 157	0 177	0 161	0 187	0 17±0 01	0 157	0 176	0 147	0 151	0 158	0 16±0 01	0 16±0 01
Findley's Model	1	81	66	101	73	79	70	78±11	78	98	83	93	100	90±9	84±12
	500	227	187	268	217	216	224	223±24	208	293	206	238	267	242±34	233±30
	1000	255	211	299	246	241	256	251±26	232	332	229	264	299	271±40	261±34
	2500	297	245	345	289	279	303	293±30	267	389	261	303	344	313±48	303±41
Direct Measurements	1	80	66	98	73	77	69	77±10	75	107	84	101	105	94±13	86±14
	500	231	182	263	215	222	225	223±24	213	298	213	245	269	248±33	236±31
	1000	252	210	299	251	240	260	252±26	234	335	221	272	304	273±42	263±36
	2500	296	247	346	281	272	302	291±30	260	380	258	300	338	307±47	299±40

Table 7.4 Summary of data for creep parameters on coupons

Condition	Coupon No	1			2			3			Total Average
	Gauge No.	1	2	Average	1	2	Average	1	2	Average	
Creep Parameters	m	139.2	120 4	130±9	131.6	124.1	128±4	132.3	112.5	122±10	127±9
	n	0.261	0.249	0.26±0.01	0.259	0.241	0.25±0.01	0.259	0 252	0.26±0 01	0 25±0.01
Findley's Model	1	140	121	131 ±10	133	125	129 ±4	133	113	123 ±10	128 ±9
	500	717	575	646 ±71	668	563	616 ±53	672	547	610 ±63	624 ±64
	1000	850	676	763 ±87	792	659	726 ±67	796	645	721 ±76	737 ±79
	2500	1074	845	960 ±115	998	818	908 ±90	1004	808	906 ±98	925 ±104
Direct Measurements	1	140	118	129 ±11	126	118	122 ±4	149	126	138 ±12	130 ±11
	500	711	572	642 ±70	667	560	614 ±54	706	561	634 ±73	630 ±67
	1000	847	671	759 ±88	785	654	720 ±66	814	660	737 ±77	739 ±79
	2500	1068	847	958 ±111	1009	828	919 ±91	976	801	889 ±88	922 ±101

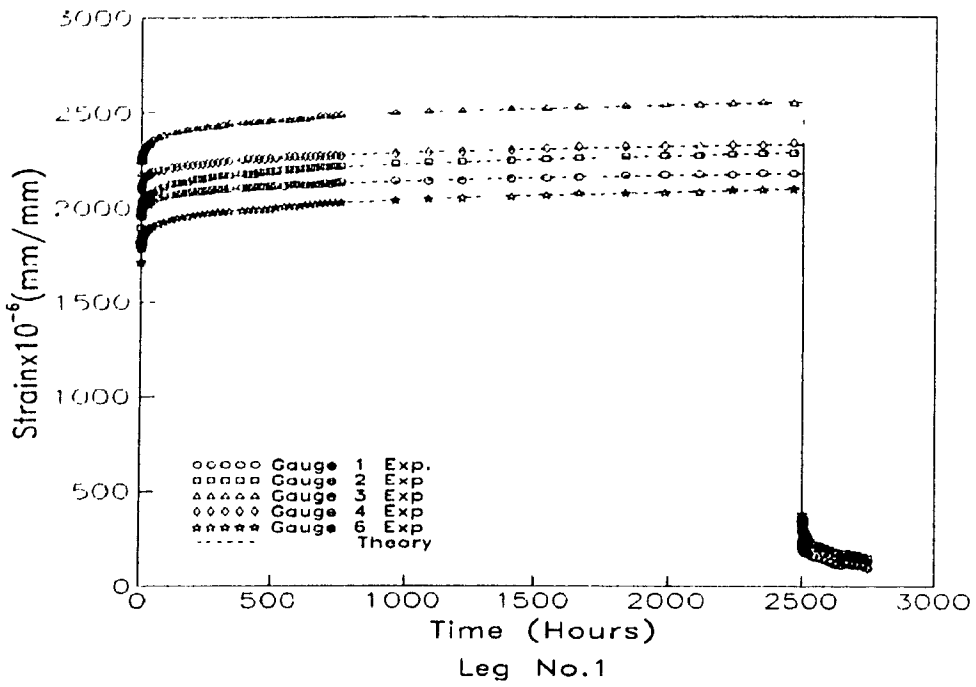

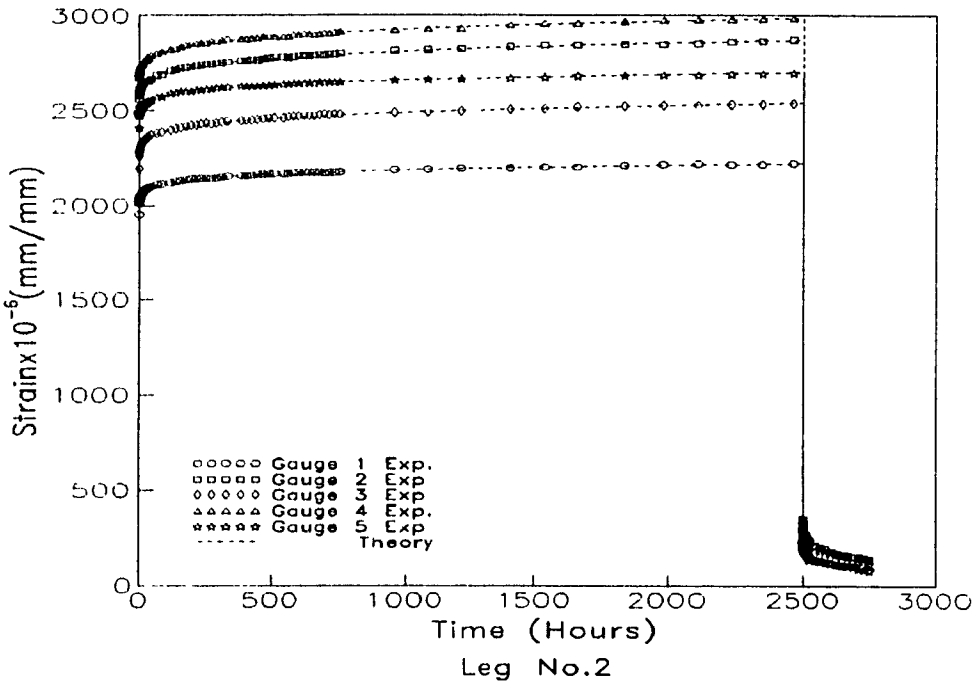

Fig. 7.5. Experimental and theoretical predictions for Angle Stub No.1

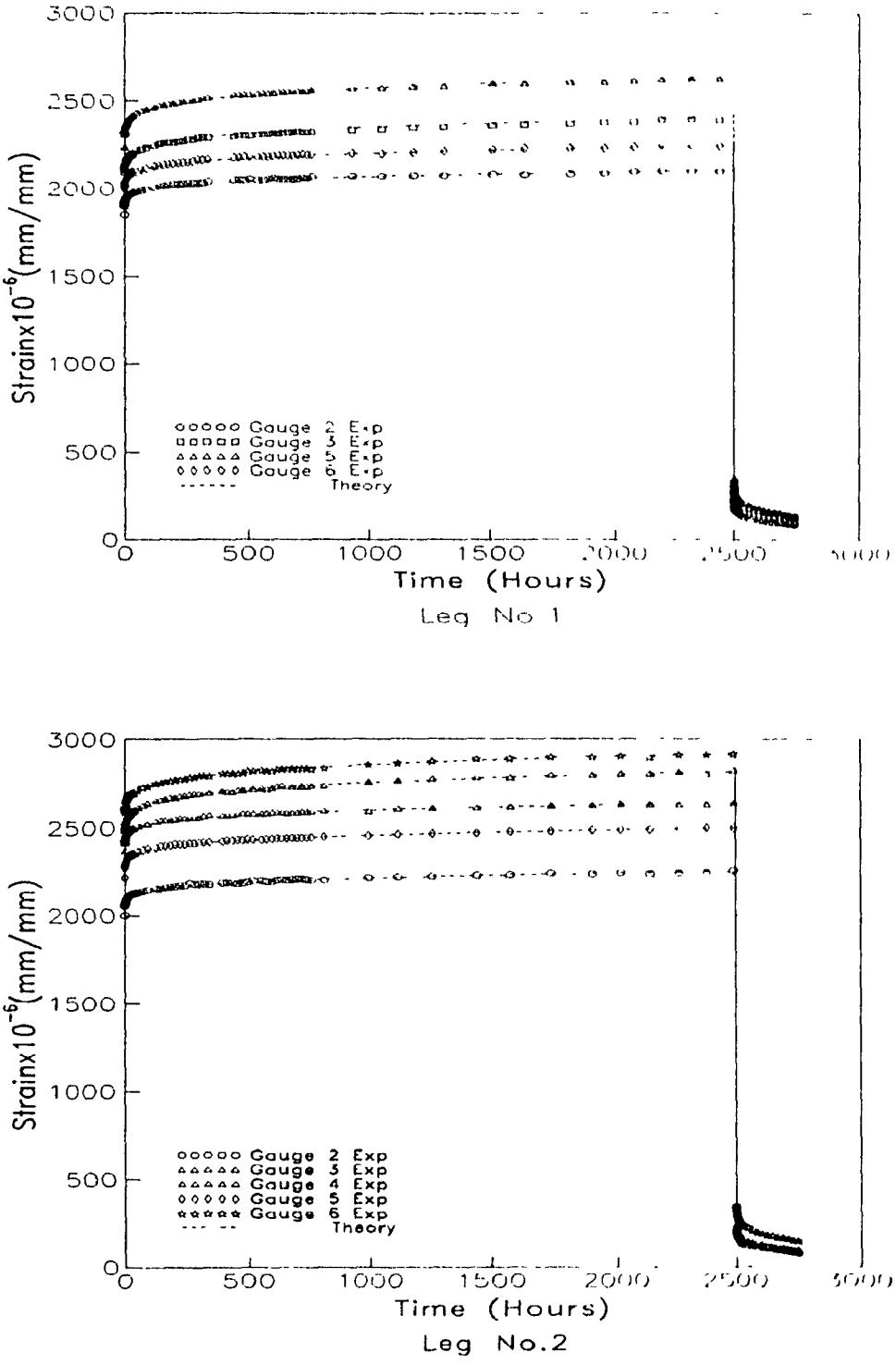

Fig. 7.6. Experimental and theoretical predictions for Angle Stub No.2

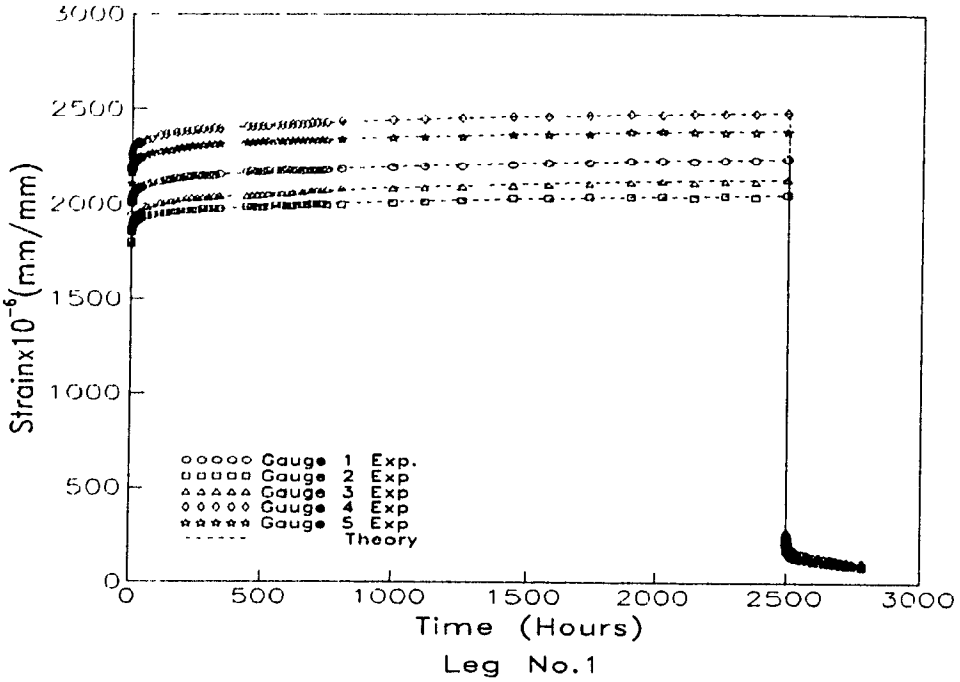

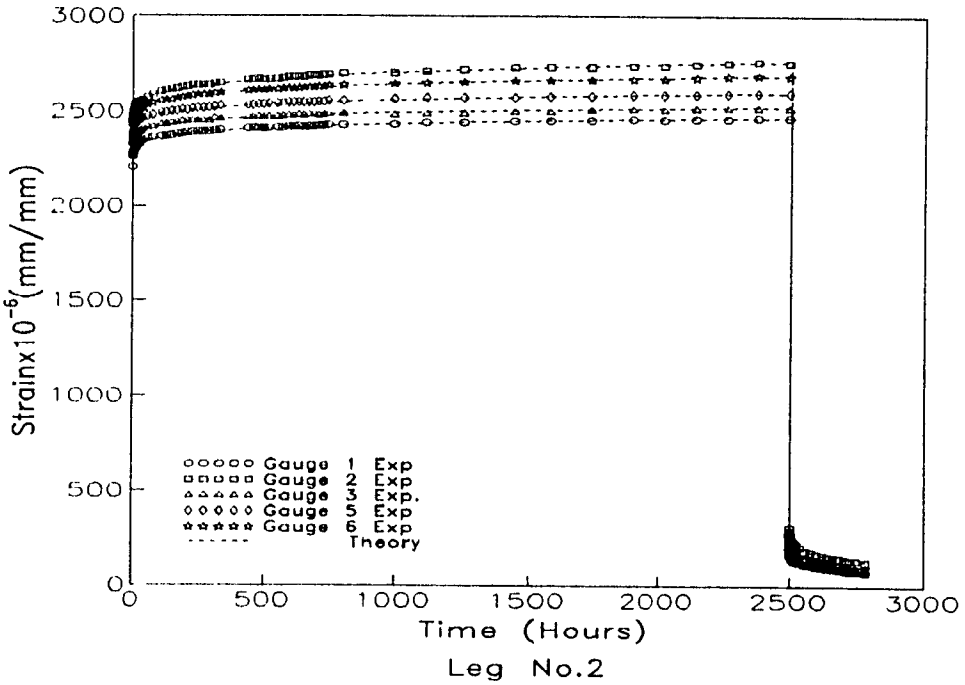

Fig. 7.7. Experimental and theoretical predictions for Angle Stub No.3

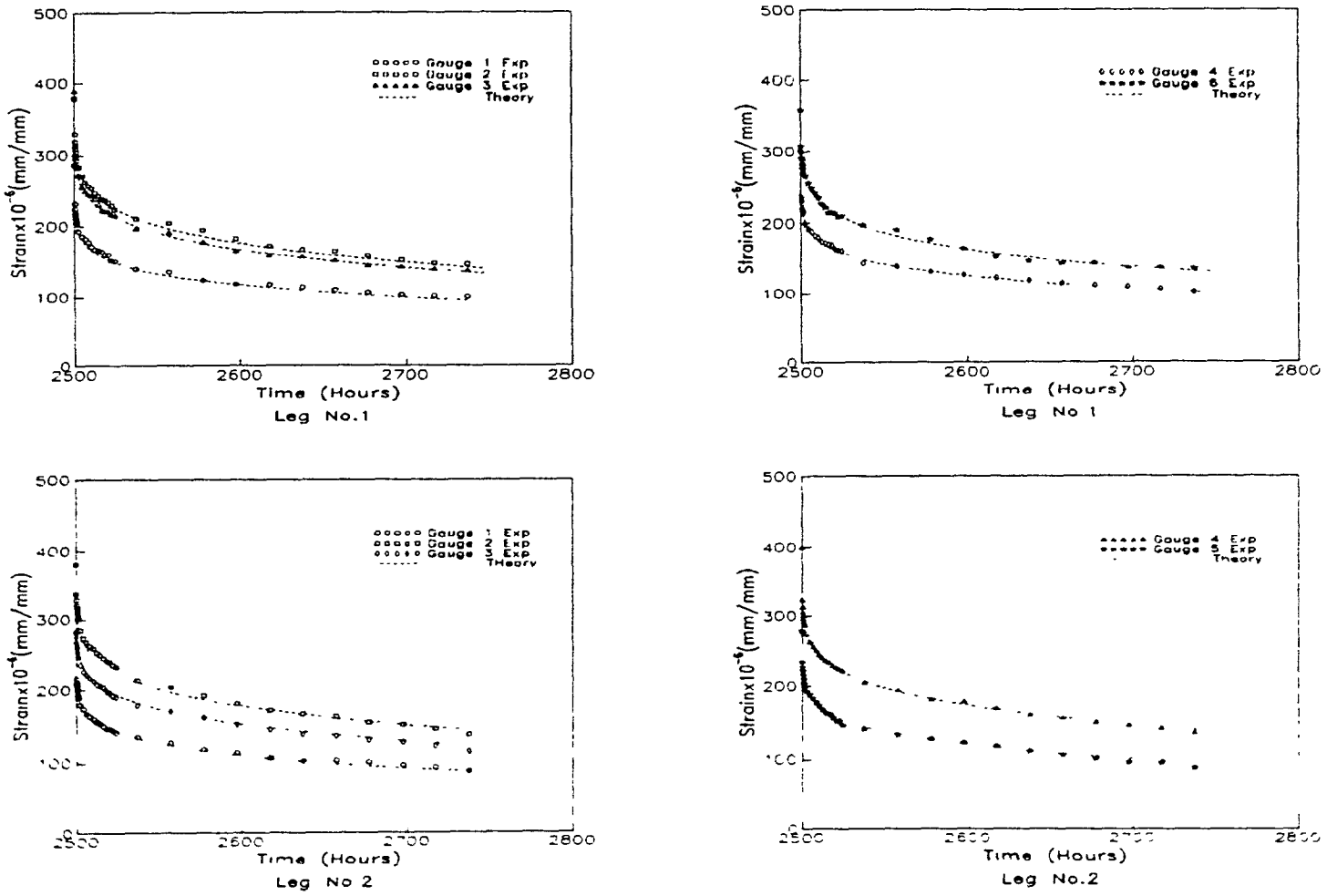

Fig. 7.8. Experimental and theoretical predictions of creep recovery for Angle Stub No.1

7.4 Predictions of Creep and Creep Recovery of Coupons

The experimental and theoretical creep curves for the three coupon tests are shown in Fig. 7.9. In these figures, excellent agreement between the experimental data and the data from Findley's power law was obtained for the entire test period. A good agreement between the actual creep strain recovery data and the predicted creep recovery using the superposition principle after 250 hours of unloading was also obtained.

As it was observed earlier, the experimental creep values for both angle stubs and coupons were slightly higher than the theoretical values for upto about 1000 hours. However, a change in this trend was noticed after this period, as indicated in Tables 7.1 to 7.5. It was also observed that a significant (95%) amount of creep occurred during the first 2000 hours of loading. This indicates that the creep parameters obtained from this reduced test period can be used to predict the long-term behaviour of both coupons and angle stubs, provided that they don't experience nonlinear tertiary creep.

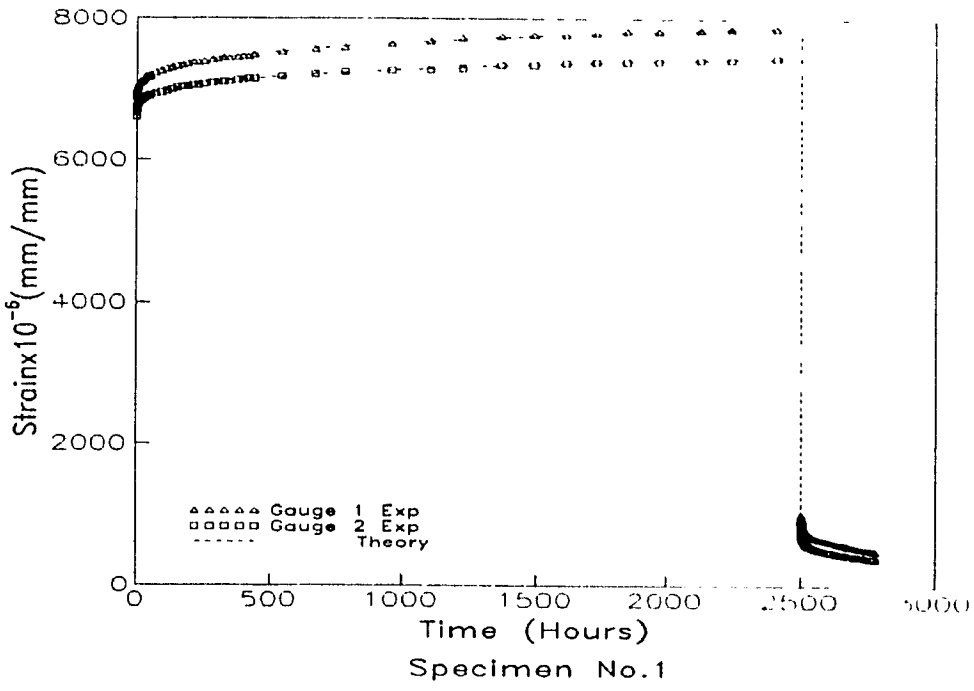

(a)

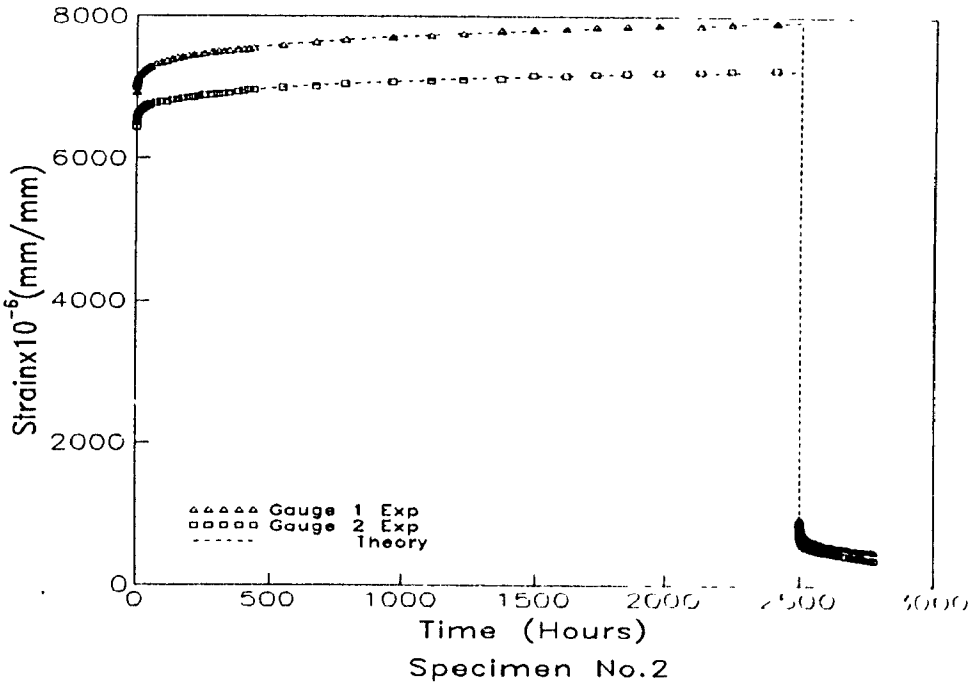

(b)

Fig. 7.9. Experimental and theoretical predictions for coupons

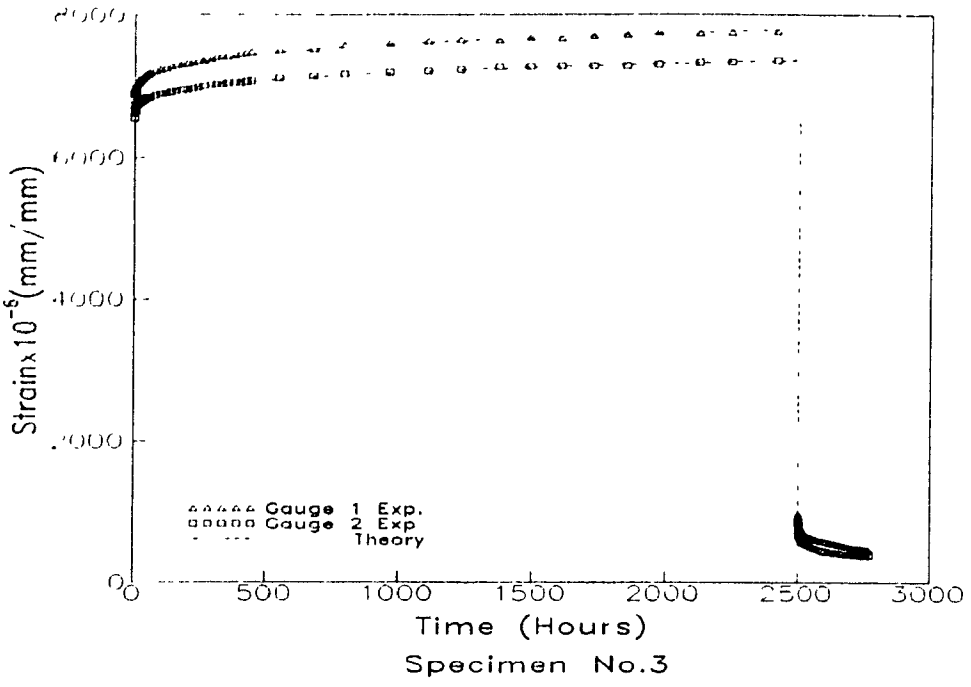

(c)

Fig. 7.9. Experimental and theoretical predictions for coupons

7.5 Summary

In this chapter, a comparison between experimental results (from angle stubs and coupons) and theoretical analysis using Findley's model has been presented. The results indicate that for a total duration of 2500 hours, the best estimate of creep strain is obtained using Findley's creep model. Creep parameters determined directly from stub tests only introduce a large scatter in the prediction. However, the estimated strain recovery values using superposition principle agree very well with the test data.

CHAPTER 8

CONCLUSION

8.1 Conclusions

This dissertation has presented a complete study of the compression creep behaviour of angle stubs and coupons constructed from commercially produced pultruded FGRP sections. Predictive models for the creep response of these composite materials have been generated and compared with experimental results.

The general conclusions drawn from the tests conducted can be summarized in the following points:

1) Tests on coupons coming from different angle legs have shown that one leg was stiffer and stronger than the other. This was attributed to mold positioning in the manufacturing process.

2) The modulus of elasticity and the ultimate stress measured were 20% higher than the nominal values guaranteed by the manufacturer.

3) The stress-strain curves in the time-independent coupon tests were linear.

4) A significant portion of the creep (96%) occurred during the first 2000 hours of loading and creep parameters obtained from this part can be used to predict the

long-term behaviour of the FGRP material.

5) Similar creep parameters were obtained using results from coupon creep, which indicate that tests on coupons can be used to predict the viscoelastic of FGRP structures.

6) The compression creep behaviour of coupons was the same as that of the angle stubs. The creepocity of coupons and angle stubs were 15%.

7) Findley's power law can be used successfully to describe the creep behaviour of pultruded FGRP angle stubs and coupons.

8) The principle of superposition can be used to describe the creep recovery of FGRP angle stubs and coupons.

9) Average creep strain predictions with both coupon and stub properties were in excellent agreement with a difference of 5%; the average creep strain corresponded to 15% of the initial strain after 2500 hours and at 45% of the ultimate failure stress.

10) The scatter on creep predictions with the stub properties ($\pm$35%) was more than twice that using the coupon properties.

11) Considering the variability of the results, Findley's model with coupon properties provides the best estimate of the scatter observed in actual measurements. Creep parameters determined directly from stub tests only introduce a larger scatter in the predictions.

8.2 Suggestions for Future Research

Although the results of this research have provided valuable information

regarding the overall behaviour of FRP pultruded materials under both short-term and long-term loading conditions, the following are some areas which have been identified by this work as needing further investigation:

1) Axial compression and tension long-term and short-term tests on the angle stubs and coupons with different load levels.

2) Long-term and short-term tests in full-size structures made from angle sections, e.g. construction of a truss section of a lattice tower.

REFERENCES

Alper, H., Barton, F.W., McCormick, F.C., Optimum Design of a Reinforced Plastic Bridge Girder, *Computer and Structures*, Vol. 7, 1977, pp. 249-256.

ASCE, Structural Plastic Design Manual, ASCE Manuals and Reports on Engineering Practice, No. 63, ASCE, New York, 1984.

ASCE, Structural Plastic Selection Manual, ASCE Manuals and Reports on Engineering Practice, No. 66, ASCE, New York, 1984.

ASTM, Standard Test Method for Compressive Properties of Rigid Plastics, *ASTM-STD-D695-89*, Annual Book of ASTM Standards, Part 35, 1990.

ASTM, Standard Test Method for Tensile Properties of Plastics, *ASTM-STD-D638-89*, Annual Book of ASTM Standards, Part 35, 1990.

ASTM, Standard Test Method for Tensile, Compressive, and Flexural Creep and Creep-Rupture of Plastic, *ASTM-STD-D2990-89*, Annual Book of ASTM Standards, Part 35, 1990.

ASTM, Standard Recommended Practice for Testing Stress-Relaxation of Plastic, *ASTM-STD-D2991-89*, Annual Book of ASTM Standards, Part 35, 1990.

Ballinger, C., Structural FRP Composites, *ASCE Civil Engineering Magazine*, Vol. 60, July 1990, pp 63-67.

Bank, L. C., Shear Properties of Pultruded Fibre Glass FRP Materials, *Journal of Materials in Civil Engineering*, Vol. 2, No. 2, May 1990, pp. 118-122.

Bank, L. C., Mosallam A.S., Creep and Failure of a Full-size Fibre-reinforced Plastic Pultruded Frame, *Composite Materials Technology*, ASME PD-Vol. 32, 1990, pp. 49-56.

Baer, E., Engineering Design for Plastics, New York, Second Edition, 1968, pp. 277-310.

Beckwith, S. W., Creep Behaviour in Kevlar/Epoxy Composite, *Proceedings of the 29th National SPMPE Symposium*, April 3-5 1985, pp. 578-591.

Benjamin, B. S., Structural Design with Plastics, New York, Second Edition, Van Nostrand Reinhold, 1982, pp. 1-12.

Bergen, R., Stress Cracking of Noncrystalline Plastics, *SPE Journal*, Vol. 24, August 1968, pp. 77-80.

Bishop, G.R., Sheard, P. A. Fire-resistant Composites for Structural Section, *Composite Structures*, 1992, pp. 85-89.

Calcote, L. R., The Analysis of Laminated Composites Structures, New York, First

Edition, Van Nostrand Reinhold Co., 1969, pp. 115-125.

Davies, R. M., Plastics In Building Construction, Proceedings of a Conference on Plastics in Building Construction, London, 1964, pp. 106-112.

Dutton, R., A Survey of Compression Creep Testing of Metals, *Materials Research and Standards*, April 1969, pp. 11-17.

Evans, R.W., Wilshire B., Creep of Metals and Alloys, London, First Edition, 1985, pp. 38-50.

Findley W. N., Mechanism and Mechanics of Creep of Plastics, *SPE Journal*, January 1960, pp. 57-65.

Findley W. N., Stress Relaxation and Combined Stress Creep of Plastics, *SPE Journal*, February 1960, pp. 192-196.

Findley, W. N., 26-Year Creep and Recovery of Polyvinylchloride and Polyethylene, *Polymer Engineering and Science*, April 1987, pp. 582-585.

Findley W. N, James S. L., Onaran K., Creep and Relaxation of Nonlinear Viscoelastic Materials, New York, First Edition, American Elsevier Pub. Co. 1976, pp. 289-303.

Findley, W. N., Khosla, G., Application of the Superposition Principle and Theories of Mechanical Equation of State, Strain, and Time Hardening to Creep of Plastics

Under Changing Loads, *Journal of Applied Physics*, 1955, pp. 821-832.

Findley W. N., Reed M.R., Concerning Strain-gauge Measurement of Creep of Plastics, *Experimental Mechanics*, January 1963, pp. 29-32.

Findley W. N., Tracy F.J., 16 Year Creep of Polyethylene and PVC, *Polymer Engineering and Science*, Vol. 14, No. 8, August 1974, pp. 577-580.

Hofer K. E., Rao N.P., A New Static Compression Fixture for Advanced Composite Materials, *Journal of Testing and Evaluation*, JTEVA, Vol. 5, No. 4, July 1977, pp. 278-283.

Hollaway, L., Glass Reinforced Plastics in Construction, Engineering Aspects, New York, First Edition, 1978, pp. 1-3.

Hollaway L., Howard C., Some Short and Long-term Loading Characteristics of a Double Layer Skeletal Structure Manufactured from Pultruded Composites, Composite Structures 3, Proceedings of the Third International Conference on Composite Structures, Paisley, Scotland, 9-11 September 1985, pp.788-808.

Holmes, M., Just, D. J., GRP in Structural Engineering, London, First Edition, Applied Science Publishers, 1983, pp. 213-228.

Holmes. M., Rahman T. A., Creep Behaviour of Glass Reinforced Plastic Box Beams, *Composites*, April 1980, pp. 79-85.

Irion, M. N., Compression Creep Testing of Composite Materials, M.S. Thesis Mechanical Engineering Department, University of Wyoming, Laramie, Wyoming, May 1980, pp. 8-13.

Irion, M. N., Adams F. D., Compression Creep Testing of Unidirectional Composite Materials, *Composites*, April 1981, pp. 117-123.

Johanson, A. E., Roll, F., A prestressed Kevlar/FRP Structural System, *Proceeding of the ASCE First Materials Engineering Congress*, Denver, Colorado, 13-15 August 1990, pp. 640-648.

Johanson, A. F., Sims, G. D., Simplified Design Procedures for Composite Plate Under Flexural Loading, Composite Structures 2, Proceedings of the 2nd International Conference on Composite Structures, Paisley, Scotland, 14-16 September 1983, pp. 302-325.

Jones, R.M., Mechanics of Composite Materials, New York, First Edition, Hemisphere, 1975.

McCormick, F. C., Laboratory Fatigue Investigation of a GRP Bridge, *Proceedings of the ASCE First Materials Engineering Congress*, Denver, Colorado, 13-15 August 1990, pp. 996-1005.

McCormick, F.C., Experimental Bridge Girder of Reinforced Plastic, *ASCE Transportation Journal*, 1975, pp. 47-63.

McClure, G., Mohammadi, Y., Compression Creep of Pultruded Angle Sections, *Ninth International Conference on Composite Materials*, Madrid, 12-16 July, 1993.

MMFG Design Manual, Morrison Molded Fiber Glass Company, Bristol, Virginia, 1990.

Mosallam, A. S., Bank L. C., Creep and Recovery of a Pultruded FRP Frame, *Advanced Composites Materials in Civil Engineering*, Las Vegas, Jan. 31-Feb. 1 1991, ASCE, pp. 24-35.

Oplinger, D. W., Plumer, J., Gandhi, K.R., Design, Fabrication and Testing of a Pultruded Framework for Tent Applications, *Proceedings of the 28th National SAMPE Symposium*, 12-14 April 1983, pp. 1478-1491.

Riddell, M. N., A Guide to Better Testing of Plastics, *Plastics Engineering*, April 1974, pp. 71-78.

Ryder, J. T., Black, E. D., Compression Testing of Large Gauge Length Composite Coupons, *Composite Materials: Testing and Design (Fourth Conference)*, ASTM STP 617, 1977, pp. 170-189.

Seymour, R. B., Deanin, R. D., History of Polymeric Composites, Proceeding of the Symposium held during the 192nd ACS National meeting, California, 10-12 September 1986, pp. 57-60.

Sheldon, R. P., Composite Polymeric Materials, Applied Science Publisher, London, 1982, pp. 1-10.

Shuart, M. J., Herakovich, C. J., An Evaluation of Sandwich Beam in Four-Point Bending as a Compressive Test Method for Composites, NASA Technical Memorandum 78783, Lanley Research Centre, September 1978.

Simonovskaya, M. V., A Machine for Long-term Strength and Creep Testing Under Compression, *Industrial Laboratory*, Vol. 41, No. 6, June 1975, pp.947-948.

Skeist, I., Plastics in Building, New York, First Edition, Reinhold, 1966, pp.72-83.

Smith, P. C., High Temperature Compressive Creep Mechanics, *Journal of Scientific Instruments*, Vol. 43, 1966, pp. 39-43.

Tsai, S W., Hahn, H. T., Introduction to Composite Materials, Technomic, Lancaster, Pennsylvania, 1980, pp. 1-457.

Thomas, D. A., Uniaxial Compressive Creep of Polytetrafluoroethylene, *Polymer Engineering and Science*, Vol. 9, No. 6, November 1969, pp. 415-422

Vinson, J. R., Chou, T. W., Composite Materials and Their Use in Structure, John Wiley and Sons, New York, 1975, pp. 1-438.

Vinson, J. R., Sierakowski, R. L., The Behaviour of Structures Composed of

Composites, Martinus Nijhoff, Dordrecht, 1987, pp. 1-323.

Whitney, J. M., Daniel, I. M., Byron, P. R., Experimental Mechanics of Fibre Reinforced Composite Materials, *SEPA*, 1982, pp. 175-185.

APPENDICES

APPENDIX A

TESTING SET-UP AND FAILURE PATTERNS OF TESTED SPECIMENS

This appendix contains some photographs for different tests performed in this research. It also shows the data logger acquisition system.

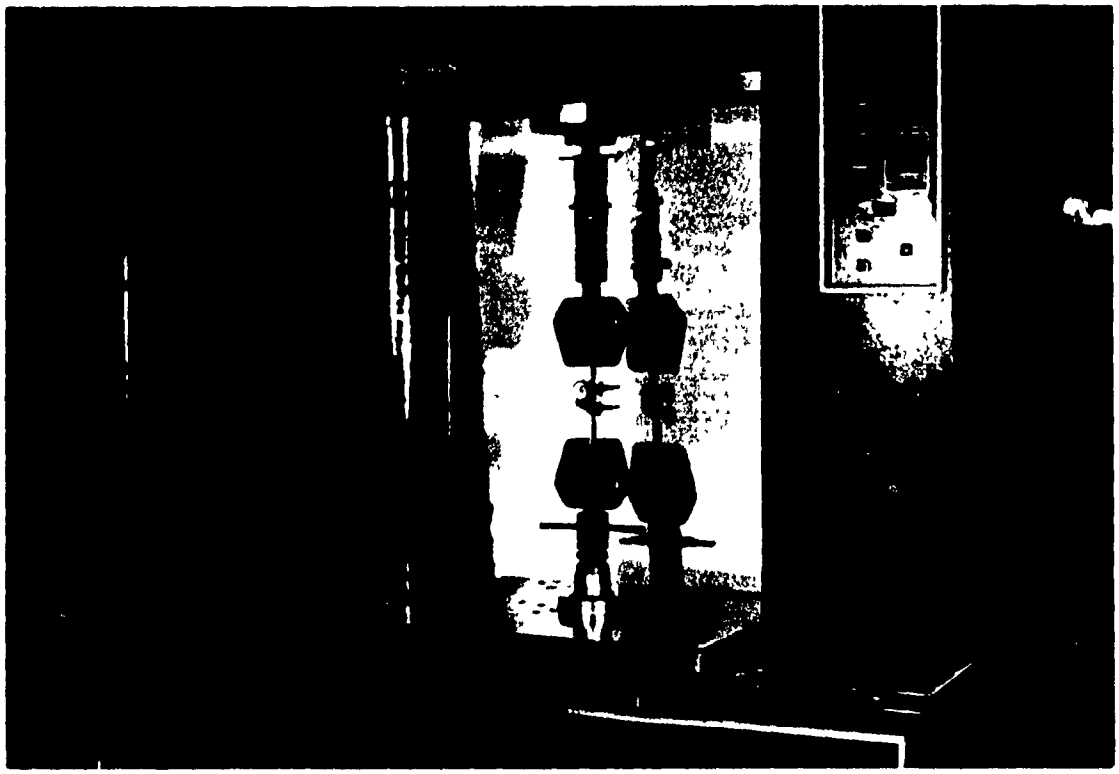

Fig. A.1. Tension coupon test

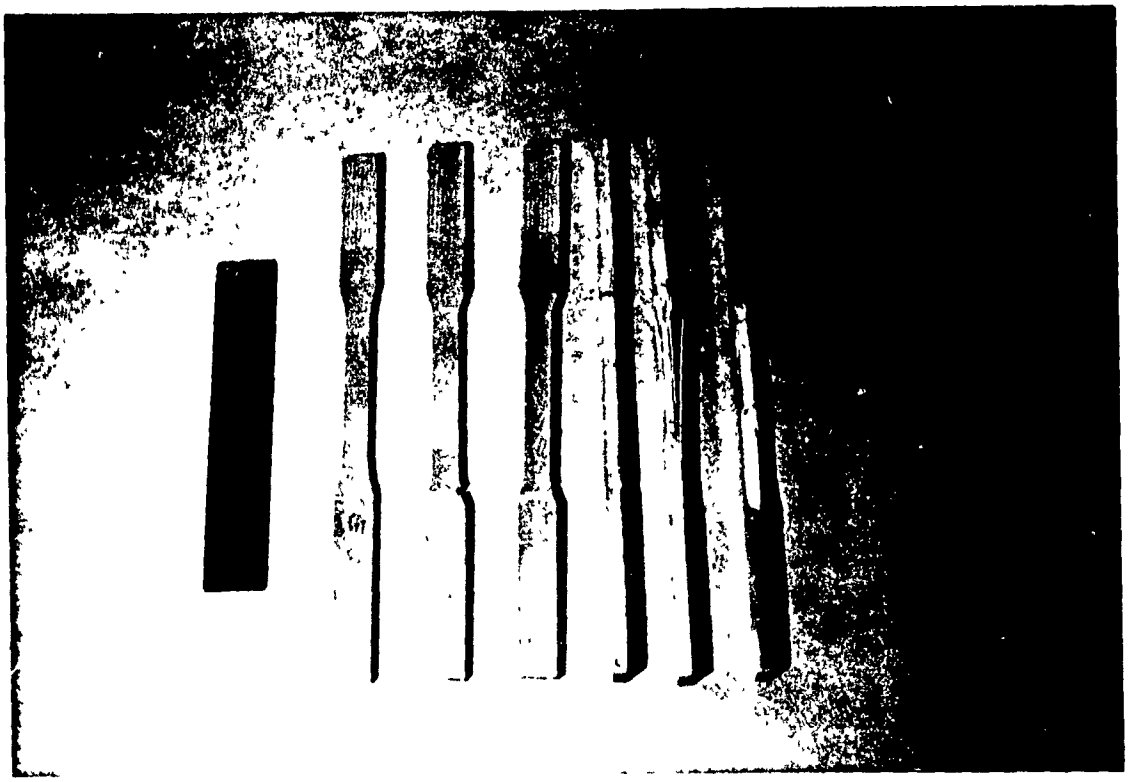

Fig A.2. Coupon failures in tension

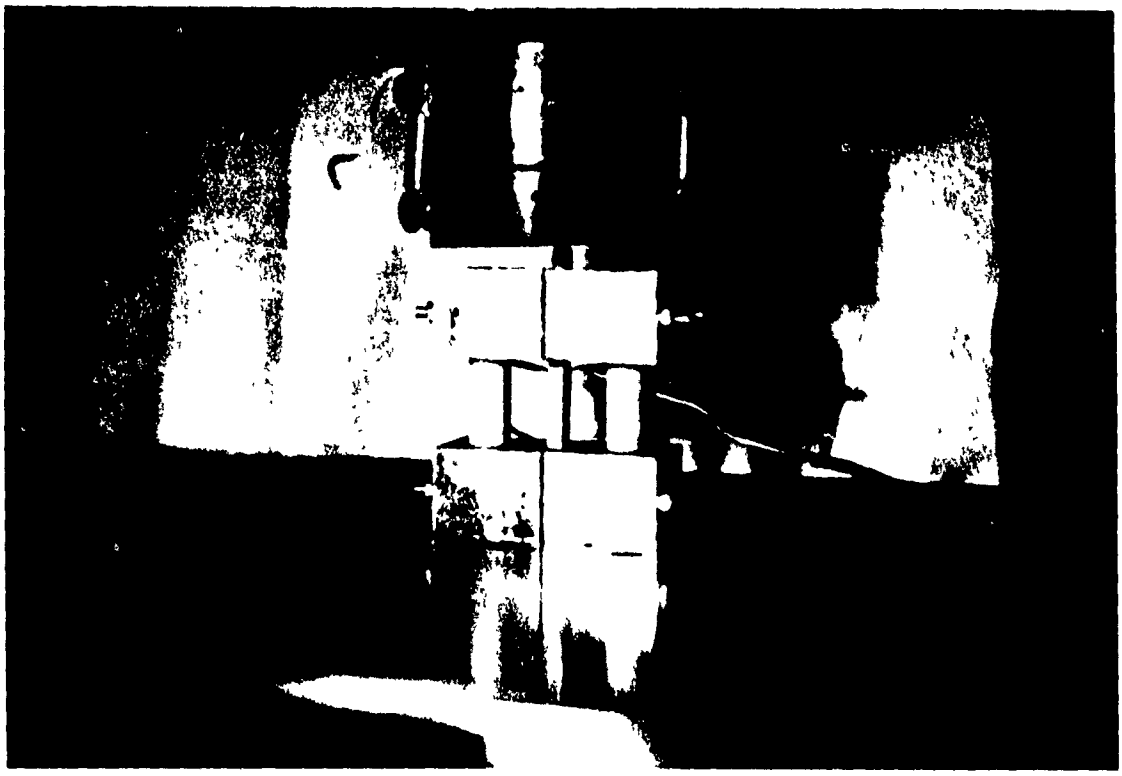

Fig A.3. Compression coupon test

Fig A.4. Coupon failures in compression

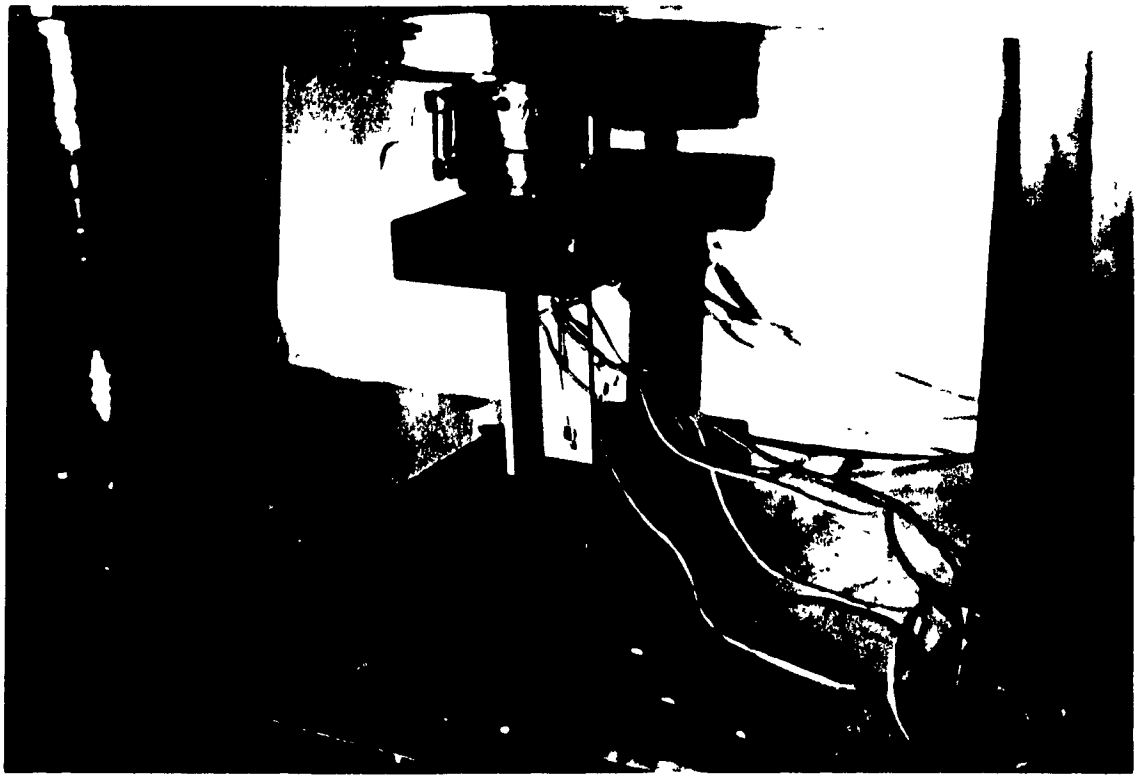

Fig. A.5. Compression angle stub test

Fig. A.6. Compression angle stub test at the onset of failure

Fig A.7. Compression angle stubs failure

Fig. A.8. Compression fixture disassembled

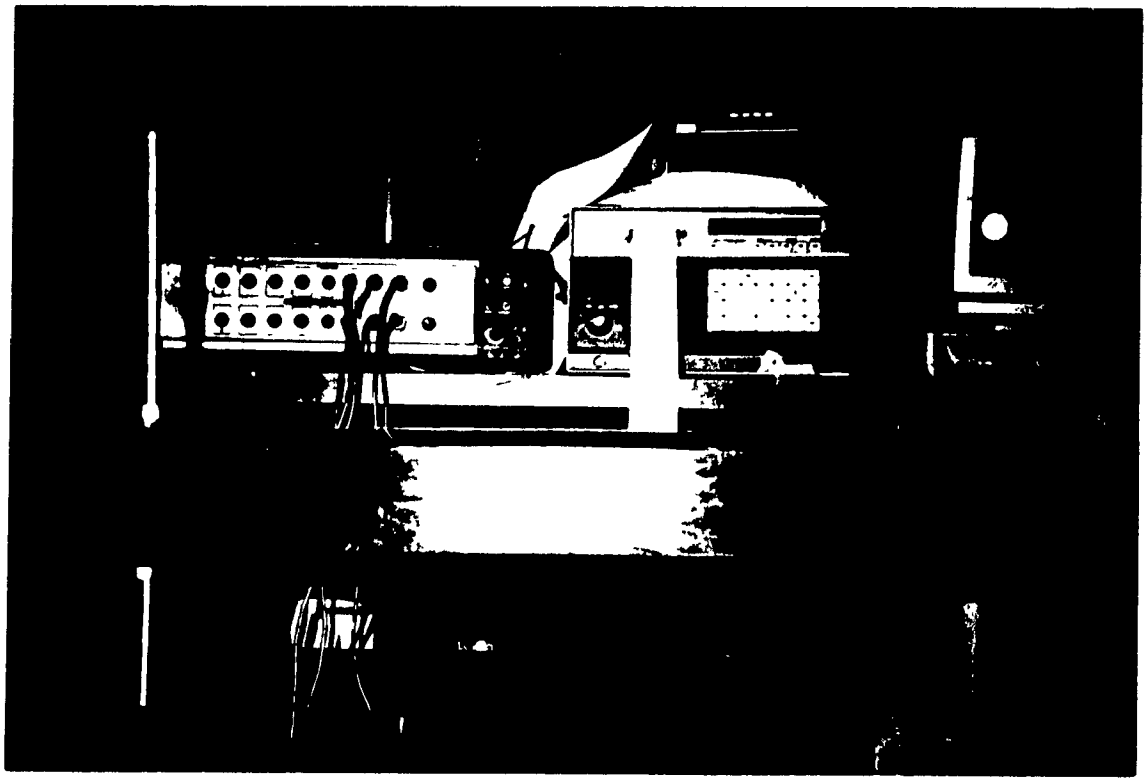

Fig. A.9. DORIC 245 DATA logger acquisition system

APPENDIX B

CREEP AND CREEP RECOVERY GRAPHS

Graphs depicting the relation between experimental and theoretical creep strain and creep recovery in the first 24 hours and 250 hours, respectively, are presented in this appendix. Theoretical values were obtained using Findley's power law with creep parameters determined experimentally.

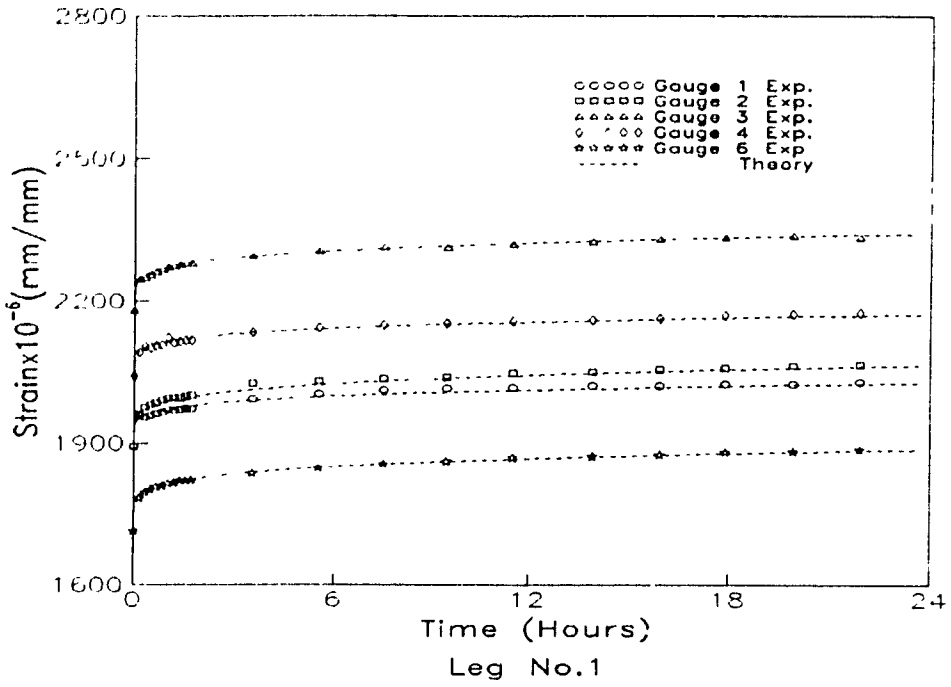

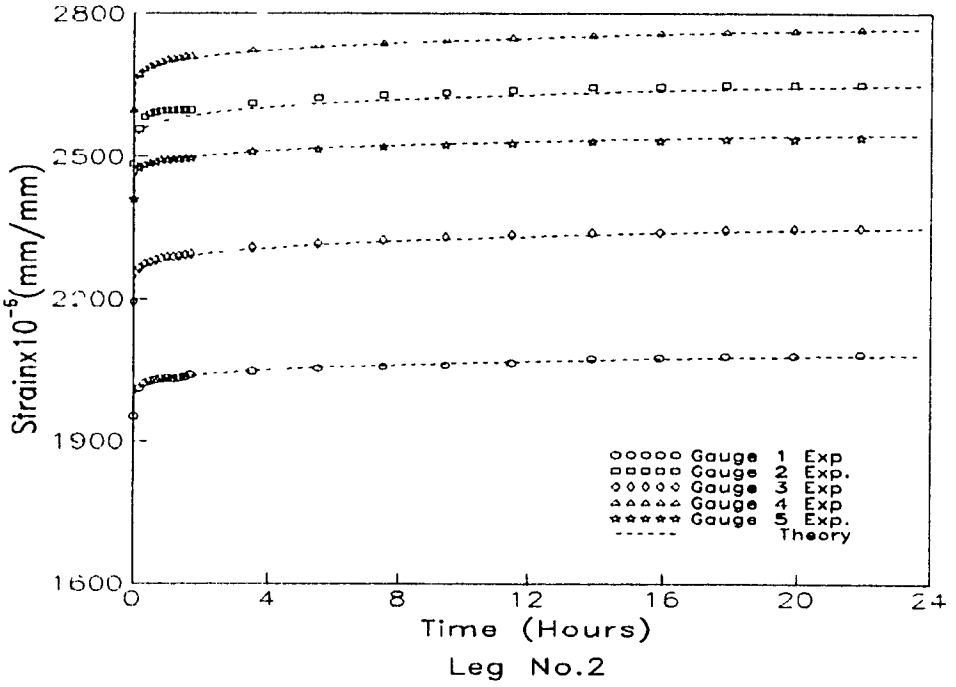

Fig. B.1. Experimental and theoretical predictions of Angle Stub No.1 for the first 24 hours of creep

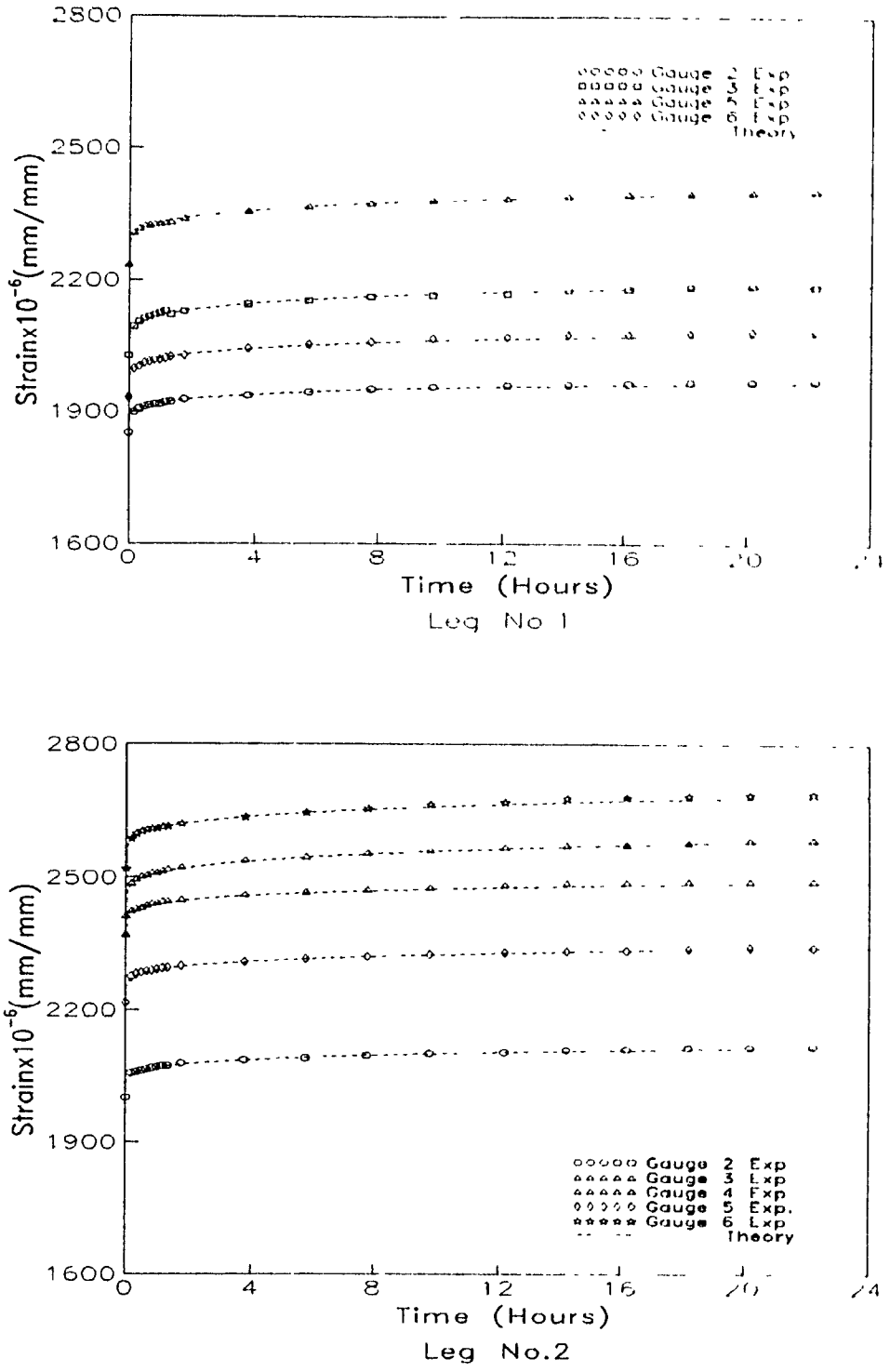

Fig. B.2. Experimental and theoretical predictions of Angle Stub No.2 for the first 24 hours of creep

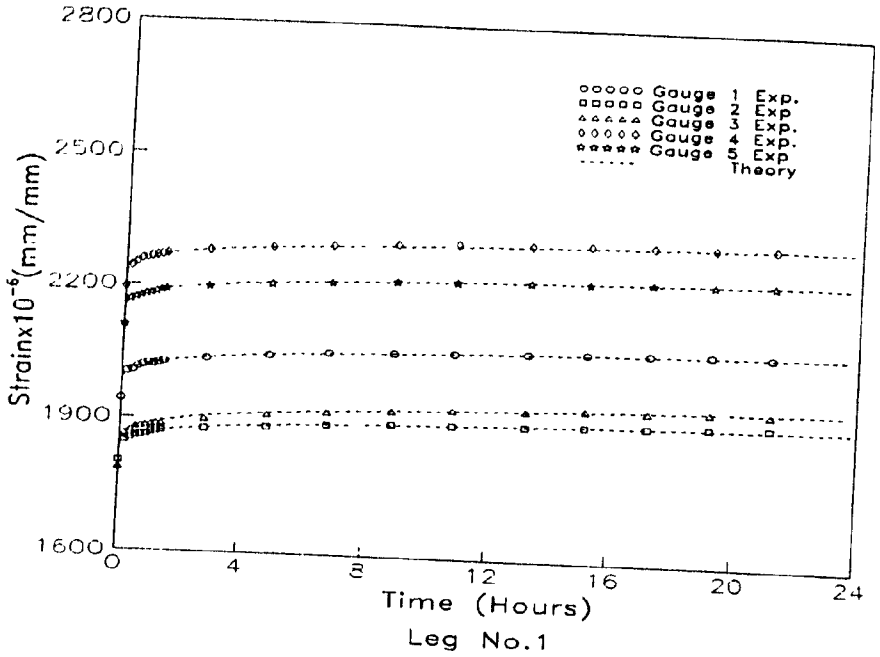

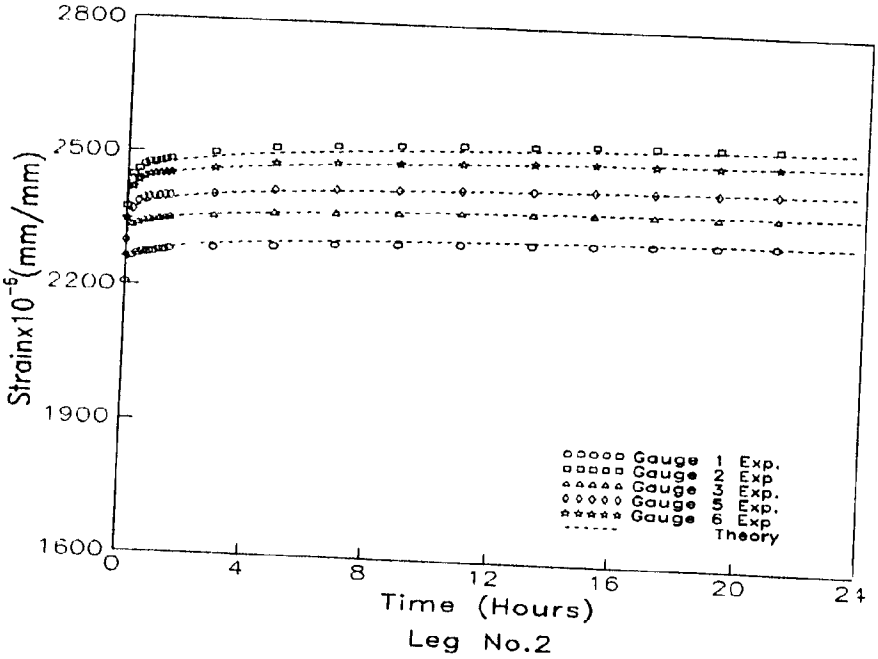

Fig. B.3. Experimental and theoretical predictions of Angle Stub No.3 for the first 24 hours of creep

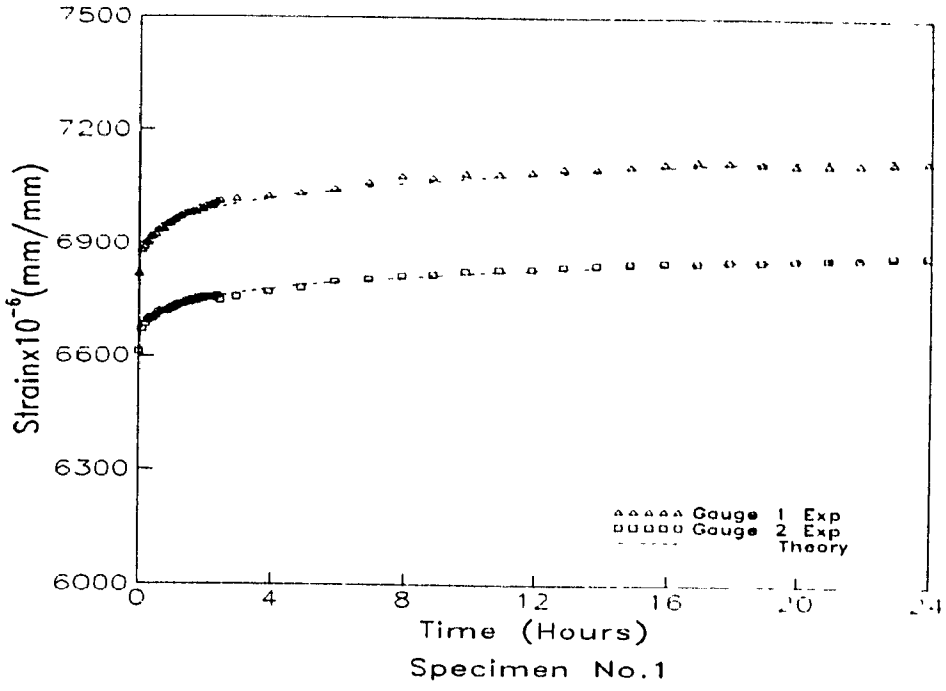

(a)

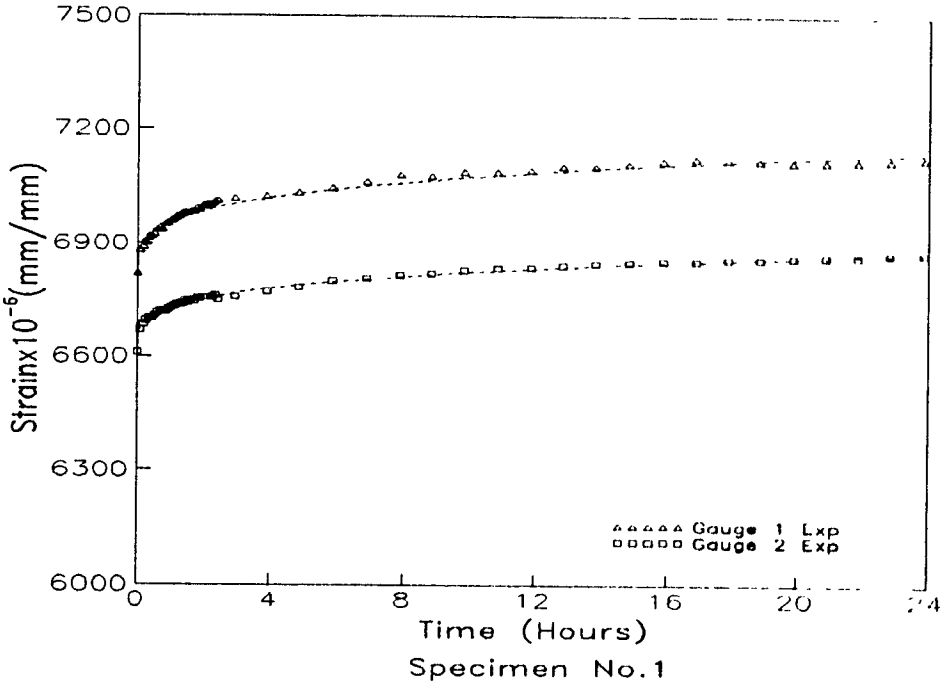

(b)

Fig. B.4. Experimental and theoretical predictions for coupons for the first 24 hours

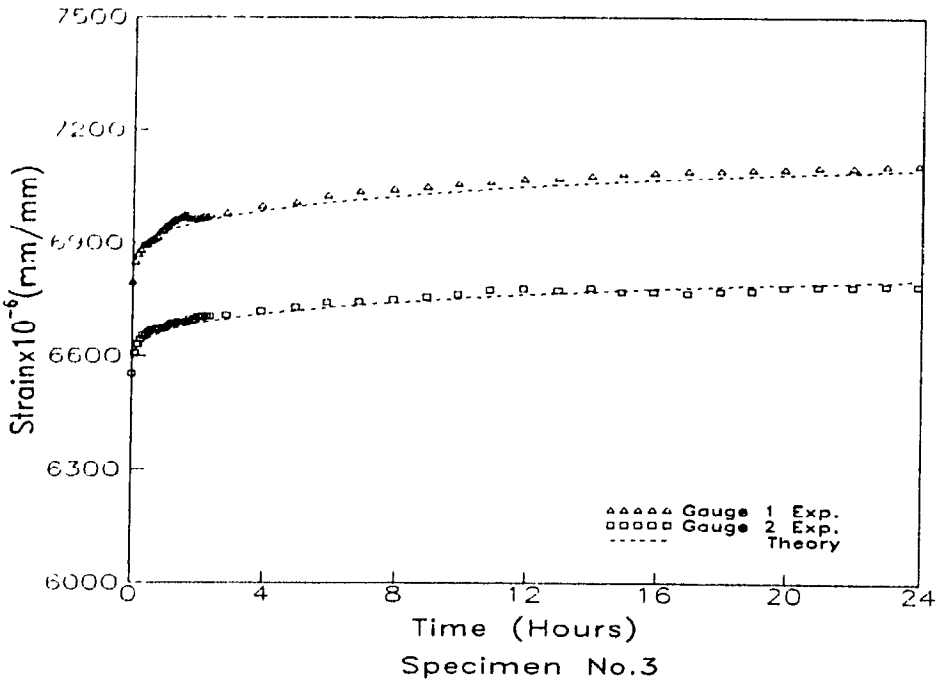

(c)

Fig. B.4. Experimental and theoretical predictions for coupons for the first 24 hours of creep

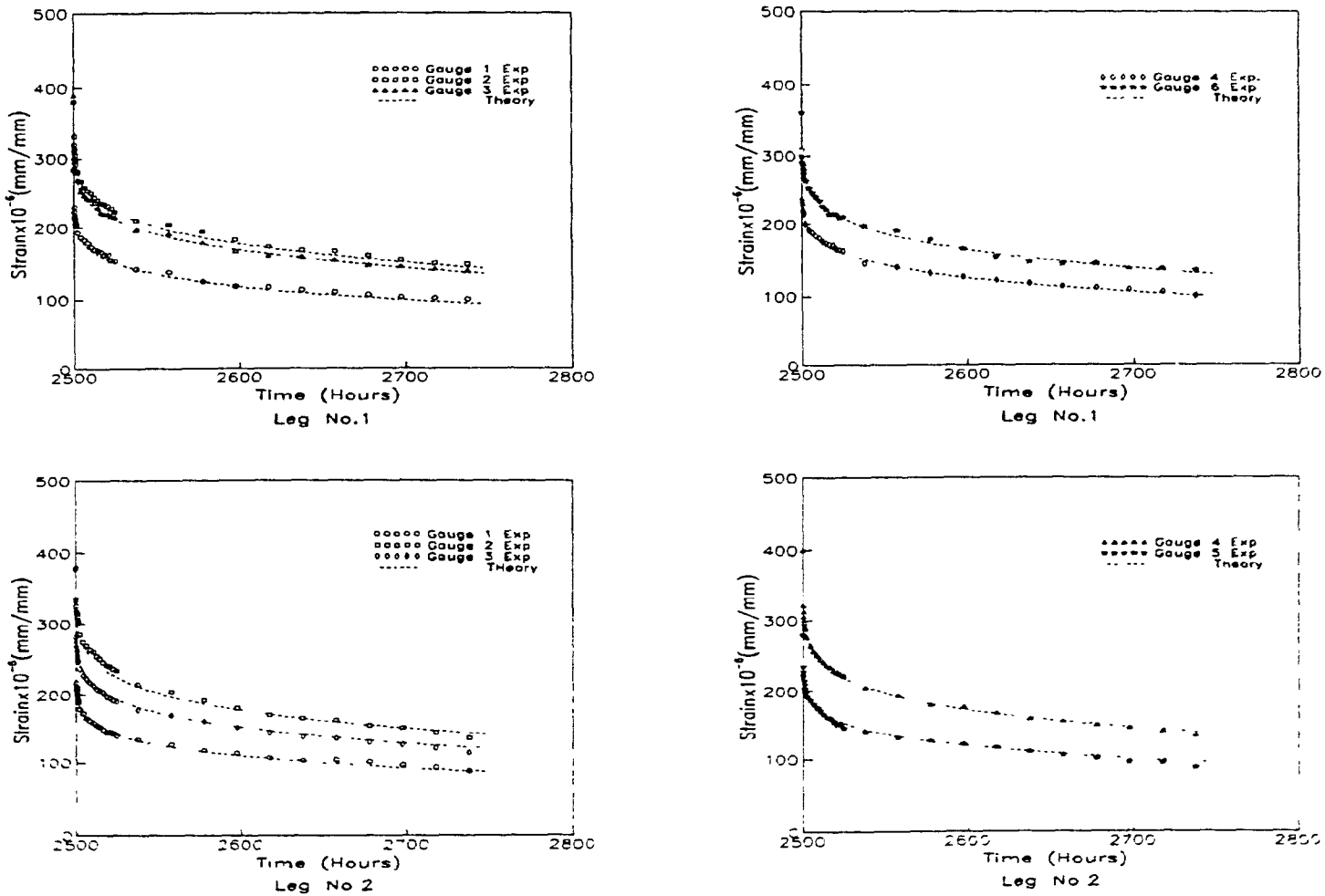

Fig. B.5. Experimental and theoretical predictions for creep recovery of Angle Stub No.1

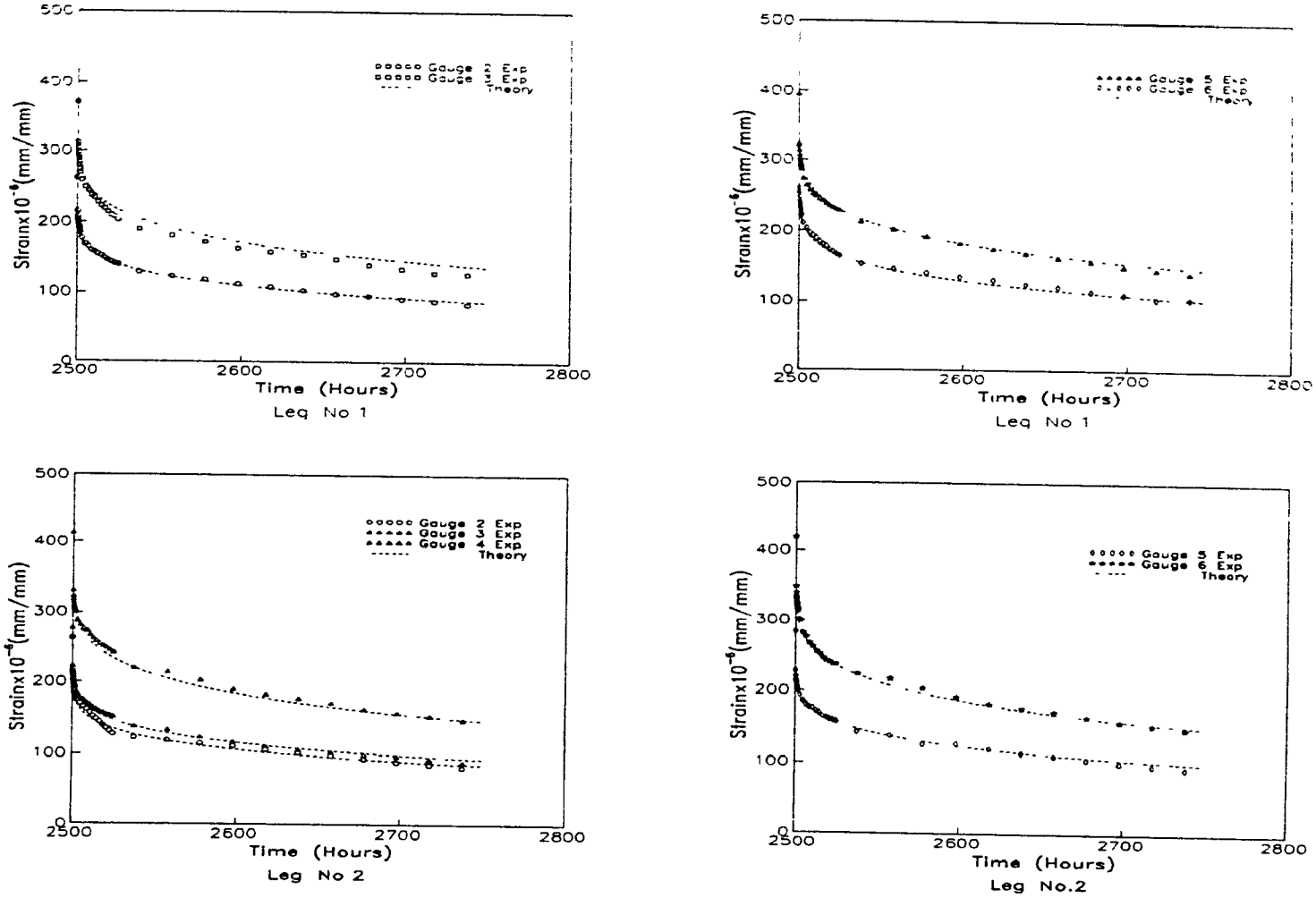

Fig. B.6. Experimental and theoretical predictions for creep recovery of Angle Stub No.2

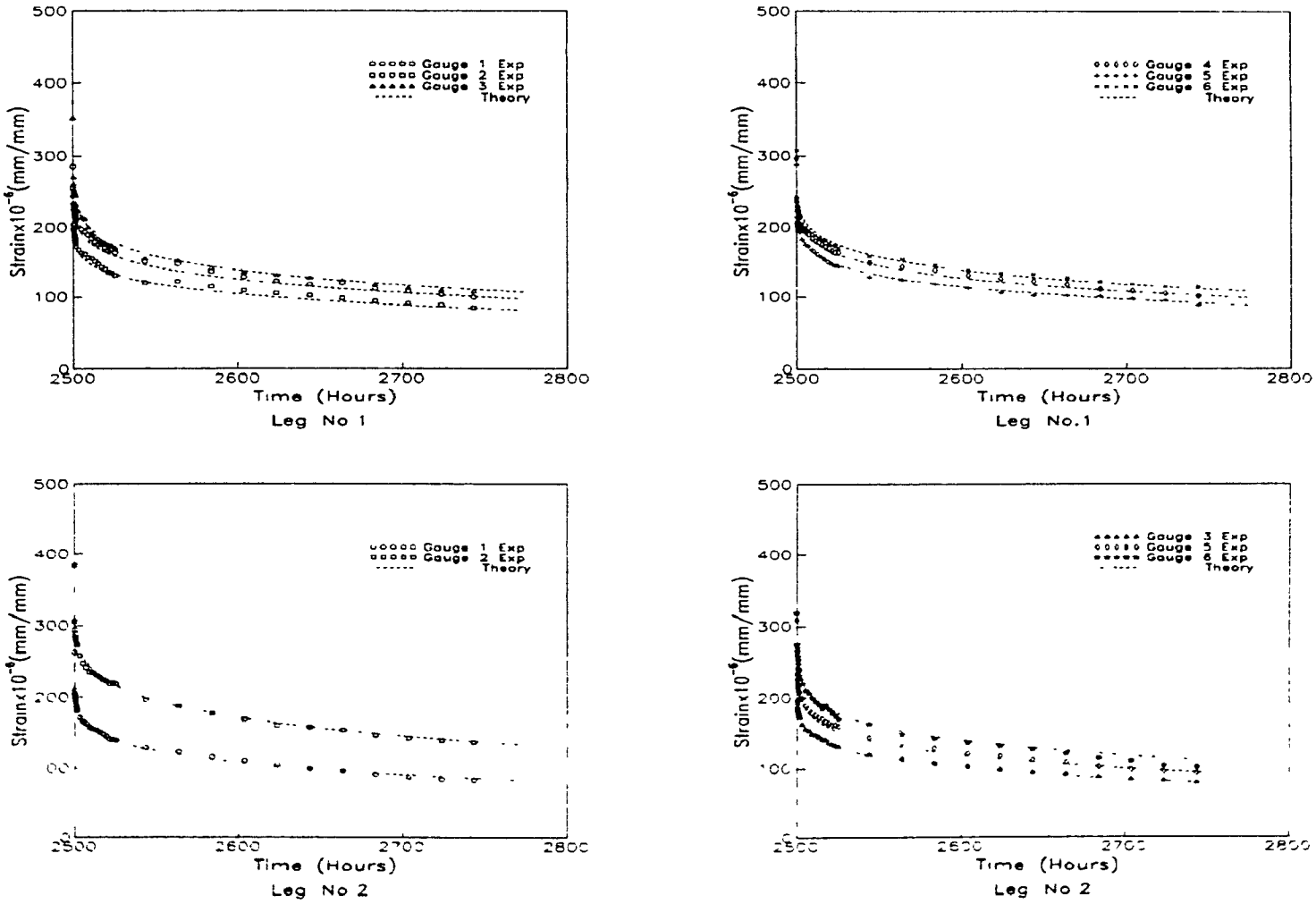

Fig. B.7. Experimental and theoretical predictions for creep recovery of Angle Stub No.3

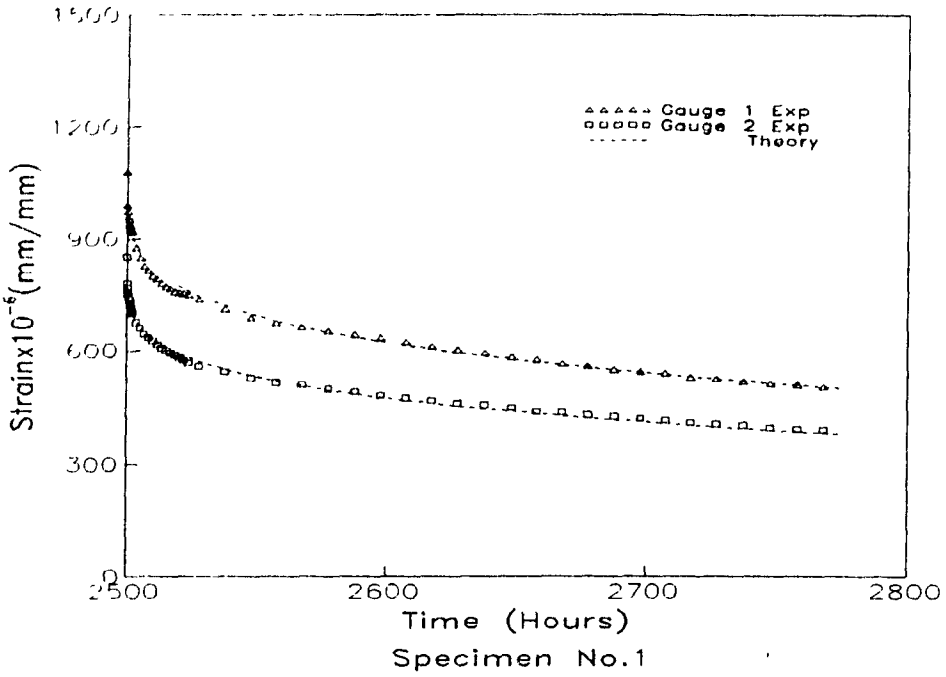

(a)

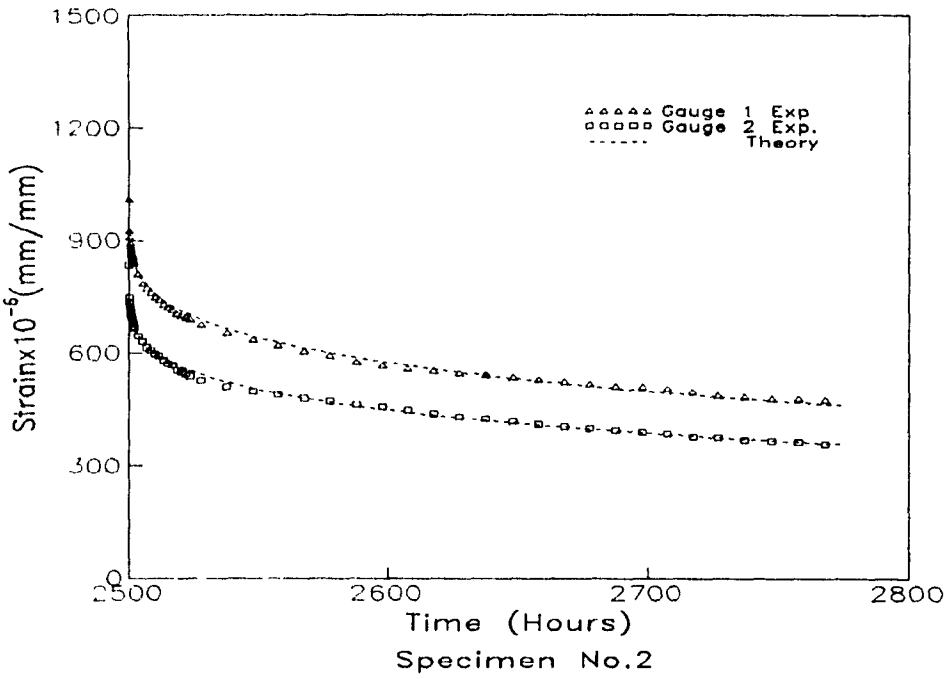

(b)

Fig. B.8. Experimental and theoretical predictions of creep recovery for coupons

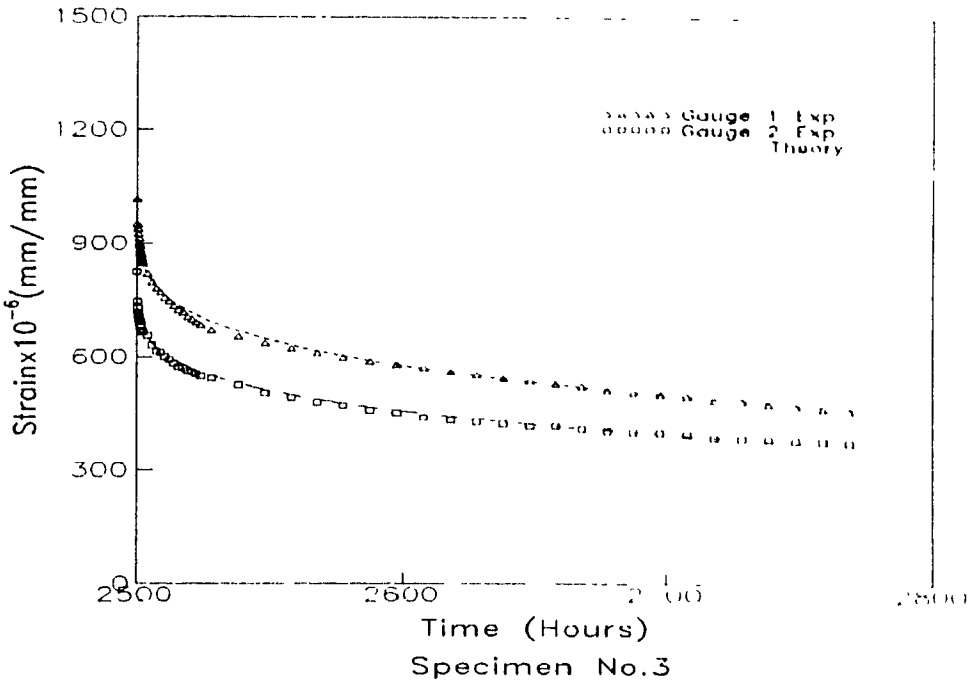

(c)

Fig. B.8. Experimental and theoretical predictions of creep recovery for coupons

APPENDIX C

MANUFACTURER'S TECHNICAL DATA SHEET

TECHNICAL PULTRUSION INC.

PROPERTIES OF CURS PULTRUDED PROFILES MAT REINFORCED

Polyester resin: high heat distortion temperature, isophtalic antiacid

Property (coupon value)	Norme ASTM	UNIT	35 TO 45% GLASS LG.	35 TO 45% GLASS TR.	45 TO 55% GLASS LG.	45 TO 55% GLASS TR.
Tensile strength	D-638	psi	30,000	7,000	45,000	9,000
Tensile modulus	--	psix10^6	2.3	.8	2.5	1.0
Flexural strength	D-790	psi	30,000	10,000	45,000	15,000
Flexural modulus	--	psix10^6	1.3	.6	1.8	.8
Compressive strength	D-695	psi	20,000	12,000	30,000	15,000
Compressive modulus	--	psix10^6	2.3	.8	2.5	1.0
Bearing stress	--	psi	20,000	20,000	30,000	30,000
Izod impact	D-256	ft-lbs/in	20	4	28	4
Barcol hardness	--	--	50	--	50	--
Shear strength	--	psi	4,500	4,500	5,500	5,500
Torque shear strength	--	psi	N.T.	N.T.	N.T.	N.T.
Dielectric strength (oil)	D-149	V/mil	200	25	200	35
Dielectric constant	D-150 at 60 Hz		4.5	--	5	--
Dissipation factor	D-669 room temp.		0.03	--	0.03	--
Arc resistance	D-495	sec.	80	--	120	--
Density	--	lbs./in^3	.058-.062	--	.060-.068	--
Specific gravity	--	--	1.61-1.75	--	1.68-1.88	--
Specific heat	--	Btu/lb/^oF	0.8616	--	--	--
Coefficient of thermal exp.	--	in/in/^oF	$3x10^{-6}$	--	$3x10^{-6}$	--
Thermal conductivity	--	Btu/h/sq.ft/in/^oF	2	--	2	--
Water absorption	D-570	Max.%	.7	--	.5	--
Flame resistance	--	--	N.T.	N.T.	N.T.	N.T.

1- Typical loading for standard profile

2- Improved construction for specific application